Mechanistic insight into gating and open channel block in prokaryotic pLGICs

Dissertation

zur

Erlangung der naturwissenschaftlichen Doktorwürde
(Dr. sc. nat.)

vorgelegt der

Mathematisch-naturwissenschaftlichen Fakultät

der

Universität Zürich

von

Carlo Bertozzi

von

Zürich ZH

Promotionskomitee

Prof. Dr. Raimund Dutzler (Leitung der Dissertation)
PD Dr. Ian Forster
Prof. Martin Jinek

Zürich 2014

Acknowledgment

Thank you - to all the people who helped and contributed to this thesis.

Ein grosser Dank gebührt meinen Eltern, für ihre finanzielle und mentale Unterstützung.

My friends for being around whenever needed.

My supervisor Raimund Dutzler for giving me the opportunity to carry out my PhD thesis in his lab and the support at any stage of my projects.

Ian Forster and Martin Jinek for being on my thesis committee and helpful advice.

I wish to thank my collaborators Prof. Dirk Trauner and his group for the custom synthesis of several compounds.

The infrastructure team of the biochemistry institute, for making it possible to focus only on my work and not having to deal with administrative, IT and maintenance work. Beat Blattmann and Céline Stutz-Ducommun of the NCCR crystallization facility, for their patience and support.

Timm Maier, Bostjan Kobe and Eugene Valkov for their introduction and valuable advice on protein purification and X-ray crystallography.

The lab former and current members for being around and their helpful input. Especially Iwan Zimmermann, Yvonne Neldner, Ricarda Hilf and Eric Geertsma.

Table of Contents

Abstract

Pentameric ligand gated ion channels (pLGIC) are key players in the fast signal transduction of nerve cells. These ion channels are present in the postsynaptic membrane of the synapses, where they convert the chemical signal originating from neurotransmitters, released by presynaptic cells, into an electrical response. pLGICs all share a common architecture. They consist of a predominantly beta-stranded extracellular domain and an alpha-helical transmembrane pore. Both domains comprise of independent folding units, which interact via an extended domain interface. Activation within the pentameric ligand-gated ion channel family is initiated by the binding of a ligand to a conserved site in the extracellular domain. The following conformational rearrangements in this part of the protein are transduced through interactions in the interface to the transmembrane part of the protein to activate a selective ion permeation pore.

The dysfunction of this activation process can lead to severe diseases like epilepsy, schizophrenia and Alzheimer's disease.

Therefore this family has been studied intensively for the last few decades using electrophysiology and biochemical techniques, which led to detailed insight into the pharmacological behavior of inhibition and modulation, ion selectivity, ligand binding mode and gating.

Only in recent years structural data became available for the family. Initially the structure of the acetylcholine binding protein, which resembles the extracellular domain of a functional acetylcholine receptor, shed light into the mechanism of agonist and antagonist binding on a molecular level. Further on the first high resolution structures of the two cation selective prokaryotic homologues (GLIC and ELIC) at two different states were determined. The homologue from *Erwinia chrysanthemi* (ELIC) was solved in a non-conductive state, while the protein from *Gloeobacter violaceus* (GLIC) resembles a potential conductive state.

In the course of my PhD studies I have used a special class of known inhibitors of the cation selective nicotinic Acetylcholine Receptor (nAChR) to study their effect on the prokaryotic homologue GLIC. This class of inhibitors called "open pore blocker" blocks the channel only in its open conformation. They are structurally diverse molecules such as quaternary ammonium compounds, local anesthetics and certain transition metal ions and vary significantly in their size and hydrophobicity. The only thing they have in common is their positive charge.

Electrophysiological experiments showed that these known inhibitors block the channel GLIC in a similar manner as seen for the nAChR. The additional structural studies revealed for the first time the molecular basis for this kind inhibition for this class of ion channels. It also allowed the discrimination of two distinct sites within the pore region responsible for block. The monovalent bulky quaternary ammoniums and local anesthetics bind in the middle of the pore and divalent transition metal ions closely interact with a conserved ring of negatively charged residues at the intracellular exit of the pore. At the same time the combination of structural and electrophysiological data could prove that the crystal structure of GLIC does indeed resemble a conductive conformation.

In a different study I had a closer look at the opening mechanism of the prokaryotic homologues GLIC and ELIC. Specifically I focused on the gating mechanism, which describes the steps between the ligand binding in the extracellular domain and the opening of the ion selective pore in the membrane region. Despite the wealth of information based on electrophysiological, biochemical and structural data, it was still unclear how the signal is transmitted through the protein and which part of the interface is important for this process.

Based on structural and electrophysiological data of mutants of the domain interface, I could show that most mutations in both homologues have the same effect on the gating mechanism, which underlines the high conservation of this process. The comparison of this data to literature shows that this conservation is not unique for these two homologues, but also can be expanded to the cation selective eukaryotic nAChR, where similar mutagenesis studies have been made. These findings indicate that both homologues share a very similar gating mechanism, and can thus be used as a model system for the entire family.

Zusammenfassung

Pentamere Liganden gesteuerte Ionenkanäle (pLGIC) sind Schlüsselfiguren in der schnellen Signalübertragung von Nervenzellen. Diese Ionenkanäle sind in der postsynaptischen Membran chemischer Synapsen präsent, wo sie durch Öffnung eines Ionenkanals nach Bindung eines Neurotransmitters das chemische Signal der presynaptischen Zelle in ein elektrisches Signal umwandeln. Alle pLGICs sing ähnlich aufgebaut. Sie bestehen im Wesentlichen aus einer extrazellulären Ligandenbindungsdomäne und einer alpha-helicalen transmembranen Pore. Diese beiden Domänen können durch ein ausgedehntes Interface miteinander interagieren. Die Aktivierung innerhalb der Familie der pentameren Liganden gesteuerten Kanäle wird durch die Bindung eines Liganden in einer konservierten Seite der extrazellulären Domäne ausgelöst. Die dadurch entstehende konformationelle Reorganisation in diesem Teil des Proteins wird über das Interface zum transmembranen Teil des Proteins weitergeleitet, welches dann eine ionenselektive Pore öffnet.
Eine Fehlfunktion in diesem Aktivierungprozess kann zu schwerwiegenden Krankheiten wie Epilepsie, Schizophrenie oder Alzheimer führen.
Aus diesem Grund wurde diese Familie in den letzten Jahrzehnten sehr intensiv mittels Elektrophysiologie und Biochemie erforscht. Diese Untersuchungen führten zu einer detaillierten Charakterisierung der Ligandenbindung, des Aktivierungsprozesses, der Ionenselektivität sowie der Pharmakologie von Inhibition und Modulation.
Trotz der Jahrzehnte dauernden Erforschung dieser Proteinfamilie standen strukturelle Daten erst in den letzten Jahren zur Verfügung. Zuerst wurde die Struktur des Acetylcholin bindenden Proteins publiziert, welches den Mechanismus der Agonisten und Antagonisten Bindung auf molekularer Ebene erklärte. Später wurden dann zwei hochaufgelöste Strukturen von zwei prokaryotischen Homologen der Familie (GLIC und ELIC) in zwei unterschiedlichen Zuständen aufgeklärt. ELIC, der Kanal aus *Erwinia chrysanthemi* nimmt eine inaktiven Konformation ein, während das GLIC, ein Protein aus *Gloeobacter violaceus* einen möglichen aktiven Zustand zeigt.

Während meiner Doktorarbeit habe ich eine spezielle Klasse von bekannten Inhibitoren des kationenselektiven nikotinischen Acetylcholin Rezeptors (nAChR) benutzt um ihren Effekt am prokaryotischen Homolog GLIC zu testen. Diese Klasse von Inhibitoren nennt sich Kanalblocker und blockiert den Kanal nur in seinem offenen Zustand. Die Inhibitoren sind strukturell sehr unterschiedlich und umschliessen quaternäre Ammoniumverbindungen, lokale Anästhetika und gewisse Übergangsmetalle. Sie unterscheiden sich deutlich in ihrer Grösse und ihrer Hydrophobizität. Ihre einzige Gemeinsamkeit ist ihre positive Ladung.
Elektrophysiologische Experimente zeigten, dass diese bekannten Inhibitoren den Kanal von GLIC in einer ähnlichen Art und Weise wie beim nAChR blockieren. Die zusätzlichen strukturellen Studien zeigten zum ersten Mal die molekulare Grundlage dieser Art von Inhibition für diese Klasse von Ionenkanälen. Es erlaubte ebenfalls die Identifizierung von zwei unterschiedlichen Stellen für den Block innerhalb der Porenregion. Die monovalenten, sperrigen quaternären Ammonium Verbindungen und die lokalen Anästhetika binden in der Mitte der Pore, während die divalenten Übergangsmetalle stark mit einem konservierten Ring von negative geladenen Resten am intrazellulären Ende der Pore interagieren. Die Kombination

der strukturellen und elektrophysiologischen Daten Unterstützt die Annahme, dass die Kristallstruktur von GLIC eine leitende Konformation zeigt.

In einer weiteren Studie befasste ich mich mit der Ligandenaktivierung in den beiden porkaryotischen Homologe GLIC und ELIC. Dabei untersuchte ich den ‚Gating' Mechanismus, welcher die Schritte zwischen der Liganden Bindung in der extrazellulären Domäne und dem Öffnen der ionenselektiven Pore in der Membran-Region beschreibt. Trotz der grossen Anzahl an Informationen basierend auf elektrophysiologischen, biochemischen und strukturellen Daten, war es noch unklar wie dieses Signal innerhalb des Proteins verbreitet wird und welche Teile des Interface an diesem Prozess beteiligt sind.
Basierend auf strukturellen und elektrophysiologischen Daten von Mutanten der Interfaceregion, konnte ich zeigen, dass die meisten Mutationen in beiden Homologen die gleichen Effekte auf den ‚Gating' Mechanismus haben, was auf eine hohe Konservierung dieses Prozesses hinweist. Der Vergleich der erhaltenen Daten mit der Literatur zeigte, dass dieser Mechanismus nicht nur in diesen beiden Homologen konserviert ist, sondern ähnlich auch im ebenfalls kationenselektiven eukaryotischen nAChR, wo ähnliche Mutationen untersucht wurden, gilt. Diese Resultate weisen darauf hin, dass die Liganden Aktivierung in der ganzen Familie nach ähnlichem Mechanismus erfolgt.

1 Introduction

1.1 Nerve cells

The core of the human nervous system consists of interconnected nerve cells. These specialized cells form a complex network throughout our body, which coordinates voluntary and involuntary movements and transmits signals between different parts of the body. These electrically excitable cells transmit information through chemical and electrical signals. Cells at the end of each axon nerve are in contact with neighboring cells in structures called synapses. These cells can be muscles or other nerve cells to which signals will be transmitted. Two different ways of signal transmission between nerve cells are known. In electrical synapses, the two adjacent cells are directly connected over a cannel forming gap-junction. Therefore, the electrical signal arriving at the cell end is directly transmitted to the adjacent cell, whereas in chemical synapses, no such direct junction exists. These cells are separated by an inter-synaptic cleft. This 20 nm wide gap cannot be directly crossed by the electrical signal.

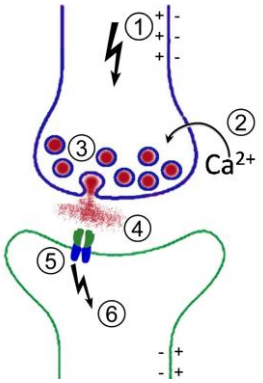

Figure 1: Signal transmission at chemical synapses. The signal is transduced by the following steps. 1) Electrical signal in form of a depolarization of the membrane. 2) Influx of calcium ions. 3) Fusion of synaptic vesicles with the presynaptic membrane. 4) Diffusion of neurotransmitter to the postsynaptic membrane. 5) Binding of the neurotransmitter and opening of an ion channel. 6) Newly generated electrical signal. (Picture taken from (*1*)).

The processes at chemical synapses involve several distinct steps (Figure 1). First the action potential of the presynaptic cells arrives at the end of the axon, causing a depolarization of the membrane. Voltage-activated calcium channels open in response, which, leads to the influx of Ca^{2+} into the cell. The increase in Ca^{2+} triggers the fusion of neurotransmitter containing synaptic vesicles with the presynaptic membrane. Upon fusion of these vesicles the neuron transmitters are released into the cleft and can then freely diffuse to the postsynaptic membrane.

On the postsynaptic membrane the neurotransmitters are recognized by specific integral membrane proteins (receptors). Upon binding of neurotransmitters these receptors undergo a conformational change which leads to an opening of a channel, thus allowing certain ions to flow along their electro-chemical gradient into the cell. Depending on the ion selectivity

of the channel this influx can lead to an excitatory or inhibitory signal which subsequently leads either to stimulation or suppression of electrical activity of the cell (*2*).

Many of the integral membrane proteins at the postsynaptic cell serving as receptors are ligand gated ion channels (LGIC). They are highly regulated by their specific neurotransmitter (ligand or agonist). The process of ligand binding and the induced conformational change (gating), which lead to the channel opening, is very fast, within the millisecond range. This timescale is crucial for fast signaling in the central nervous system and at neuromuscular junctions.
There are three major families of LGICs: the ionotropic glutamate receptors, the nucleotide gated ion channels and the pentameric ligand gated ion channels (pLGIC).

1.2 Pentameric Ligand Gated Ion Channels

The family of pentameric ligand gated ion channels consist of activatory members like acetylcholine (nAChR), serotonine (5-HT3R), and inhibitory receptors such as γ - amino-butyric acid Receptors ($GABA_AR$ and $GABA_CR$), glycine Receptors (GlyR) and invertebrate glutamate-gated chloride channels (GluCl) (*3-6*).
The electrical response, is dependent on the selectivity on these channels. The inhibitory channels are anion selective, thus their activation leads to a hyperpolarization of the cell, which in turn prevents further downstream signaling. The excitatory members, in contrast, the cation selective acetylcholine and serotonin receptors are key players in fast electrical signal transmission.
It is therefore not surprising that this protein family is involved in cognitive processes such as learning and memory. Since being part in these important processes dysfunction of these channels are associated with severe diseases such as epilepsy, Alzheimers disease and Schizophrenia (*7*).

1.3 Activation of pLGICs

Due to the importance and the pharmacological potential of pLGICs (*7*), they have been studied intensively for decades. It has been shown that pLGICs can be activated by a variety of chemical compounds, which are called ligands or agonists. Not all of the identified agonists play a role in the physiology of pLGICs, but they have served in the characterization of these channels, due to differences in the activation and deactivation properties.
Models used to describe the activation and deactivation process of an agonist on a receptor have been invented and refined over the years. These models are based on classical enzyme kinetics and try to link the experimental observation to the events on the molecular level. Initial experiments on pLGIC from *Torpedo electroplax* and Frog endplates showed that agonist binding to the channel does not follow the classical single-site binding mechanism. It rather showed a cooperative behavior of the channel exposed to its ligand. Due to this

fact it had to be assumed that the protein must contain several allosterically linked binding sites.

Further on Del Castillo and Katz realized that this classical model of cooperation does not explain all observed effects. It was seen that different ligands evoke different maximal responses on the same channel. Therefore, an even more complex model had to be derived, where these partial agonists were taken into account. In this Del Castillo – Katz model two states were postulated. Initially both the agonist **A** and its receptor **R** are in their free form. The first step is only the binding of **A** to **R** to from an **AR** complex. In this step only the binding affinity to the site is essential. Only in the second step the activation of the channel occurs. The opening of the channel leads to the formation of the **AR*** state, where the ***** on the **AR** indicates its activation. In this step a second equilibrium constant describes the ability of the bound ligand to trigger the opening of the channel. This property has been named efficacy. Using this model they could explain why some agonists, even at full occupancy, evoke a smaller response to the channel than others. The lower response could be simply explained by a smaller efficacy (*8*).

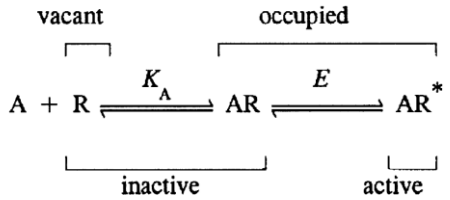

Figure 2: A schematic representation of the Del Castillo-Katz model of receptor activation. The vacant receptor binds the agonist to form an agonist-bound but inactive complex. This step only depends on the affinity of the agonist to the receptor. In the second step, the receptor undergoes a conformational change which leads to the active and conductive state. This transition is dependent on the efficacy *E*, a measure of the ability of the agonist to convert the receptor to its active state. (Adapted from (*8*)).

In a standard dose-response experiment the response of the channel to the exposure of different ligand concentrations is measured. The characteristic quantity obtained from this experiment is the EC_{50}, which describes the concentration of the ligand at half maximal evoked response. Generally this quantity is called the apparent affinity. The term apparent is used since the EC_{50} takes into account the real affinity and the efficacy of the ligand. The relationship between both constants is described in the equation below:

$$EC_{50} = \frac{K_D}{1 + E}$$

Therefore, mutations on the channel characterize by a 2EVC experiments only shows the contribution of both the affinity and efficacy (*9*).

Yet, this model did not fully explain the experiments on pLGIC. In an additional attempt, Monod, Wyman and Changeux (MWC) used the theory of cooperative enzymes. In the model, they proposed that the protein could coexist in an open and a closed state in the presence and absence of ligands (*10*). This model, like the Del Castillo – Katz model, takes into account a two-step model of agonist binding. But additionally it states that the receptor can also open when no ligand is bound and also considers binding of two agonists to the channel.

Experimentally, it was proven that the channel exists in an open state even in the absence of a ligand (*11, 12*). Despite the fact that population of this state is very low. This model not only explains the opening of a free receptor, but also takes into account the possibility of several agonists bound to the receptor and therefore describes its cooperative behavior.

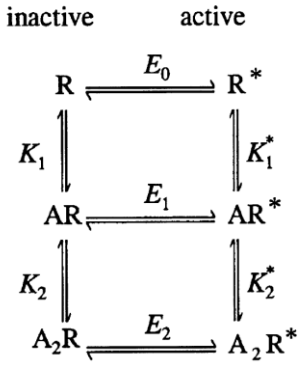

Figure 3: The schematic representation of the Monod-Wyman-Changeux (MWC) model of allosteric receptor activation. In this model, the receptor can adopt both the inactive and the active conformation in the presence or absence of agonist. The agonist can stabilize the active conformation and as a result, the efficacies increase from the unliganded to the bi-liganded state. This implies that the active conformation has a much higher affinity to the agonist than the inactive conformation, which can explain the cooperative behavior in the activation of pLGICs. (Adapted from (*10*)).

1.4 Desensitization

The prolonged exposure of the channel to its ligand leads to a progressive reduction of the response. This phenomenon is called desensitization and is abundant in pLGICs. The activation upon application of the agonist is thus only transient. If the agonist is applied for longer the response decreases. This reduction is due to the fact that the channel adopts a different closed, the desensitized, state. The recovery time from this state is a rather slow process and can only happen if the agonist is not present in the solution as the desensitized state has a much higher affinity to its ligand than the open or closed state (*13-17*). To explain this phenomenon one has to again take a different model into account. In this circular model the receptor can adopt three states: Resting (**AR**), Active (**AR***) and Desensitized (**D**) (Figure 4). In contrast to the transition from **AR** to **AR***, which requires high ligand concentrations, the transition from **AR** to **D** can occur already at much lower concentrations. Consequently **D** must have a much higher affinity (*13*).

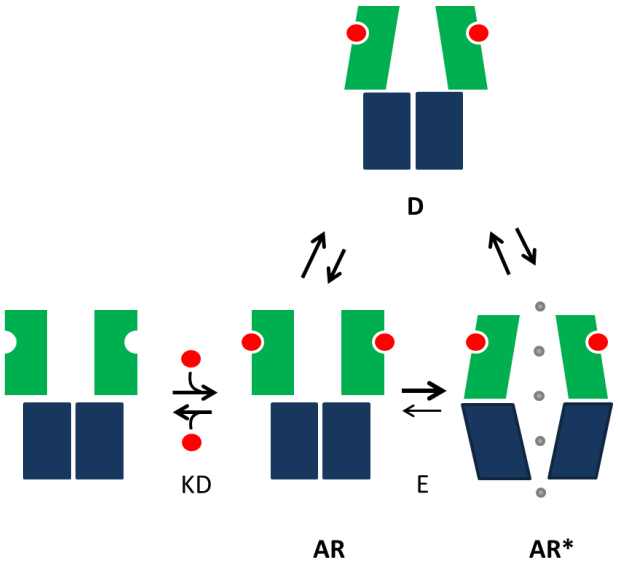

Figure 4: Schematic representation of the circular desensitization model. The first two steps (bottom) are identical to the Del Castillo-Katz model of receptor activation. The additional desensitized state (top) can either directly change into the ligand bound resting state or the activated open state (although with different rate constants).

Desensitization is a classical property of allosteric proteins. Experimental models showed that for allosteric proteins all states are populated at any time with different probabilities. Quantifications on nAChR for example showed that up to 1 % of the receptor is present in **D** in the absence of any ligand (*16*). Due to the high affinity of the **D** state to the agonist, the receptors can be quantitatively desensitized even by concentrations of agonist too low to activate the receptor. On the other hand, the estimated rate of dissociation of the agonist from the desensitized state is much faster than the rate of recovery and it is therefore assumed that the recovery from desensitization is independent of the agonist affinity (*14*). Desensitization is an intrinsic feature of almost all pLGICs. However, its physiological function is still ambiguous. In synapses, neurotransmitters are instantly reabsorbed or degraded and only present for several milliseconds, but the desensitization rates of most pLGICs are on the second time scale and thus much slower. Desensitization nevertheless could still accumulate during repetitive excitations of a synapse. The most common explanations are that desensitization is either a mechanism for the protection of the cells against excitotoxicity (*15*) or a mechanism to shape the short term plasticity of synapses (*18*).

1.5 Modulation of pLGICs

As pLGICs play an important role in the central nervous system, it is not surprising that they are also influenced by a variety of natural and artificial compounds. These modulating drugs either enhance or inhibit the receptor response in a process called positive or negative modulation. The way these modulators can interact with the receptor are diverse, nevertheless they can be grouped based on their interaction with the channel. (1) Open pore blockers are interacting with the pore region in the activated channel, (2) orthosteric ligands bind to the same location as the agonist and (3) modulators where the binding site and the effectory site are different from one another. The off-site modulators (3) will be discussed in detail in the appendix (8.1.1.2)

1.5.1 Open pore block

The inhibition of ion flow by the obstruction of the channel is called open pore block. Certain chemical compounds, frequently carrying a net charge corresponding to the ion selectivity of the channel, are attracted to the open pore, but are too big to pass the channel, which leads to a blockage of the ion flow (*19*).Electrophysiological and crosslinking experiments shed light in to the mechanism of open pore block (*20-22*). It was shown that open pore blocker bind in an uncooperative, voltage dependent way. The voltage dependence shows that these compounds have to pass part of the membrane potential to reach their binding site, which implies that the actual event of blockage has to be within the membrane. Additionally, many blockers can only block the channel from one side. Due to the fact that open channel blockers can only bind to the channel in a conductive conformation their binding leads to a stabilization of the open conformation and the channel can only close once the inhibitor diffuses off (*23-25*). This phenomenon has been described by Armstrong as the ‘‘foot-in-the-door’’ (*26, 27*).

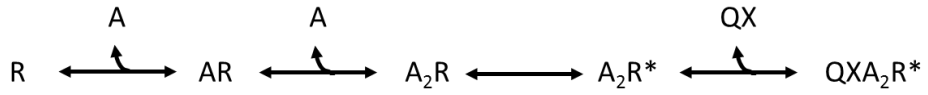

Figure 5: A schematic representation of the mode of of action of open channel blockers. Until the last step this model represents a simplified version of the Monod-Wyman-Changeux (MWC) model of activation. Therefore once the channel is activated (AR_2*) it can become blocked (i.e. by QX, a quaternary lidocaine derivative) and the binding of the drug then prevents the channel from closing (Adapted from (*19*)).

To measure the potency of inhibition of an open pore blocker a dose response experiment is performed. In this experiment the responses of the channel at a specific agonist concentration for different pore blocker concentrations are measured. These responses normalized to the current in the absence of inhibition are then plotted against the concentration of the inhibitor. The concentration which leads to half maximal inhibition is termed IC50. The IC50 is also called apparent affinity (similar to the EC_{50}) and can be used to compare the potencies of pore blockers at a certain membrane potential (*28*). It is apparent that the binding is strongly influenced by the membrane potential.

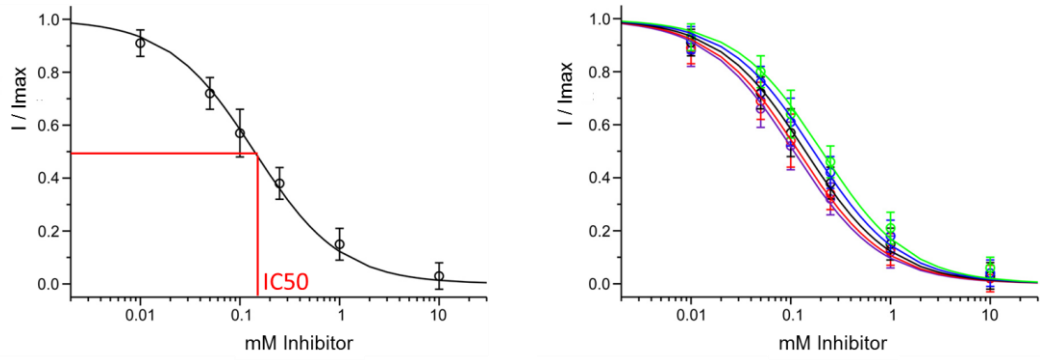

Figure 6: (left) Example of a dose response experiment at a specific holding potential (-80mV) for an open pore blocker. The response of the channel at a certain agonist concentration is measured at different open pore blocker concentrations and then fitted by a single-site binding isotherm. The concentration which leads to half maximal response is termed IC50 (apparent binding affinity) and can be used to compare the potency of different pore blockers at a certain holding potential. (right) The same dose response experiment as on the left at different holding potentials. Starting from a holding potential of -40mV (light green) to -120mV (violet). It clearly shows that the apparent affinity is higher at higher holding potentials.

For the cation-selective members of the pLGIC family structurally diverse molecules (i.e. quaternary ammoniums, local anesthetics and certain transition metal ions (*21*, *29*-*32*) have been found to exhibit such a behavior. The only common property is their positive charge, whereas they vary significantly in their size and hydrophobicity. These open pore blockers can be subdivided into two different classes: (1) the large and bulky monovalent and (2) the divalent transition metal ions.

While the first group (1) is site specific and can only block the channel from the extracellular side, for the second group (2) this is not the case. Divalent ions have been shown to directly interact with a conserved stretch of negatively charge residues at the pore end from both sides of the membrane (*33*). Thus these ions can modulate the channel from the intra- and extracellular side.
This tight interaction has already been proposed in the absence of structural data, since it has been observed that small divalent ions pass the pore, whereas larger transition metal ions lead to either a reduction or a complete disappearance of the currents. The reduction of the flow arises from a tighter interaction of divalent ions with the pore lining which in turn becomes rate limiting for ion flow. This feature indicates a close relationship between permeation and blockage for these divalent ions (*34*-*36*). Despite the wealth of information about open pore block the structural basis of this mechanism is still unclear.

1.5.2 Competitive inhibition

In contrast to the open pore blockers, which bind in the pore region, competitive inhibitors bind in the extracellular domain. They belong to the second group – the orthsteric ligands and compete with the actual ligand for the same binding site, but contrary to the ligand, they do not trigger any response upon binding. By exposing the receptor to a higher concentration of ligand the effect of the competitive inhibitor can be removed. Inhibition thus only depends on the binding affinities and concentration differences between the ligand and its competitor. Therefore, the inhibitor leads to a shift of the dose repose curve

to higher ligand concentration, but is not changing the shape or the maximal response of the curve (Figure 7). Competitive inhibitors are known for all member of the pLGIC family. They can be, either similar to their agonists or protein based as found for certain snake toxins. Well-known small molecule antagonists are DhβE and d-tubocuracine for nAChR, strychinnie for GlyRs, biculline for GABARs and morphine and methadone for the $5HT_3$Rs.

To determine the affinity of a competitive inhibitor, the agonist displacement in a dose response experiment can be quantified by a Schild plot (*37*, *38*).

$$\log(DR - 1) = \log[B] - pA_2$$

DR is the dose ratio, meaning the ratio of equiactive agonist concentrations in the absence and presence of inhibitor (e.g.$\frac{EC50'}{EC50}$), [B] is the concentration of the inhibitor and pA2 corresponds to the logarithm of the dissociation constant KB of the inhibitor. A plot of [B] against (DR-1) in a double logarithmic graph gives a linear relationship with a slope of unity and the intercept pA_2 which is the logarithm of the inhibitor concentration that is required to double the equiactive concentration of the agonist. This value corresponds to the dissociation constant of the inhibitor.

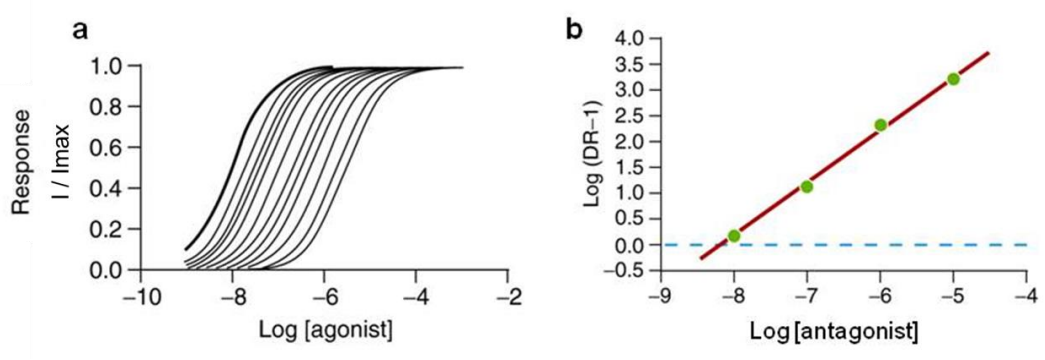

Figure 7: (a) Dose response curves of a receptor activated by its agonist at different concentrations of a competitive inhibitor. Due to the presence of the inhibitor, the curves shift to higher agonist concentrations. The data is transformed to the dose ratio at the corresponding antagonist concentrations and plotted in a Schild plot (b). The dissociation constant of the inhibitor can be deduced from the X-axis intercept. (Picture taken and text adapted from (*18*)).

1.6 Prokaryotic homologues

Initially all functional data on pLGICs was obtained from eukaryotic family members as prokaryotic members have not yet been identified.

With the abundance of genomic data, more and more prokaryotic species and their genes could be analyzed. These advances have led in 2005 to the first identification of prokaryotic homologues by Tasneem and coworkers (*39*). Despite the very low sequence identity, which is below 30%, the key residues of the family are conserved. This was in a way

surprising, since it was thought that pLGICs were only abundant in the tree of higher organisms, which have a central nerve system.
The first characterization of such a prokaryotic pLGIC (GLIC) from the bacterium *Gloeobacter violaceus* was published in 2007 by Boquet and colleagues (*40*). They identified GLIC as a homopentameric pH gated cation selective channel and confirmed the pentameric structure by electron microscopy and unspecific crosslinking.

1.7 Structural information

Whereas the organization of pLGICs was revealed from electron microscopy high resolution structures of pLGICs became available only recently. This started in 2001 when Brejc and colleagues (*41*) determined the structure of the acetylcholine binding protein (AChBP) of the mollusk *Lymnaea stagnalis*. Sequence alignment underlines its conservation to the extra cellular domain of the nAChR. This high resolution (2.7 Å) X-Ray structure gave detailed insight into the ligand binding pocket and it revealed the relation between key residues for the interaction with ligands and competitive inhibitors.
It took some time until the first full length pLGIC became available at high resolution. The first EM structures on the nicotinic receptor from the electric organ of *torpedo* (*42-44*) shed light into the architecture of the protein. Despite the comparably low resolution, this pioneer work significantly contributed to understanding of ion selectivity and the gating mechanism (*45-47*).
Due to bottlenecks in the production of eukaryotic membrane proteins and since the receptors purified from its natural source did not allow the growth of diffracting crystals, structural studies of this family initially failed. However, with the identification of prokaryotic homologues has allowed to overcome this bottleneck (*48*). Thus only few years after prokaryotic homologues were identified, the first high resolution structures of such proteins were determined (*33, 49, 50*). These high resolution structures allowed detailed interpretations of functional properties of the channels. The first X-Ray structures for cation selective pLGICs came from two prokaryotic organisms. The first structure was from *Eriwinia chrysanthemi* (ELIC). This ligand activated channel was crystallized in the absence of its ligand in a non – conductive state. The second structure from *Gloeobactoer violaceus*, a pH activated channel, was solved in a potential open, conductive, conformation.
Only in 2011 did the first eukaryotic member of the family become available. The protein from *Caenirhabditis elegans* was the first anion selective member of the family. It shed light on anion selectivity, ligand binding and allosteric modulation (*6*).

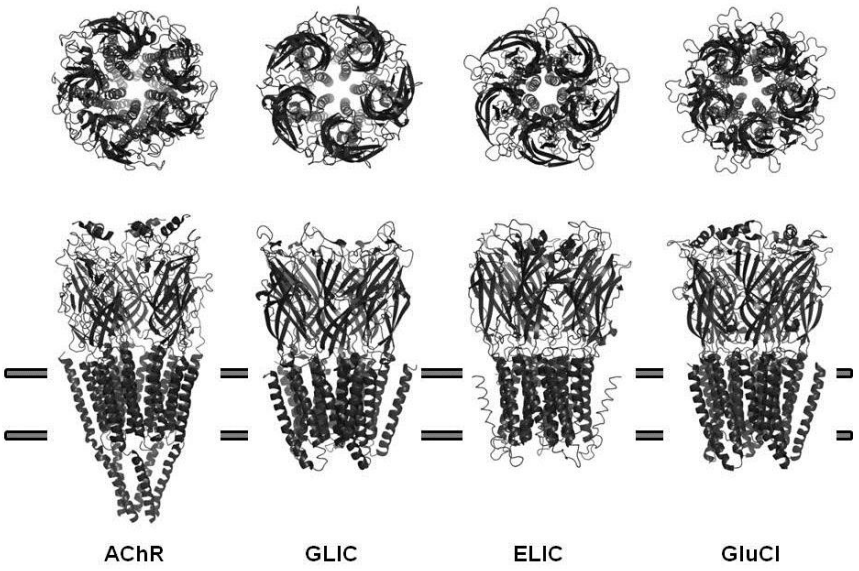

Figure 8: Top and side view of the available structures of pLGICs. The membrane is indicated as grey bars. A comparison of the cartoon representations of the secondary structure elements reveals the strong structural conservation within the family. Each of the five protomers is formed by an extracellular domain which consists of two β-sheets and a transmembrane domain of four α-helices. The residues of the second transmembrane helix line the pore which spans the membrane along the symmetry axis of the pentamer. (Picture and text taken from (*18*))

Despite the very low sequence identity between homologues, their structural conservation is striking (Figure 8). Whether pLGICs are inhibitory or excitatory, they all share the same overall architecture. The Receptor is formed by five subunits, which are either identical or very homologous. Each subunit consists of an extracellular cellular and a membrane spanning domain. The extracellular ligand binding domain is an open water-filled chamber that provides access to the channel forming pore of the transmembrane domain.

1.7.1 The extracellular domain

The extracellular domain resembles a cylindrical tube. Its height is 60 Å and its diameter is 80 Å. The open aqueous chamber in the middle of the pentamer is 20 Å wide (Figure 9).
The extracellular part of the protein resembles a turbine, with five blades along its symmetry axis. Each subunit is enclosed by two neighbors, with a buried surface of around 2500 $Å^2$. A subunit consists of 10 β - strands forming a β - sandwich of two sheets with an immonuglobin like fold.
The ligand binding site is formed at the subunit interface as shown in Figure 9.

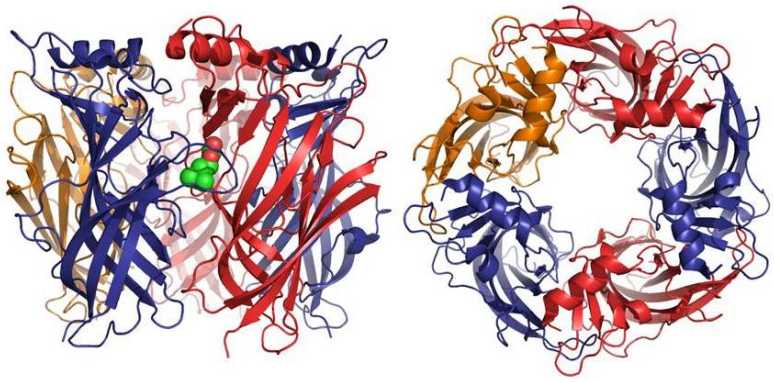

Figure 9: The structure of the acetylcholine binding protein of *T. Californica* representing the extracellular domain of the nAChR with the typical pentameric assembly of the pLGIC family. (left) The side view shows the ligand binding site, indicated by the bound agonist carbachol. It is located in the large interface between the principal (blue) and the complementary (red) subunit. (right) The top view along the fivefold axis depicts the windmill-like structure of the pentamer formed by five subunits, which resembles a turbine. It encloses a large vestibule in the center of the pentamer, which gives access to the pore in the full receptor. (Picture taken from (*18*)).

1.7.2 The pore

Adjacent to the extracellular domain is the membrane spanning pore domain. Only the first full-length structures (*6, 33, 42, 44, 49, 50*) did show a clear picture of how the pore is constructed.

The four helical segments per subunit are arranged around a five-fold axis of symmetry, forming an inner ring of α helices (α2), which line the pore, and an outer shell of α helices (α1, α3 and α4), which surround the inner ring and shield it from lipids (Figure 10).

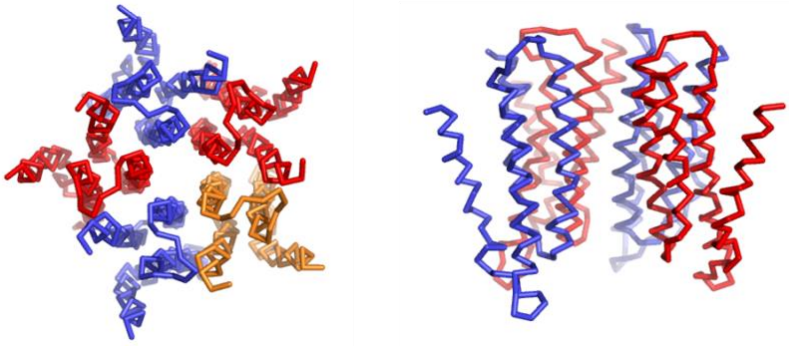

Figure 10: The structure of the transmembrane region of ELIC (ribbon representation) illustrates the typical pentameric assembly of the pLGIC family. (left) The top view shows the pore formed by the α2 of each subunit. (right) side view perpendicular to the pore axis. One subunit has been removed for clarity. This view as well shows that the pore is formed by the membrane spanning α2. α1 and α3 are at the subunit interface while α4 is loosely attached.

The pore facing residues form a distinct pattern of residues with physico-chemical properties that are conserved for the cation selective members of the family (top Figure 11). It is lined by three consecutive rings of hydrophobic residues, followed by two rings of polar residues and a negatively charged ring.

The first high resolution structure (ELIC) was crystallized in the absence of its agonist in a non-conductive conformation. There, the α2 helices are arranged almost parallel to each other in the membrane. In ELIC the first pore lining amino acid at the constriction is a ring of phenylalanines. This aromatic residue occludes the pore (*51*). The phenylalanine ring is followed by two additional rings of hydrophobic residues, none of which is water accessible. In the other prokaryotic homologue, GLIC, the pore shows a potential open conformation. There the α2 helices are bent in a slight angle with regard to one another, thus forming a funnel shaped, water accessible, pore. In this structure the hydrophobic residues of the first ring have moved apart and are no longer occluding the pore. At the intracellular end of the α2 helix, the negatively charged residues have moved closer to from a selectivity filter (Figure 11).

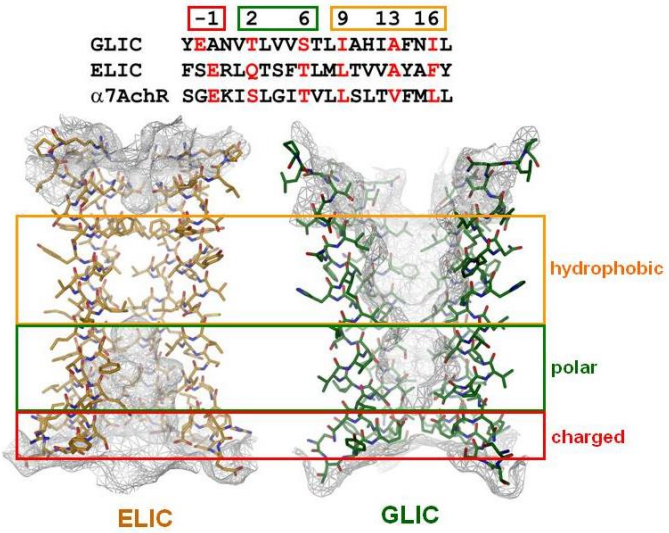

Figure 11: (top) Sequence alignment of the pore forming α2 helix of GLIC, ELIC and nAChR. The pore lining residues are conserved and form six rings with distinct chemical properties. The three hydrophobic rings on the extracellular side constitute the gate, whereas the inner two polar and the intracellular charged ring form a selectivity filter. (bottom) Comparison of the pore structures of ELIC and GLIC showing two conformational states. ELIC is in a non-conductive state, in which the hydrophobic rings obstruct the pore. The GLIC pore is in the open conformation, where the hydrophobic rings separated from each other to open the gate whereas the polar and charged rings contracted to form a selectivity filter (Adapted from (*52*)).

Due to the high degree of structural conservation between known structures (prokaryotic and eukaryotic) (*53*), it is quite likely that the underlying mechanism for gating is conserved (*5*). This emphasizes the potential of the prokaryotic homologues to serve as a model for the complex and diverse family.

1.7.3 Ion selectivity

The structures of pLGICs have provided structural insight into the ion selectivity of the family.

The main determinants of ion selectivity in an ion channel are frequently found at the narrowest part of the channel. This constriction can limit the size of the ions which can still permeate the channel (see also “Open pore block” 1.5.1), whereas the pore lining residues

and their chemical interaction to the solvent can discriminate different ions and influence the solvent permeation (*53*). The hydrophilic or charged amino acids in the pore reduce the energetic barrier of the hydrophobic membrane and thus allow ion flux through the channel across the membrane (*54*). The combination of the steric features and the polar and charged residues make an ion channel capable to discriminate between different ions.
In pLGICs the pore region is not the only site for the ion selectivity. The vestibule of extracellular domain is as well narrow enough (~20 Å wide) to ensure that charged groups lining their surfaces would interact electrostatically with the permeating ions. Nevertheless these vestibules are wide enough not to directly interact, which could slow the movement of the ions, as it has seen in the pore region for certain divalent ions (*55, 56*).
At a closer look on the surface potential of the known cation selective channels, it is apparent that the extracellular and the intracellular vestibules are almost entirely negatively charged (Figure 12). The resulting cation-stabilizing environment would increase the concentration of cations relative to that of anions at both entrances of the narrow membrane pore, and in that way promote bidirectional transport of cations through the open channel. It is therefore likely that the vestibules contribute significantly to the charge selectivity of the channel, and that the "selectivity filter" at the end of the pore is not the only region for ion selectivity (*57*).

The pLGIC are not selective for a certain kind of ion. Their selectivity is mainly based on the charge of the ion. Therefore barely any discrimination exists between different monovalent ions and even divalent ions and bigger organic cations were shown to permeate certain channels. A similar behavior has been also seen for the anion selective part of the family. Due to this rather poor selectivity, these channels are termed charge selective.

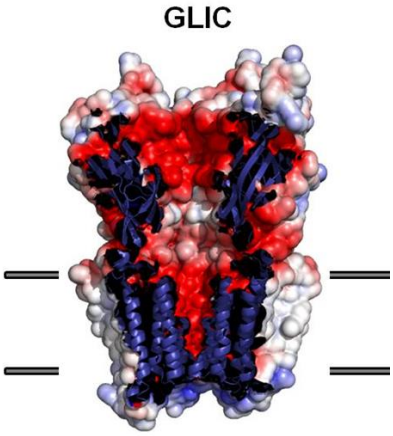

Figure 12: The calculated surface potential of the cation selective GLIC is shown (negative potential red and positive potential blue). The figure highlights the role of the electrostatic potential on the underlying mechanism of the charge selectivity of pLGICs. They create an attractive environment for the conducted ions and an insurmountable barrier for their counter ions. (Picture and text adapted and taken from (*18*)).

1.8 Ligand recognition and conformational changes in the extracellular domain

To form an ion selective pore the channel first needs to be activated by its ligand. For cation selective pLGICs, the mode of ligand binding to the ligand binding pocket is very similar (*58*). The pocket is located in the extracellular domain at the interface between two adjacent subunits, called the principal and complementary site (Figure 9).
The ligand binding domain itself can exist in various conformations with different affinities for the ligand. As previously discussed in the so called resting sate, the affinity to the ligand is low. However after the opening of the channel, which induces underlying conformational changes, the ligand binding affinity increases. After a longer exposer of the ligand to the channel enters the desensitized state. In this state, the ligand has an up to 1000 fold higher affinity than in the open state. These different affinities indicate the existence of at least three different states with potentially unique conformations of the ligand binding domain.
The induced conformational changes upon ligand binding were extensively investigated using the AChBP. The protein was crystallized with several agonists and antagonists (*59*). The biggest structural changes in the structure were seen in the C loop. The tip of this loop does in the apo state only loosely interact with the rest of the protein. Upon binding of the ligand this loop closes the ligand binding pocket (Figure 13). This closing is called the C – loop capping. In contrast to the agonist the binding of the antagonist leads to a further opening of the C – loop (red conformation in Figure 13).

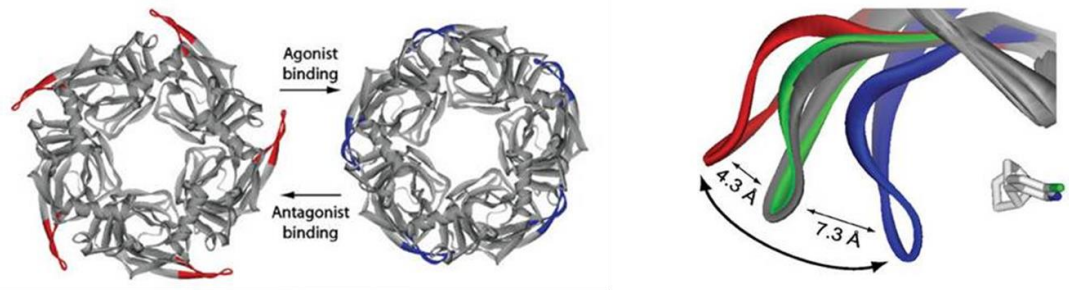

Figure 13: Mechanism of C-loop capping derived from structures of the AChBP, crystallized in the apo-, agonist- and antagonist bound state. The C-loop experiences a contraction from the apo structure (in green) to the agonist bound structure (in blue). This conformational change is believed to be the first step in the activation process of pLGICs. Antagonists on the other hand were found to push the C-loop outwards, corresponding to the observed difference between the apo structure (in green) and the antagonist bound structure (in red). Competitive inhibitors are therefore believed to inhibit receptor activation by preventing the C-loop capping. (Adapted from (*59*))

The use of the AChBP to serve as a model for the activation of the receptor is limited since ligand binding is not cooperative as it is for pLGICs. Nevertheless a functional chimera of the AChBP with the $5HT_3$ receptors transmembrane part could be produced (*60*). This chimera shows that the AChBP can serve as functional part of a full length receptor. Remarkably as part of a full receptor it also shows the observed cooperative behavior of the family.

With the structures of the first full-length receptors in two different states (a conductive in GLIC and a non-conductive in ELIC), it was shown that the C – capping was conserved in these cases (*5, 33, 49, 50*). The structures also indicated potential changes in the extracellular domain upon ligand binding. Differences were observed in the F – loop and in the β1 – β2 turn at the interface of the extracellular domain to the pore domain. The best way to describe the differences in the extracellular domian between GLIC and ELIC is a 12º rotation around an axis parallel to the two β sheets of the extra cellular domain (Figure 14).

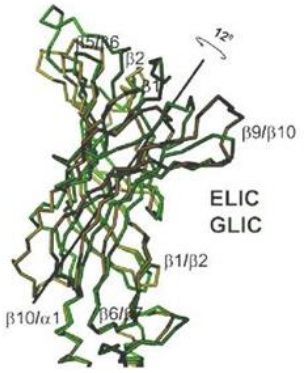

Figure 14: Conformational differences between the structures of ELIC and GLIC. The extracellular domain is rotated along an axis between the β-sheets (adapted from (*5*)).

1.9 From binding to opening - Gating

Despite the insight gained form the structures of AChBP one very important question still remained unclear: How are the ligand binding and the pore opening connected? These two events must be directly linked despite the several nanometer distances between the locations.

The AChBP shows no structural differences upon ligand binding in the area, which would form the interface to the pore domain in intact receptors. An interesting feature of the extracellular domain in the known chimeras is that these won't work unless the extracellular loop β1 – β2 is exchanged with the corresponding loop of the homologue which forms the pore domain (*60, 61*). This indicates, that this specific loop interaction between the α2 – α3 pore loop to the β1 – β2 turn is crucial for pore opening.

The full length receptor structures offered insight into the potential structural rearrangements during activation, since they show two different states, a conductive channel for GLIC and a non-conductive channel for ELIC. The most obvious change at the interface of the pore and the extracellular domain are observed in the β1 – β2 turn of the extracellular domain and the α2 - α3 loop of the pore. In GLIC, these two loops are in direct contact with one another. A lysine at the tip of the β1 – β2 turn interacts directly with a conserved proline of the α2 – α3 loop. In ELIC these residues are approximately 7 Å apart from each other (Figure 15, left). This β1 – β2 turn in GLIC is stabilized by a conserved bridge salt-bridge (Figure 15, right middle). In ELIC this salt-bridge is absent and the

conserved negatively charged residue, which forms this interaction in GLIC, is a polar threonine. This disruption of the salt bridge might be the cause of this big difference of the loop position. The importance of this conserved salt bridge for gating has previously been described as part of the 'principal pathway of gating' by Sine and colleagues (*45*). In the nAChR and in GLIC this salt bridge is formed by a conserved aspartate residue of the cys–loop and an equally conserved arginine of the β10 - α1 linker.

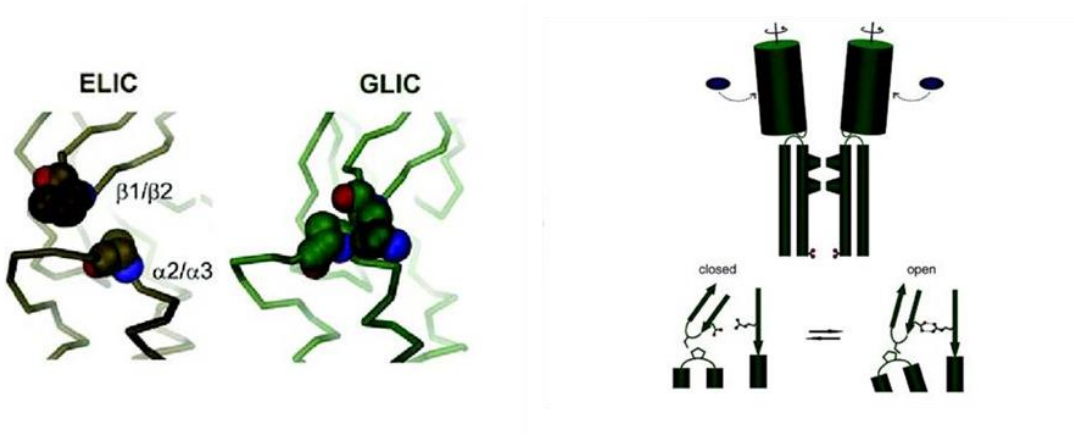

Figure 15: Differences between the ELIC and the GLIC structures in the coupling interface of the extracellular and the transmembrane domain. The interaction of the residue at the tip of the β1 - β2 turn with the α2 - α3 loop is believed to couple the movement of the domains. The schematic representation depicts the interactions in the principal pathway of coupling where the signal of agonist binding is transmitted to the α2 - α3 loop via the β1 - β2 turn which is additionally stabilized by a hydrogen bond to the pre α1 region. (adapted from (*5*))

The comparison of the ELIC and GLIC structures shows that the conformation of the cys-loop in both prokaryotic homologues is similar. Therefore the importance of this highly conserved motif and its role in the gating cycle remains unclear (*5*). Remarkably, mutations within this loop in other receptors have shown a significant alteration in the activation pattern thus underlining its involvement in gating (*46*). One residue of the cys-loop, which is slightly above the interface of the pore and the extracellular domain, is part in the previously mentioned conserved salt bridge of the 'principal pathway of gating' (*45*). This indicated that at least the location of the cys-loop must be important for activation. In further studies it has then been proposed that this pathway contributes jointly together with another pathway, the 'cys-loop pathway' in the transducing of agonist binding to the gating of the nAChR channels (*46*). The 'cys-loop pathway' contains residues, which form a hydrophobic core between the cys-loop, the β10 - α1 linker and the α2 – α3 loop (Figure 16). Mutations of these residues show significant reduced channel activity (*46*).

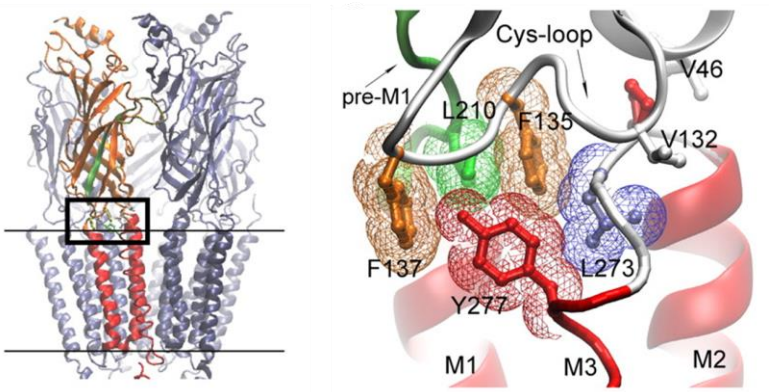

Figure 16: Cryo-electron microscopic structure of the Torpedo nAChR (PDB code 2bg9). [left] The pentameric nAChR in the membrane (parallel black lines) is shown with one of the α-subunits highlighted; β-strands are orange and α-helices red. β-Strand 10 preceding transmembrane domain α1 region is green. The boxed region is the junction of extracellular and pore domains, shown at higher magnification on the right. [right] Residues from three converging regions of the α-subunit (Cys-loop, β10-α1 linker, α2–α3 loop) which are important in the 'cys-loop pathway' are shown in stick representation overlaid with colored van der Waals surfaces. (Taken from (*46*))

The full length receptor structures also offered insight into the potential structural rearrangements of the pore domain. In ELIC this pore is occluded and not permeable to ions, while in GLIC the pore shows a funnel shaped water accessible cavity (Figure 11 and Figure 17, left) that would allow ions to flow through the membrane. The biggest differences in this region between these two structures (Figure 17, left) are found in the helices α2 and α3. Based on these structural differences a rotation of the α2 and α3 helices of around 12º along an axis in the pore region perpendicular to the pore axis was proposed as potential mechanism for pore opening. This movement would separate the three hydrophobic rings, which occlude the pore in the non – conductive state. While at the intracellular region of the pore the polar and charged rings are getting closer, thus allowing the formation of a polar constriction, that allows desolvated ions to permeate the pore (*5*). In contrast to this model crosslinking experiments in GLIC show a different conformational change in the pore domain as potential mechanism for channel closing (Figure 17, right). In these experiments a local unwinding on the extracellular end of the pore forming helix α2 was observed while helix α3 remained unchanged (Figure 17, right (*62*)). In this model the polar constriction and the 'selectivity filter' have similar conformations also in the closed conformation thus suggesting that the structure of ELIC does neither describe a resting nor an activated conformation.

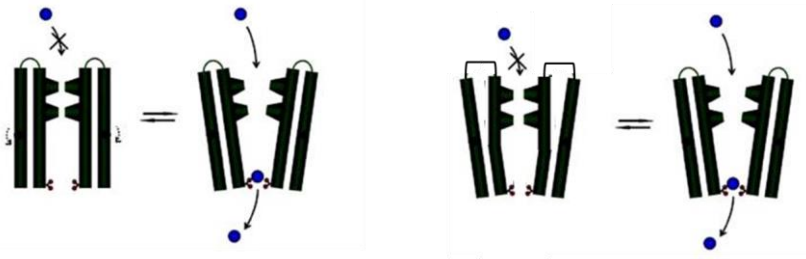

Figure 17: Comparison of the two proposed mechanism of pore opening. On the left is the mechanism based on the two different prokaryotic structures ELIC and GLIC. The helix α2 and α3 undergo a combined rotation around an axis perpendicular of the pore axis. On the right is the mechanism based on crosslinking experiments. In this mechanism does the α2 helix collapse and thus occlude the pore, while the α3 remains unchanged (Adapted from (*5, 62, 63*)).

Although there are several potential scenarios for the processes underlying ligand binding to the pore opening, in all cases the interface region between the extracellular and the transmembrane must couple these different events. In summary, studies have identified interactions of the β1 – β2 turn and the cys-loop to the α2 – α3 loop, the linker of the β10 - α1 as the main element for the coupling (*45*, *64*, *65*). The location of the residues between the extracellular and pore domains and their sequence conservation suggest that they form a functionally coupled network that contributes to the rapid and efficient channel gating characteristic of the nAChR (*46, 66*). Despite the wealth of functional data and due to the problem of assigning the available structures to a state within the activation cycle it was still unclear which network of interactions lead to the activation of the channel. Therefore questions concerning the gating mechanism still remain to be answered.

1.10 Aim of Thesis

Detailed models for pLGICs function were developed over the last few decades. In combination with the recent high-resolution structures of the prokaryotic homologues ELIC and GLIC and the eukaryotic protein GluCl these studies have led to a deeper understanding of structure-function relationships. However, despite all efforts of combining structural and functional data, the detailed mechanistic understanding of channel activation is still not fully understood. Currently all available structures and model systems to study the mechanism of gating have their drawbacks. Firstly, there is currently no model protein whose structure has been determined at high resolution in more than one state. Therefore the different states seen in the structures could arise from distinct properties of each particular channel.
The homologue GLIC is not activated by a ligand, but by the protonation state of the channel itself. Such mechanism has never been seen in any other family member. GluCl, on the other hand, is a truncated version of a homopentamer that is only partially activated by the addition of its ligand. For full activation ivermectin, an allosteric enhancer molecule, has to be added. Such a behavior is not seen in the naturally abundant GluCl channels. Therefore, the use of GluCl as a model system for functional studies is limited. In contrast, ELIC has promising properties required for a model system. It is activated by a variety of small molecules and is desensitized by prolonged application of its ligand. The major drawback of this model, however, is the fact that the structure shows an inactive, non-conductive conformation, which so far could not be assigned to a specific state in the activation cycle and despite different approaches, no other conformation could be determined.

The first aim of this thesis was to investigate whether known open pore blockers of cation selective nAChRs act in a similar way on the prokaryotic homologue GLIC. As part of the study I wanted to use the potential conductive state of the crystal structure of GLIC to visualize this pore block for the first time in the family. The combination of electrophysiological and structural data should also confirm that the GLIC structure is indeed an open, conductive, conformation of the channel.
In a second study, I aimed to investigate which residues of the interface between the extracellular and the pore domain are important in the gating mechanism of the two prokaryotic homologues ELIC and GLIC and then relate these findings with the published data available for the family to gain a deeper understanding of the activation mechanism.

2 Results

2.1 Pore Block

The pharmacology of pLGICs has been characterized for decades with a variety of chemical compounds. A well-studied group of compounds are ‘open channel blockers’. The charged pore blockers are attracted into the channel region by their positive net charge. However, due to their bulky size, they cannot pass the pore and therefore block the open channel. This leads to a reduction or elimination of the overall measured current flow since some or all pores are occluded and ions cannot pass the membrane along their electrochemical gradient. Open pore blockers are pharmacologically interesting and were also used to gain information about pLGICs. In a combination of electrophysiological recording and the use of the substituted cysteine accessibility (SCAM) method the general mechanism of open channel block could be studied for the nAChR. With the first high-resolution structure of a, potential, conductive state structural studies of complexes with these modulating compounds came within reach. The prokaryotic homologue GLIC was identified as a pH activated member of the pLGIC family. Its crystal structure showed a potential conductive conformation, which made it a perfect system to study channel blockers for the first time on a structural level and by electrophysiology and thus gain insight to which degree the conductive state seen in the structure agrees with the experiments found in the lipid environment. The following publication describes the work on open channel block in GLIC that reveals for the first time the detailed structural basis of this mechanism for the family.

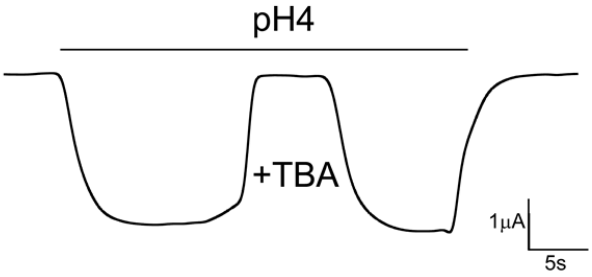

Figure 18: Open channel block. 2EVC recording of a GLIC-RNA injected *Xenopus Laevis* oocyte at a holding potential of -50mV. The figure shows the opening of GLIC at pH 4 followed by its reversible inhibition by 10 mM TBA^+ (tetrabutylammonium).

nature structural & molecular biology

Structural basis of open channel block in a prokaryotic pentameric ligand-gated ion channel

Ricarda J C Hilf[1,3,4], Carlo Bertozzi[1,4], Iwan Zimmermann[1], Alwin Reiter[2], Dirk Trauner[2] & Raimund Dutzler[1]

The flow of ions through cation-selective members of the pentameric ligand-gated ion channel family is inhibited by a structurally diverse class of molecules that bind to the transmembrane pore in the open state of the protein. To obtain insight into the mechanism of channel block, we have investigated the binding of positively charged inhibitors to the open channel of the bacterial homolog GLIC by using X-ray crystallography and electrophysiology. Our studies reveal the location of two regions for interactions, with larger blockers binding in the center of the membrane and divalent transition metal ions binding to the narrow intracellular pore entry. The results provide a structural foundation for understanding the interactions of the channel with inhibitors that is relevant for the entire family.

Open channel blockers occlude the narrow aqueous pore of an ion channel and in that way interfere with conduction[1]. They often carry the corresponding net charge of the permeating ions but are usually too bulky to pass the channel constriction that contains selective ion-binding sites. The cation-selective members of the pentameric ligand-gated ion channel (pLGIC) family are inhibited by structurally diverse molecules such as tetraethylammonium, local anesthetics and certain transition metal ions[2–4]. Although these compounds vary in size and hydrophobicity, they are all positively charged. The interactions between pore blockers and different nicotinic acetylcholine receptor (nAChR) subtypes have been investigated in detail by electrophysiology and chemical cross-linking, which has provided insight into the general mechanism of channel block[5–9]. The molecules inhibit the nicotinic receptor in the open state[10]. Large pore blockers enter the channel from the extracellular side and bind to a site in the narrow transmembrane pore that is located partly within the transmembrane field[8]. Whereas small divalent ions are generally permeant, larger divalent transition metal ions inhibit conduction, thus indicating a close relationship between permeation and block[11–13]. Still, despite the wealth of functional data, which has allowed the identification of single residues of the pore lining involved in the interaction with the blocking molecules, the structural basis for open channel block is currently unclear.

The X-ray structures of two prokaryotic pLGICs have recently revealed a first view of the family at high resolution, with one structure, from a protein of the cyanobacterium *Gloeobacter violaceous* (GLIC), showing an open conformation of the channel[14–17]. GLIC is activated by an increase of the proton concentration on the extracellular side[18]. The protein is cation selective; it also allows the permeation of different mono- and divalent ions and in that way resembles the nAChR[18]. Similar permeation characteristics are also reflected in the conservation of the pore between the proteins[15] (**Supplementary Fig. 1a**). GLIC is a homopentamer and consists of an extracellular ligand-binding domain that encloses a wide aqueous vestibule and a transmembrane domain that forms a narrow channel (**Fig. 1**). The latter is formed by four membrane-spanning helices, one of which, the second helix α2 (or M2), contributes to the pore lining. Because of the pentameric symmetry of the protein, the side chains of solvent-exposed residues form rings with distinct physicochemical properties (**Fig. 1**). Whereas the extracellular half of the pore is lined by three rings of hydrophobic residues, the cytoplasmic half is hydrophilic; it consists of two rings of polar residues followed by a ring of negatively charged glutamates at the intracellular membrane boundary that have been shown to play an important role in conduction and selectivity in the nAChR[19,20]. The pore is funnel shaped with a large diameter on the hydrophobic extracellular side that narrows toward the cytoplasm. The extracellular pore entry is filled with water and thus provides sufficient space to accommodate solvated ions. The residues at the narrow intracellular part, in contrast, provide a hydrophilic and negatively charged environment that interacts with ions that have shed a large part of their hydration shell. Ions were localized in this region at different sites: divalent Zn^{2+} ions were found at the intracellular pore entry, and Cs^{+} ions were located at a site within the pore, coordinated by threonine side chains that constitute the inner of the two polar rings[16] (**Fig. 1**).

Besides the similar selectivity properties, GLIC also shares with its eukaryotic counterparts the sensitivity to blockers such as quaternary ammonium compounds, and derivatives of lidocaine and quinacrine, and thus provides an ideal system to study the mechanism of open channel block in pLGICs. Here we investigated the binding of positively charged inhibitors to the open channel of GLIC. We determined the crystal structures of the channel in complex with different compounds and used

[1]Department of Biochemistry, University of Zürich, Zürich, Switzerland. [2]Department of Chemistry, University of Munich, Munich, Germany. [3]Present address: Vollum Institute, Oregon Health and Science University, Portland, Oregon, USA. [4]These authors contributed equally to this work. Correspondence should be addressed to R.D. (dutzler@bioc.uzh.ch).

Received 15 May; accepted 7 September; published online 31 October 2010; doi:10.1038/nsmb.1933

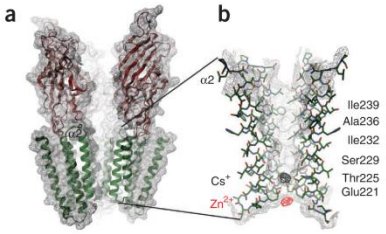

Figure 1 GLIC structure. (**a**) Ribbon representation of GLIC viewed from within the membrane with the extracellular solution above. The extracellular domain and the pore are colored in red and green respectively. The molecular surface is shown as gray mesh. The front subunit is removed for clarity. (**b**) View of the α2 helices of GLIC defining the pore region. The front subunit is removed for clarity. The molecular surface is shown as gray mesh. The anomalous difference densities of Cs^+ (black, calculated at 4.0 Å and contoured at 6 σ) and Zn^{2+} (red, calculated at 4.0 Å and contoured at 4.5 σ) are shown. The position of residues of the pore lining is indicated. Structures in **Figures 1**–**4** were prepared with DINO (http://www.dino3d.org/).

electrophysiology to investigate the energetics of the interaction. Our studies reveal the location of two regions for interactions, with larger molecules binding in the center of the membrane and divalent transition metal ions binding to the narrow intracellular pore entry.

RESULTS

Channel block by quaternary ammonium compounds

To gain insight into the mechanisms of open channel block, we expressed GLIC in *Xenopus laevis* oocytes and studied its activation and inhibition by two-electrode voltage clamp recording. One to two days after the injection of mRNA, GLIC mediates robust and non-desensitizing currents upon acidification of the extracellular medium with a midpoint of activation at pH 4.8 (**Supplementary Fig. 1b**,**c**). In its open state, the channel is reversibly inhibited by quaternary ammonium compounds added to the extracellular side, whereas their addition to the intracellular side does not show any effect on conduction (**Supplementary Fig. 2a**,**b**). The block is slightly dependent on the external pH, with an apparent affinity that is stronger at pH 4, where the open probability is close to one, than at higher pH values (**Supplementary Table 1** and **Supplementary Fig. 2c**). For all quaternary ammonium molecules, the inhibition is well described by a single-site binding isotherm (**Fig. 2a**,**b**). The binding affinity is dependent on the size of the blocker, thus indicating that hydrophobic interactions make an important contribution to binding (**Supplementary Table 1** and **Supplementary Fig. 2c**).

As expected for an open pore blocker, the binding of quaternary ammonium compounds is stronger at negative voltages[1]. By quantifying the voltage dependence of block using the Woodhull equation, it is possible to estimate the fraction of the field that the blocker has to cross to reach its binding site[21]. For tetrabutylammonium (TBA) and tetraethylammonium (TEA), this number

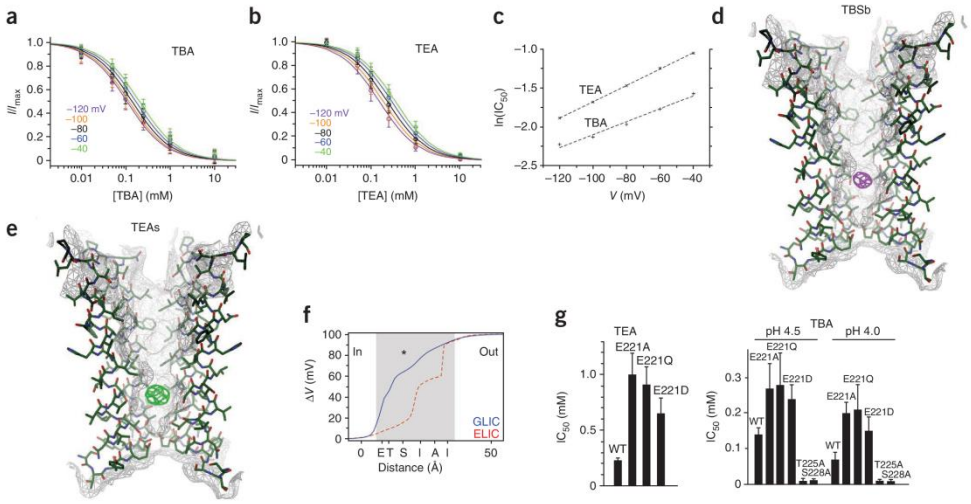

Figure 2 Inhibition of GLIC by quaternary ammonium compounds. (**a**,**b**) Dose-response curves of TBA (**a**) and TEA (**b**) block recorded from GLIC expressed in *X. laevis* oocytes by two-electrode voltage clamp at an extracellular pH of 4.5. The averages of data from 22 (for TBA) and 12 (for TEA) oocytes and their s.d. are shown. Measurements at different membrane potentials (ranging from −120 to −40 mV in 20-mV steps) are colored as indicated with a fit to a single-site binding isotherm shown in the same color. (**c**) Voltage dependence of TEA and TBA block, suggesting that TBA and TEA cross 20% ($z\delta = 0.2$) and 24% ($z\delta = 0.24$) of the electric field, respectively, to reach their binding sites. (**d**,**e**) Structure of the pore region of GLIC in complex with TBSb (**d**) and TEAs (**e**). The anomalous difference electron densities (calculated at 4.0 Å and contoured at 4.5 and 6 σ for TBSb and TEAs, respectively) are shown as mesh. (**f**) Falloff of the transmembrane potential over the pores of GLIC (blue) and ELIC (red, dashed). The membrane region is indicated (gray), and the Cα positions of residues of the pore lining are labeled. * indicates the center of the bound TBSb molecule. (**g**) Influence of pore mutations on TEA and TBA binding. The average IC_{50} values at −80 mV and their s.d. for WT and pore mutants are shown. TEA block (left) was measured from at least ten oocytes at pH 4.5, TBA block (right) from at least six oocytes at pH 4.5 and pH 4.0.

Table 1 Data collection and refinement statistics

	WT–$Cd2^+$	WT–TEAs	WT–$Zn2^+$	WT–TBSb	WT–TMAs	WT–Br-lido	E221D–TEAs	WT–Cs^+	E221A–$Zn2^+$
Data collection									
Space group	*C2*	*C2*	*C2*	*C2*	*C2*	*C2*	*C2*	*C2*	*C2*
Cell dimensions									
a, *b*, *c* (Å)	182.0, 129.0, 163.2	180.1, 133.3, 161.1	179.1, 131.8, 160.2	177.6, 133.0, 160.0	178.5, 134.3, 160.3	181.9, 133.9, 162.5	180.0, 133.3, 161.4	181.3, 133.6, 162.3	180.5, 132.7, 161.2
α, β, γ (°)	90.0, 103.4, 90.0	90.0, 102.1, 90.0	90.0, 102.4, 90.0	90.0, 102.4, 90.0	90.0, 102.0, 90.0	90.0, 102.4, 90.0	90.0, 102.2, 90.0	90.0, 102.4, 90.0	90.0, 102.6, 90.0
Resolution (Å)	50–3.4	50–3.5	50–3.6	50–3.7	50–3.4	50–3.5	50–3.2	50–3.7	50–3.7
R_{merge}[a]	9.9 (39.1)	8.4 (42.7)	13.0 (56.7)	12.3 (45.1)	7.8 (53.2)	10.2 (58.6)	8.4 (42.7)	14.1 (74.8)	13.1 (68.4)
$I / \sigma I$ [a]	9.8 (3.1)	13.7 (3.2)	15.5 (3.0)	7.0 (2.3)	12.4 (2.4)	10.6 (2.3)	13.7 (3.2)	8.9 (2.1)	10.0 (2.3)
Completeness (%)[a]	87.1 (68.9)	91.1 (73.1)	99.0 (100)	78.6 (64.5)	89.1 (71.2)	86.8 (63.3)	91.1 (73.7)	88.9 (71.8)	90.2 (72.3)
Redundancy[a]	3.0 (2.7)	3.5 (3.3)	6.3 (6.0)	1.3 (1.2)	1.7 (1.6)	3.5 (3.3)	3.4 (3.0)	3 (2.7)	3.4 (3.2)
Refinement									
Resolution (Å)	40–3.4	40–3.4	40–3.6	40–3.7	40–3.6	40–3.5	40–3.2	40–3.7	40–3.7
No. reflections	49,956	49,333	42,999	39,853	42,618	44,467	66,454	38,628	39,690
R_{work}/R_{free}	24.3/26.6	25.0/26.6	23.8/24.8	25.7/27.4	26.0/27.2	24.8/25.7	25.2/25.7	24.6/24.7	21.2/23.1
No. atoms									
Protein	12,605	12,605	12,605	12,605	12,605	12,605	12,600	12,605	12,585
Ligand/ion	5	1	3	1	1	1	1	1	4
B-factors									
Protein	92.3	92.1	92.9	92.5	91.7	83.3	92.1	108.0	102.0
Ligand/ion	144.0	132.4	164.6	151.0	206.6	171.9	130.9	212.8	107.0
R.m.s. deviations									
Bond lengths (Å)	0.01	0.01	0.01	0.01	0.01	0.01	0.01	0.01	0.01
Bond angles (°)	1.3	1.3	1.5	1.4	1.3	1.4	1.3	1.4	1.5

[a]Values in parentheses are for highest-resolution shell. Br-lido, bromo-lidocaine.

ranges between 20% and 25%, which indicates that the molecules bind on the extracellular periphery of the electric field (**Fig. 2c**).

To visualize the inhibited channel, we crystallized GLIC in the presence of quaternary ammonium compounds of different length and determined the structures by X-ray crystallography (**Tables 1** and **2**). The interpretation of the binding interaction is complicated by the symmetry mismatch between the pentameric channel and the tetrahedral molecules, which results in an ensemble of energetically equivalent conformations. We thus used analogs of the blocking molecules in which the central nitrogen atom is replaced by heavier atoms such as antimony or arsonium that were readily detected by their anomalous scattering properties. The two heavy atom derivatives tetrabutylantimony (TBSb) and tetraethylarsonium (TEAs) show a similar voltage-dependent inhibition behavior to their quaternary ammonium analogs and thus likely block the channel in the same way (**Supplementary Fig. 2d–f**). The higher affinity of TBSb is probably due to its higher free energy in solution, which is reflected in the lower solubility of the compound.

The heavy atom components TBSb and TEAs in complex with GLIC are readily detectable from their anomalous difference densities (**Fig. 2d,e**), which correspond to the respective centers of the bound pore blockers. In both cases, the molecule is located in a cavity close to residue Ser229 at the boundary between the hydrophobic and hydrophilic part of the pore. Modeling suggests that the alkyl chains of the blockers fill the space and thus obstruct the pore and prevent ion permeation. Whereas both molecules bind to the same location, the position of TEAs is shifted toward the intracellular side, probably because of its smaller size. Strong electron density somewhat deeper in the pore was also observed for the poor inhibitor tetramethylarsonium (TMAs) (**Supplementary Fig. 2g,h**). In no case did the structure of the protein visibly change upon binding of the inhibiting molecule, an observation that underlines the conformational stability of the channel region.

The binding sites of TBSb and TEAs are geometrically located at about 0.67 fractional distance from the extracellular solution to the cytoplasm, less than the distance for the previously located binding site of Cs^+ ions. The respective positions of these sites within the pore substantially exceeds the relatively short electrical distance ($z\delta$ = 0.2–0.24) that is inferred from the voltage dependence of inhibition. These differences are qualitatively explained by a numerical solution of the Poisson-Boltzmann equation, suggesting that in GLIC the major potential drop occurs across the region located intracellular to the binding site, whereas it occurs at the extracellular half of the pore in the non-conducting conformation of ELIC (**Fig. 2f**).

To investigate the contribution of pore residues in GLIC to inhibitor binding, we mutated the side chains of residues in the lower part of the pore lining and studied the mutants by X-ray crystallography and electrophysiology. The respective mutations did not affect the overall structure of the protein, which is in all cases very close to that of the wild type (WT). The mutation S229A increases the binding affinity of TBA, probably by increasing the volume of the binding cavity (**Fig. 2g** and **Supplementary Table 1**). The position of the bound blocker is consequently shifted toward the intracellular side (**Supplementary Fig. 3a**). A similar structural and functional behavior is also found for the more distant residue T225A. Different mutations of Glu221 at the intracellular pore entry weaken the binding of TBA and TEA without affecting their binding position and thus indicate a long-range electrostatic interaction of the negatively charged side chain with the positively charged inhibitors (**Fig. 2g** and **Supplementary Fig. 3b,c**). Electrophysiological experiments show that channel block is dependent on the charge of the side chain in the respective position: whereas mutations to alanine and glutamine decrease the binding

Table 2 Data collection and refinement statistics

	E221A–Cd2+	S229A–Cd2+	E221A–TEAs	S229A–TBSb	T225A–TBSb	E221A–TBSb	E221D–TBSb	E221Q–TEAs	E221Q–TBSb
Data collection									
Space group	*C*2	*C*2	*C*2	*C*2	*C*2	*C*2	*C*2	*C*2	*C*2
Cell dimensions									
a, *b*, *c* (Å)	184.3, 133.9, 164.2	186.5, 137.5, 165.8	183.3, 128.3, 164.4	179.1, 133.8, 161.1	181.6, 133.1, 162.2	182.4, 133.7, 163.4	179.7, 134.4, 161.3	182.1, 135.5, 163.2	181.2, 133.7, 162.8
α, *β*, *γ* (°)	90.0, 103.5, 90.0	90.0, 102.0, 90.0	90.0, 104.0, 90.0	90.0, 101.8, 90.0	90.0, 102.8, 90.0	90.0, 103.1, 90.0	90.0, 101.7, 90.0	90.0, 103.1, 90.0	90.0, 102.4, 90.0
Resolution (Å)	50–3.5	50–3.9	50–3.6	50–3.7	50–3.6	50–3.8	50–3.6	50–3.6	50–3.6
R_{merge}[a]	10.0 (46.9)	10.1 (81.9)	12.4 (53.2)	9.7 (41.2)	11.9 (61.7)	16.7 (73.3)	11.8 (49.5)	10.6 (56.6)	17.4 (58.7)
$I / \sigma I$[a]	7.3 (2.0)	10.2 (2.5)	10.0 (3.2)	9.2 (3.1)	8.4 (2.4)	7.7 (2.1)	10.0 (2.9)	10.8 (2.8)	7.5 (2.7)
Completeness (%)[a]	86.5 (71.0)	89.8 (71.6)	88.6 (76)	90.0 (76.9)	89.2 (72.7)	97.2 (89.4)	91.6 (79.1)	88.7 (69.6)	85.2 (72.6)
Redundancy[a]	3.6 (2.8)	2.4 (2.3)	3.5 (3.4)	3.4 (3.2)	3.5 (3.3)	3.4 (3.2)	3.4 (3.1)	3.5 (3.4)	1.4 (1.3)
Refinement									
Resolution (Å)	40–3.6	40–3.9	40–3.7	40–3.7	40–3.6	40–3.9	40–3.6	40–3.6	40–3.6
No. reflections	42,828	33,629	39,145	38,315	42,166	37,741	43,375	46,402	25,595
R_{work}/R_{free}	24.6/26.1	27.4/27.7	23.4/25.5	22.7/25.2	21.9/22.7	22.3/24.1	22.7/25.0	22.6/24.1	22.4/27.3
No. atoms									
Protein	12,585	12,600	12,585	12,600	12,595	12,585	12,600	12,605	12,605
Ligand/ion	4	4	1	1	1	1	1	1	1
B-factors									
Protein	90.6	144.3	105.7	99.6	103.1	106.8	95.8	105.4	101.5
Ligand/ion	192.3	222.0	192.1	252.2	172.1	187.1	205.8	192.4	206.1
R.m.s. deviations									
Bond lengths (Å)	0.01	0.01	0.01	0.01	0.01	0.01	0.010	0.01	0.01
Bond angles (°)	1.5	1.5	1.4	1.5	1.5	1.4	1.5	1.4	1.2

[a]Values in parentheses are for highest-resolution shell.

affinity, the negatively charged aspartate partly reverses the effect, as the mutant shows binding closer to WT (**Fig. 2g**).

Channel block by lidocaine

Apart from symmetric quaternary ammonium compounds, cation-selective pLGICs are also inhibited by larger and more complex substances that include tricyclic antidepressants, chlorpromazine, lidocaine and quinacrine[7–9,22–24]. This diverse set of molecules combines a positively charged amino group with a hydrophobic aromatic ring system. To reveal the mechanism of block by such compounds, we investigated the inhibition of GLIC by lidocaine. Lidocaine blocks GLIC with an apparent affinity similar to that of TBA (**Fig. 3a** and **Supplementary Table 1**). Like those from quaternary ammonium compounds, this block is voltage dependent ($z\delta$ = 0.27, **Supplementary Fig. 4a**). To localize lidocaine within the pore of GLIC, we synthesized a derivative that carries a bromine atom at the phenyl ring of the molecule and collected data from a crystal of the protein in complex with the inhibitor. A strong peak in the anomalous difference electron density locates the bromine atom in the hydrophobic part of the pore above Ile232 (**Fig. 3b** and **Supplementary Fig. 4b**,**c**). If this position is used to place a model of bromo-lidocaine into the pore, the positively charged part of the molecule would occupy the previously identified binding site of TEAs, thus indicating that the overall mechanism of lidocaine block is very similar to that of block by quaternary ammonium compounds.

Channel block by cadmium ions

After investigating the binding of large inhibitors, we turned our attention to a smaller blocker, the divalent transition metal ion cadmium (Cd^{2+}). Unlike the molecules previously described, which reach their binding site only from the extracellular side, Cd^{2+} blocks the channel from both sides of the membrane, as indicated by the reversible decrease of outward currents in an inside-out patch-clamp experiment (**Supplementary Fig. 2b**). When applied to the outside, Cd^{2+} lowers the current passed by GLIC. A gradual, steady decrease that starts at low ion concentrations and levels off at about 70% of the original value is irreversible and not voltage dependent, thus indicating that

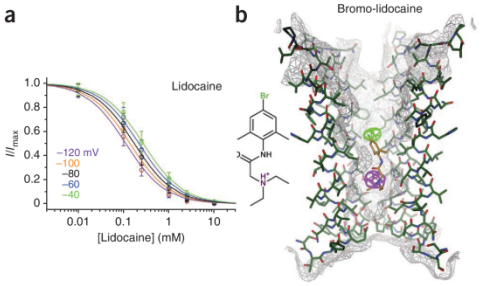

Figure 3 Inhibition of GLIC by lidocaine. (**a**) Dose-response curves of lidocaine block recorded from GLIC expressed in *X. laevis* oocytes by two-electrode voltage clamp at an extracellular pH of 4.5. The averages of data from 16 oocytes and their s.d. are shown. Measurements at different membrane potentials (ranging from −120 to −40 mV in 20-mV steps) are colored as in **Figure 1b** with a fit to a single-site binding isotherm shown in the same color. (**b**) Structure of the pore region of GLIC in complex with bromo-lidocaine. The anomalous difference electron density of the bromine position of the blocker (calculated at 4.5 Å) is contoured at 4.5 σ and shown as green mesh. For comparison the anomalous difference density of TEAs (calculated at 4.0 Å and contoured at 6 σ) is shown in indigo. A model of lidocaine was placed to illustrate a probable binding mode. The chemical structure of bromo-lidocaine is illustrated.

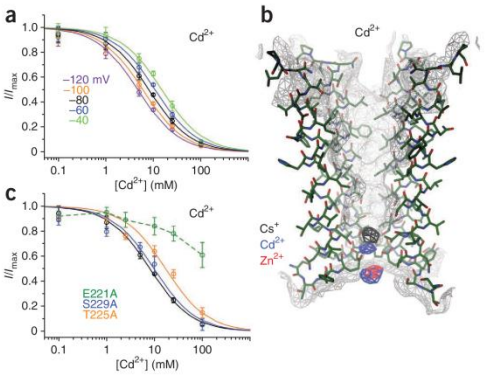

Figure 4 Inhibition of GLIC by Cd^{2+}. (**a**) Dose-response curves of Cd^{2+} block recorded from GLIC expressed in *Xenopus laevis* oocytes by two-electrode voltage clamp at an extracellular pH of 4. The averages of data from ten oocytes and their s.d. are shown. Measurements at different membrane potentials (ranging from −120 to −40 mV in 20-mV steps) are colored as in **Figure 2a** with a fit to a single-site binding isotherm shown in the same color. (**b**) Structure of the pore region of GLIC in complex with Cd^{2+}. The anomalous difference electron density of Cd^{2+} (contoured at 4.5 σ) is shown as blue mesh. The anomalous difference electron densities of Zn^{2+} (contoured at 4.5 σ) and Cs^{+} (contoured at 6 σ) are shown for comparison. All anomalous densities were calculated at a resolution of 4 Å. (**c**) Dose-response curves of Cd^{2+} block of WT and the pore mutants E221A, T225A and S229A were recorded at −80 mV. For the mutants the averages of data from at least 10 oocytes and their s.d. are shown. WT is as in **a**.

the effect is not due to binding in the pore region (**Supplementary Fig. 5a**). The steep drop of the current at higher concentration, by contrast, is reversible and strongly voltage dependent and is thus likely caused by open channel block (**Fig. 4a**). The fraction of the electric field crossed by this divalent ion ($z\delta = 0.17$), as inferred from the voltage dependence of the block, is comparable to the previously analyzed larger blockers and would thus indicate binding to the same location in the channel (**Supplementary Fig. 5b**). However, it can be expected that the voltage drop in the blocked channel is influenced by the size and position of the bound molecule and that large pore blockers and divalent ions thus may, despite their similar electrical distance, still bind to different sites in the protein. At high ion concentrations, the currents essentially vanish, which is indicative of either complete block or a very low residual conductance of Cd^{2+} (**Fig. 4a** and **Supplementary Fig. 5c**). This behavior differs from the properties of the related divalent transition metal ion Zn^{2+}, whose addition to the outside of the channel also causes a voltage-dependent decrease of the current. In this case, however, the current saturates at negative potentials, thus indicating that although Zn^{2+} also binds to a site in the channel, it is still permeant (**Supplementary Fig. 5d**).

The anomalous difference electron density of a GLIC–Cd^{2+} complex shows several positions of bound Cd^{2+} ions, some of which are located in the wide vestibule of the extracellular domain (**Supplementary Fig. 6a**). Within the pore, strong electron density is found in the narrow intracellular region (**Fig. 4b**). Separated peaks indicate binding to two positions, one overlapping with the previously identified Zn^{2+} binding site and one located about 5Å in the extracellular direction (**Supplementary Fig. 6b**). The correspondence of both positions with the site of block is supported by mutagenesis: although Cd^{2+} block is weakened in the mutant T225A, it is essentially abolished in the mutant E221A (**Fig. 4c**). Both mutants truncate side chains that likely interact with Cd^{2+} ions. Remarkably, the same mutants had a comparably smaller influence on TBA block. The functional phenotype is also reflected in the X-ray structure of the mutant E221A in high concentrations of Cd^{2+}. Whereas the binding of Cd^{2+} at sites in the extracellular domain is still detectable, the electron density in the pore region is absent (**Supplementary Fig. 6c**). In contrast, the mutant S229A, which concerns a residue that is not in contact with the bound ion, behaves similarly to WT with respect to Cd^{2+} block in both structural and functional experiments (**Fig. 4c** and **Supplementary Fig. 6d**).

The dominant role of Glu221 for the interaction with divalent ions is also observed for Zn^{2+}. The saturation of the current at negative potentials upon addition of extracellular Zn^{2+} is not seen in the mutant E221A, which shows a nearly linear current-voltage relationship (**Supplementary Fig. 5e**). At the same time, the strong density of bound ions in the pore region seen in WT is not detectable in the anomalous electron density of the mutant crystallized in the presence of Zn^{2+} (**Supplementary Fig. 6e,f**). This similarity in the structural and functional behavior thus underlines the mechanistic resemblance between Cd^{2+} block and the anomalous conduction properties of divalent cations through cation-selective pLGICs.

DISCUSSION

Inhibition by large pore blockers

Ion conduction through GLIC is inhibited by a structurally diverse set of molecules that have previously been identified as open channel blockers of the nicotinic acetylcholine receptor. We investigated the structural and energetic basis of this process; the results are

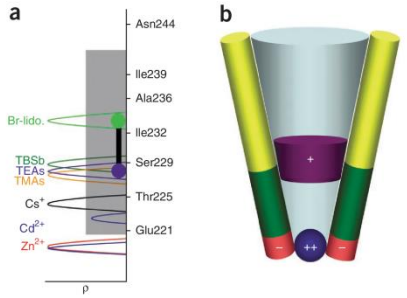

Figure 5 Mechanisms of open channel block. (**a**) Distribution of anomalous difference electron densities of GLIC in complex with different inhibitors. The electron densities (ρ) were sampled in the transmembrane region along the pore axis and normalized at their respective maximum. The hydrophobic core of the membrane is indicated (gray box). The Cα positions of pore residues are marked. Inhibitors and ions, except for Cd^{2+}, bind to a single site within the pore region. Cd^{2+} ions bind to two sites (shown as blue peaks). The electron density for bromo-lidocaine corresponds to the bromide atom attached to the aromatic ring. The extended binding region of the blocker is indicated by two connected circles. (**b**) Schematic representation of open pore block in GLIC. The α2 helices of two subunits are approximated as cylinders and colored according to the properties of the side chains (yellow hydrophobic, green polar, red negatively charged). A large blocker is colored in purple, a divalent cation is shown as blue sphere.

summarized in **Figure 5**. Large molecules such as quaternary ammonium compounds bind to a site about halfway across the membrane. A deeper penetration is prevented by the taper of the funnel shaped pore, as suggested by the progressive shift in the binding position of quaternary ammonium compounds of decreasing size toward the intracellular side. The affinity is determined by long-range electrostatics and by hydrophobic interactions with the alkyl chains that cause a stronger binding of larger molecules such as TBA and TPA. The binding site of the positively charged amine moiety in a cavity at the boundary between the hydrophobic and hydrophilic part of the channel is shared by quaternary ammonium compounds and larger blockers such as lidocaine, whose bulky and hydrophobic end is located in the wider and hydrophobic region at the extracellular half of the pore. The observed interaction is consistent with previous studies on the block of lidocaine derivatives to the nAChR[8]. After analysis of the effects of the changed reactivity of mutants of pore-lining residues to methanethiosulfonate (MTS) reagents upon addition of the inhibitor, a very similar binding mode was proposed[9]. The wide diameter in the vicinity of the aromatic ring would also provide sufficient space to accommodate the larger polycyclic groups of quinacrine, chlorpromazine and tricyclic antidepressants. However, their position would, for steric reasons, likely be shifted toward the extracellular side, as was also suggested by the changed reactivity of pore residues in the inhibited state of the nAChR, in different experimental studies[22,24].

It is noteworthy that the discussed inhibitors are not specific for pLGICs but also block other families of ion channels. Quaternary ammonium compounds have been known for a long time as blockers of K^+ channels[25], whereas lidocaine acts as local anesthetic that inhibits Na^+ channels[1,26]. The dominant mode of inhibition in both cases is caused by binding to the ion conduction path from the intracellular side. The similar mechanism in structurally unrelated families of ion channels underlines the general properties of the open pores of cation-selective channels that usually combine spacious hydrophobic entrances at one side of the membrane with an overall negative electrostatic potential throughout the pore and selective ion-coordination sites in a narrow selectivity filter on the other end of the pore. The difference in the sidedness of block reflects the reversed overall topology of ligand-gated channels in comparison to their voltage-gated counterparts.

Permeation and block by divalent ions

In contrast to larger blockers, the divalent transition metal ion Cd^{2+} inhibits ion conduction by binding to the narrow intracellular end of the pore. This region is hydrophilic and has previously been shown to provide coordination sites for permeant ions that have shed part of their hydration shell[16]. Cd^{2+} block resembles the anomalous conduction properties of divalent ions through the cation-selective members of the pLGIC family[12], properties that in certain cases are believed to play an important physiological role in the uptake of Ca^{2+} (ref. 27). Divalent ions generally show a tighter interaction with residues of the pore region than do their monovalent counterparts, and they dominate ion conduction at higher concentrations. Such properties are observed for Zn^{2+}, which binds to a single site in the intracellular pore entry of GLIC and causes a saturation of the inward currents when added from the extracellular side. The strong block by Cd^{2+} could either originate from tight binding of the ion to a site in the pore or from the presence of a large energy barrier on the translocation path. Because the IC_{50} values for extracellular Cd^{2+} indicate a comparably low affinity, the second possibility appears likely. The electron density of a GLIC–Cd^{2+} complex shows two peaks in the pore region, one at the location identified for Zn^{2+} binding and another at a nearby position toward the extracellular side. It is thus conceivable that the barrier that prevents permeation is located between the two positions, which might for energetic reasons represent alternately occupied sites, one site being accessible from the outside and the other from the cytoplasm. Like the partial block by Zn^{2+}, Cd^{2+} block is essentially removed by the mutation of a conserved glutamate residue at the intracellular entry of the pore. In the structure of GLIC, this residue projects into the channel and constricts the pore, but it is possible that its conformation is biased by the low pH of the crystallization conditions. Alternative conformations of the side chain remove the constriction and put the residue into place for a direct interaction with divalent ions without changing the overall conformation of the pore (**Supplementary Fig. 7**). An analogous phenotype has previously been observed for the nAChR. Mutations in the equivalent position, which was termed the 'intermediate ring of charges', have been found to interfere with the binding and conduction of divalent ions[20,28,29]. Besides their role in ion binding, the intermediate ring of charges was also proposed to dominate the strong negative electrostatic potential at the intracellular part of the pore[30], which attracts cations into the transmembrane channel. In our study on GLIC, we observed a similar long-range electrostatic influence on the interaction with TBA and TEA, which bind far from the negatively charged glutamate residues and whose binding was weakened upon mutation to uncharged residues.

The results of our study provide a structural framework for understanding the interaction of GLIC with a diverse class of pore blockers and divalent ions that is likely conserved within the family. Although the open pore conformation lasts for only milliseconds in eukaryotic pLGICs, it is much more stable in GLIC. Therefore, our data makes it possible to reconcile previous studies on the role of residues within the pore domain for ion permeation and open channel block. Our work also reinforces the structural similarity between the open state of the GLIC pore and that of eukaryotic pLGICs.

METHODS

Methods and any associated references are available in the online version of the paper at http://www.nature.com/nsmb/.

Accession codes. Coordinates have been deposited with the Protein Data Bank under codes 2XQA (WT–TBSb complex), 2XQ5 (WT–TEAs complex), 2XQ9 (E221D–TEAs complex), 2XQ4 (WT–TMAs complex), 2XQ3 (WT–bromo-lidocaine complex), 2XQ7 (WT–Cd^{2+} complex), 2XQ8 (WT–Zn^{2+} complex), 2XQ6 (WT–Cs^+ complex).

Note: Supplementary information is available on the Nature Structural & Molecular Biology website.

ACKNOWLEDGMENTS

We would like to thank the staff of the X06SA beamline for support during data collection and members of the Dutzler lab for help in all stages of the project. Data collection was done at the Swiss Light Source of the Paul Scherrer Institute. The research leading to these results received funding from a grant from the Swiss National Science Foundation (SNF) and from an EC FP7 grant for the European Drug Initiative on Channels and Transporters consortium (HEALTH-201924). R.J.C.H. received the support of the Forschungskredit of the University of Zurich. C.B. and I.Z. are affiliated with the Biomolecular Structure and Mechanism PhD program of the University of Zurich (UZH) and the Swiss Federal Institute of Technology (ETH) Zurich.

AUTHOR CONTRIBUTIONS

R.J.C.H. and C.B. carried out all experiments. I.Z. assisted in electrophysiological and crystallographic data collection. A.R. and D.T. synthesized the channel blockers. R.D., R.J.C.H. and C.B. jointly planned the experiments and analyzed the data. R.D. wrote the manuscript with the help of all coauthors.

COMPETING FINANCIAL INTERESTS
The authors declare no competing financial interests.

Published online at http://www.nature.com/nsmb/.
Reprints and permissions information is available online at http://npg.nature.com/reprintsandpermissions/.

1. Hille, B. *Ion Channels of Excitable Membranes* 3rd edn. (Sinauer Associates Inc., Sunderland, Massachusetts, USA, 2001).
2. Sine, S.M. & Engel, A.G. Recent advances in Cys-loop receptor structure and function. *Nature* **440**, 448–455 (2006).
3. Corringer, P.J., Le Novere, N. & Changeux, J.P. Nicotinic receptors at the amino acid level. *Annu. Rev. Pharmacol. Toxicol.* **40**, 431–458 (2000).
4. Karlin, A. Emerging structure of the nicotinic acetylcholine receptors. *Nat. Rev. Neurosci.* **3**, 102–114 (2002).
5. Adler, M., Oliveira, A.C., Albuquerque, E.X., Mansour, N.A. & Eldefrawi, A.T. Reaction of tetraethylammonium with the open and closed conformations of the acetylcholine receptor ionic channel complex. *J. Gen. Physiol.* **74**, 129–152 (1979).
6. Leonard, R.J., Labarca, C.G., Charnet, P., Davidson, N. & Lester, H.A. Evidence that the M2 membrane-spanning region lines the ion channel pore of the nicotinic receptor. *Science* **242**, 1578–1581 (1988).
7. Revah, F. *et al.* The noncompetitive blocker [^{3}H]chlorpromazine labels three amino acids of the acetylcholine receptor gamma subunit: implications for the alpha-helical organization of regions MII and for the structure of the ion channel. *Proc. Natl. Acad. Sci. USA* **87**, 4675–4679 (1990).
8. Charnet, P. *et al.* An open-channel blocker interacts with adjacent turns of alpha-helices in the nicotinic acetylcholine receptor. *Neuron* **4**, 87–95 (1990).
9. Pascual, J.M. & Karlin, A. Delimiting the binding site for quaternary ammonium lidocaine derivatives in the acetylcholine receptor channel. *J. Gen. Physiol.* **112**, 611–621 (1998).
10. Neher, E. & Steinbach, J.H. Local anaesthetics transiently block currents through single acetylcholine-receptor channels. *J. Physiol. (Lond.)* **277**, 153–176 (1978).
11. Nutter, T.J. & Adams, D.J. Monovalent and divalent cation permeability and block of neuronal nicotinic receptor channels in rat parasympathetic ganglia. *J. Gen. Physiol.* **105**, 701–723 (1995).
12. Adams, D.J., Dwyer, T.M. & Hille, B. The permeability of endplate channels to monovalent and divalent metal cations. *J. Gen. Physiol.* **75**, 493–510 (1980).
13. Dani, J.A. & Eisenman, G. Monovalent and divalent cation permeation in acetylcholine receptor channels. Ion transport related to structure. *J. Gen. Physiol.* **89**, 959–983 (1987).
14. Hilf, R.J. & Dutzler, R. X-ray structure of a prokaryotic pentameric ligand-gated ion channel. *Nature* **452**, 375–379 (2008).
15. Hilf, R.J. & Dutzler, R. A prokaryotic perspective on pentameric ligand-gated ion channel structure. *Curr. Opin. Struct. Biol.* **19**, 418–424 (2009).
16. Hilf, R.J. & Dutzler, R. Structure of a potentially open state of a proton-activated pentameric ligand-gated ion channel. *Nature* **457**, 115–118 (2009).
17. Bocquet, N. *et al.* X-ray structure of a pentameric ligand-gated ion channel in an apparently open conformation. *Nature* **457**, 111–114 (2009).
18. Bocquet, N. *et al.* A prokaryotic proton-gated ion channel from the nicotinic acetylcholine receptor family. *Nature* **445**, 116–119 (2007).
19. Imoto, K. *et al.* Rings of negatively charged amino acids determine the acetylcholine receptor channel conductance. *Nature* **335**, 645–648 (1988).
20. Konno, T. *et al.* Rings of anionic amino acids as structural determinants of ion selectivity in the acetylcholine receptor channel. *Proc. Biol. Sci.* **244**, 69–79 (1991).
21. Woodhull, A.M. Ionic blockage of sodium channels in nerve. *J. Gen. Physiol.* **61**, 687–708 (1973).
22. Gumilar, F., Arias, H.R., Spitzmaul, G. & Bouzat, C. Molecular mechanisms of inhibition of nicotinic acetylcholine receptors by tricyclic antidepressants. *Neuropharmacology* **45**, 964–976 (2003).
23. Sepúlveda, M.I., Baker, J. & Lummis, S.C. Chlorpromazine and QX222 block 5–HT3 receptors in N1E–115 neuroblastoma cells. *Neuropharmacology* **33**, 493–499 (1994).
24. Yu, Y., Shi, L. & Karlin, A. Structural effects of quinacrine binding in the open channel of the acetylcholine receptor. *Proc. Natl. Acad. Sci. USA* **100**, 3907–3912 (2003).
25. Armstrong, C.M. Interaction of tetraethylammonium ion derivatives with the potassium channels of giant axons. *J. Gen. Physiol.* **58**, 413–437 (1971).
26. Hille, B. Common mode of action of three agents that decrease the transient change in sodium permeability in nerves. *Nature* **210**, 1220–1222 (1966).
27. Weisstaub, N., Vetter, D.E., Elgoyhen, A.B. & Katz, E. The alpha9alpha10 nicotinic acetylcholine receptor is permeable to and is modulated by divalent cations. *Hear. Res.* **167**, 122–135 (2002).
28. Bertrand, D., Galzi, J.L., Devillers-Thiéry, A., Bertrand, S. & Changeux, J.P. Mutations at two distinct sites within the channel domain M2 alter calcium permeability of neuronal alpha 7 nicotinic receptor. *Proc. Natl. Acad. Sci. USA* **90**, 6971–6975 (1993).
29. Imoto, K. *et al.* Location of a delta-subunit region determining ion transport through the acetylcholine receptor channel. *Nature* **324**, 670–674 (1986).
30. Wilson, G.G., Pascual, J.M., Brooijmans, N., Murray, D. & Karlin, A. The intrinsic electrostatic potential and the intermediate ring of charge in the acetylcholine receptor channel. *J. Gen. Physiol.* **115**, 93–106 (2000).

ONLINE METHODS

Protein preparation. GLIC was expressed and purified as described previously[16]. Briefly, the protein was expressed in *Escherichia coli* as a fusion to the C terminus of maltose binding protein (MBP) that was preceded by an *E. coli* pelB signal sequence and a decahistidine (His_{10}) tag. The fusion protein was extracted from isolated membranes with the detergent dodecyl maltoside (DDM), which was subsequently used for purification and crystallization. After centrifugation, the fusion protein was purified on Ni-NTA. MBP was cleaved off the channel with herpes simplex (HRV) 3C protease at a specific site located between the MBP and GLIC and removed by binding to Ni-NTA resin. The channel was subsequently concentrated and subjected to gel filtration on a Superdex 200 column (GE Healthcare) in a buffer containing 10 mM Tris, pH 7.5, 150 mM NaCl, 0.5 mM DDM. The protein peak corresponding to the GLIC pentamer was pooled and concentrated to 10 mg ml^{-1} and used for crystallization. Mutations were introduced with the QuikChange method (Stratagene) and confirmed by sequencing. The mutant proteins were expressed and purified as WT.

Synthesis. TEAs nitrate and TMAs nitrate were synthesized as described[31]. The compounds were confirmed by electron spray mass spectrometry and ^{1}H and ^{13}C NMR spectrometry. Bromo-lidocaine was synthesized following a protocol outlined in **Supplementary Figure 8** (ref. 32). The compound was purified by flash chromatography and confirmed by electron spray mass spectrometry and ^{1}H and ^{13}C NMR spectrometry.

Crystallization and crystal preparation. GLIC was crystallized in sitting drops at 4 °C. Crystals were obtained by mixing protein containing additional 0.5 mg ml^{-1} *E. coli* polar lipids (Avanti Polar Lipids, Inc.) in a 1:1 ratio with reservoir solution containing between 200 and 500 mM $(NH_4)_2SO_4$, 50 mM sodium acetate (pH 4.0), 9–12% (w/v) PEG 4000. For structural studies on channel block, the complexes were obtained either by cocrystallization or by soaking of native crystals in solutions containing the respective inhibitors (5 mM TBSb (Aldrich), 10 mM TEAs, 30 mM TMAs, 15 mM bromo-lidocaine) added to the standard conditions. For divalent ions, NaCl was replaced by the respective Cl^- salt (100 mM $ZnCl_2$ or 50 mM $CdCl_2$). For cryoprotection, the crystals were transferred into mother liquor containing 30% (v/v) ethylene glycol and flash-frozen in liquid propane.

Crystallography. Data sets were collected on frozen crystals on the X06SA beamline at the Swiss Light Source (SLS) of the Paul Scherrer Institut (PSI) on a PILATUS detector (Dectris) at a suitable wavelength to maximize the anomalous diffraction of the bound inhibitors. The data were indexed, integrated and scaled with the programs XDS[33] and further processed with CCP4 programs[34] (**Tables 1** and **2**). All WT and mutant complexes crystallized in space group C2 (cell dimensions: $a = 178.5$ Å, $b = 133.5$ Å, $c = 160.5$ Å, $\alpha = \gamma = 90°$, $\beta = 106.1°$) and were isomorphous to WT. The structure of GLIC at 3.1 Å (PDB code 3EHZ without water molecules) served as starting model that was improved by rigid-body refinement in PHENIX[35]. The electron density was inspected and mutations were introduced in O[36]. For datasets exceeding a resolution of 3.6 Å, the structures were additionally subjected to refinement of individual atom positions in PHENIX maintaining strong NCS constraints. R and R_{free} were monitored throughout. R_{free} was calculated from the same 5% set of reflections that were initially selected for the structure determination of GLIC at 3.1 Å (PDB code 3EHZ) and that were omitted in refinement. For the calculation of the anomalous difference densities, a high resolution cutoff of $I/\sigma I > 5$ was used throughout. The one-dimensional density profile along the pore was sampled using the program MAPMAN[37]. The molecular surface was calculated with MSMS[38].

Electrophysiology. Constructs containing the gene of either the WT channel or point mutants preceded by the signal sequence of the human α7nAChR were cloned into the pTLN vector for expression in *X. laevis* oocytes[39]. After linearization of the plasmid DNA by MluI, capped complementary RNA was transcribed with the mMessage mMachine kit (Ambion) and purified with the RNeasy kit (Qiagen). For expression, 1–50 ng of RNA was injected into defolliculated oocytes. Two-electrode voltage-clamp measurements were taken 1–2 d after injection at 20 °C (OC-725B, Warner Instrument Corp.). Currents were recorded in bath solutions containing 130 mM NaCl, 2 mM KCl, 1.8 mM $CaCl_2$, 5 mM $MgCl_2$ and the specified inhibitor concentrations. The respective pH values were stabilized by addition of 10 mM HEPES (pH 7.0) or 10 mM of citrate (pH 4.0–pH 5.0). For recording in solutions containing either Zn^{2+} or Cd^{2+}, citrate was replaced by 10 mM glucuronate. Low-salt solutions contained 30 mM NaCl, 100 mM mannitol, 2 mM KCl, 1.8 mM $CaCl_2$, 1 mM $MgCl_2$ and 10 mM glucuronate at pH 4.0. Inside-out patch clamp measurements were recorded 3 d after injection with an Axopatch 200B amplifier (Axon Instruments). Electrodes had a resistance of 1–3 MΩ. Bath solution contained 150 mM NaCl, 1 mM $CaCl_2$ and 5 mM $MgCl_2$. The respective pH values were stabilized by addition of 10 mM HEPES (pH 7.0) or 10 mM of glucuronate (pH 4.0–5.0) and the indicated concentration of the inhibitor. The pipette solutions contained 150 mM NaCl, 1 mM EGTA and 5 mM MgCl and 10 mM glucuronate at pH 5.5. Electrodes were bathed in 1 M KCl solution connected to the bath solution by agar bridges.

Poisson Boltzmann calculations. The drop of a 100-mV transmembrane potential across GLIC was calculated by solving the linearized Poisson Boltzmann equation in CHARMM[40,41] on a 110 × 110 × 150 Å grid (1 Å grid spacing). Polar hydrogen positions were generated in CHARMM, and protein charges were set to zero. The protein was assigned a dielectric constant of two. Its transmembrane region was embedded in a 30-Å-thick slab ($\varepsilon = 2$), representing the membrane that contained a cylindrical hole around the water-filled pore region, and was surrounded by an aqueous environment ($\varepsilon = 80$). Calculations were carried out with a mobile ion concentration of 150 mM of monovalent salt in the solvent region.

31. Lenaeus, M.J., Vamvouka, M., Focia, P.J. & Gross, A. Structural basis of TEA blockade in a model potassium channel. *Nat. Struct. Mol. Biol.* **12**, 454–459 (2005).
32. Heravi, M.M., Abdolhosseini, N. & Oskooie, H.A. Regioselective and high-yielding bromination of aromatic compounds using hexamethylenetetramine–bromine. *Tetrahedr. Lett.* **46**, 8959–8963 (2005).
33. Kabsch, W. Automatic processing of rotation diffraction data from crystals of initially unknown symmetry and cell constants. *J. Appl. Cryst.* **26**, 795–800 (1993).
34. Collaborative Computational Project Number 4. The CCP4 suite: programs for X-ray crystallography. *Acta Crystallogr. D Biol. Crystallogr.* **50**, 760–763 (1994).
35. Adams, P.D. *et al.* PHENIX: building new software for automated crystallographic structure determination. *Acta Crystallogr. D Biol. Crystallogr.* **58**, 1948–1954 (2002).
36. Jones, T.A., Zou, J.Y., Cowan, S.W. & Kjeldgaard, M. Improved methods for building protein models in electron density maps and the location of errors in these models. *Acta Crystallogr. A* **47**, 110–119 (1991).
37. Kleywegt, G. & Jones, T.A. In *Proceedings of the CCP4 Study Weekend.* (eds. Bailey, S., Hubbard, R. & Waller, D.), 59–66 (Daresbury Laboratory, Daresbury, UK, 1994).
38. Sanner, M.F., Olson, A.J. & Spehner, J.C. Reduced surface: an efficient way to compute molecular surfaces. *Biopolymers* **38**, 305–320 (1996).
39. Lorenz, C., Pusch, M. & Jentsch, T.J. Heteromultimeric CLC chloride channels with novel properties. *Proc. Natl. Acad. Sci. USA* **93**, 13362–13366 (1996).
40. Brooks, B.R. *et al.* CHARMM: a program for macromolecular energy, minimization, and dynamics calculations. *J. Comput. Chem.* **4**, 187–217 (1983).
41. Im, W., Beglov, D. & Roux, B. Continuum solvation model: computation of electrostatic forces from numerical solutions to the Poisson-Bolztmann equation. *Comput. Phys. Commun.* **111**, 59–75 (1998).

The structural basis of open channel block in a prokaryotic pentameric ligand-gated ion channel

Ricarda J. C. Hilf, Carlo Bertozzi, Iwan Zimmermann, Alwin Reiter, Dirk Trauner and Raimund Dutzler

a

```
                -1' 2'  6' 9' 13'16'
GLIC       TSYEANVTLVVSTLIAHIAFNILVETNLPKT
ELIC       ESFSERLQTSFTLMLTVVAYAFYTSNILPRL
α7AChR     ADSGEKISLGITVLLSLTVFMLLVAEIMPAT
αAChR      TDSGEKMTLSISVLLSLTVFLLVIVELIPST
βAChR      PDAGEKMSLSISALLALTVFLLLLADKVPET
```

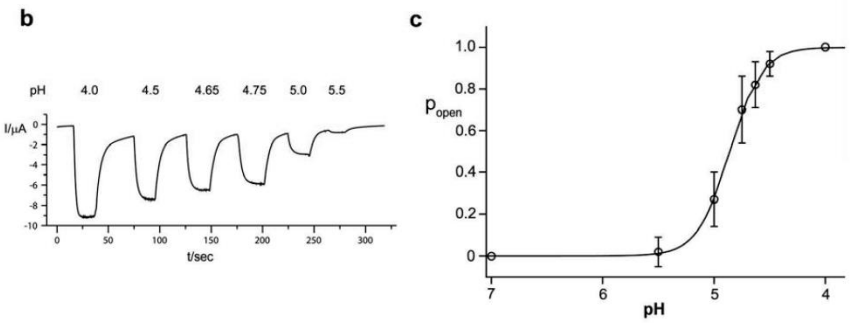

Supplementary Figure 1 Sequence conservation and pH activation of GLIC. **a** Sequence alignment of the pore region of the pLGICs from *Gloeobacter violaceous* (GLIC), *Erwinia chrysanthemi* (ELIC), the homopentameric human α7 acetylcholine receptor (α7AChR), and the α and β chains of the heteropentameric muscle-type acetylcholine receptor (AChR) from *Torpedo marmorata*. Conserved positions contributing to the pore lining are highlighted in red. The previously introduced numbering for the pore of the nAChR is shown above. For GLIC -1' corresponds to position Glu221. **b** Two electrode voltage clamp recordings of *Xenopus* oocytes expressing GLIC. Currents were recorded at -60 mV. The pH of bath solutions is indicated above. The solution was changed back to pH 7 after each activation step. **c** Open probability of GLIC plotted as function of the proton concentration. The currents were normalized to the value at pH 4. The averages of 5 oocytes and their standard deviations are shown. The solid line shows a fit to a hill equation with a coefficient of 3.0.

Nature Structural & Molecular Biology: doi:10.1038/nsmb.1933

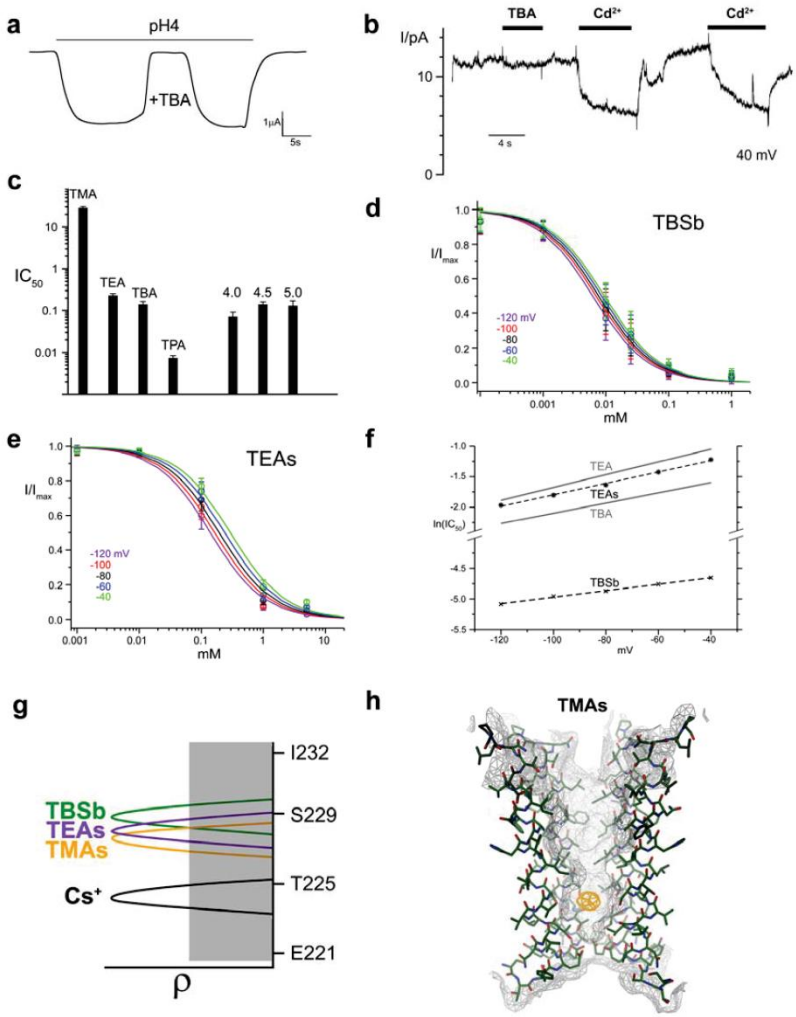

Supplementary Figure 2 Block by QA compounds. (**a**) Reversible block of currents mediated by GLIC in response to the addition of 10 mM TBA. Currents were recorded at -80 mV. (**b**) GLIC-mediated macroscopic currents recorded by the inside-out patch clamp technique at 40 mV. The pipette solution was at pH 5.5. The perfusion with bath solution (at pH7) containing 10 mM TBA or 10 mM Cd^{2+} is indicated. (**c**) Dependence of channel block on the size of the QA compounds and the pH of the extracellular solution. IC_{50} values of different QA compounds (left, measured at pH4.5) and the dependence of TBA block on the pH of the bath solutions (right) are shown. Data

Nature Structural & Molecular Biology: doi:10.1038/nsmb.1933

was recorded at -80 mV, the average of at least 12 independent measurements and their standard deviation are shown. (**d**) Dose-response curves of TBSb and (**e**) TEAs block recorded from GLIC expressed in *Xenopus laevis* oocytes by 2-electrode voltage clamp at an extracellular pH of 4.5. The averages of currents from 7 (TBSb) and 5 (TEAs) oocytes and their standard deviations are shown. Measurements at different membrane potentials (ranging from -120 to -40 mV in 20 mV steps) are colored as indicated with a fit to a single site binding isotherm shown in the same color. (**f**) Voltage dependence of TEAs and TBSb block. The voltage dependence of TEA and TBA are shown for comparison. (**g**) Distribution of anomalous difference electron densities of QA analogues bound to GLIC. The electron densities (ρ) were sampled in the transmembrane region along the pore axis and normalized to their maximum value. The hydrophobic core of the membrane is indicated (grey box). The Cα positions of pore residues are marked. (**h**) Structure of the pore region of GLIC in complex with tetramethylarsonium (TMAs). The orange mesh shows the anomalous difference electron density calculated at 4.0 Å and contoured at 5σ.

	IC_{50}^{-80} / mM	n	pH	Nr
WT TBA	0.07	1	4.0	15
WT TBA	0.14	1	4.5	22
WT TBA	0.13	1	5.0	15
WT TEA	0.24	1	4.5	12
WT TMA	29.0	1	4.5	12
WT TBSb	0.0067	1	4.5	7
WT TEAs	0.20	1	4.5	5
WT TPA	0.008	1	4.5	13
E221A TBA	0.32	0.78	4.5	6
E221Q TBA	0.25	0.65	4.5	6
E221D TBA	0.24	1	4.5	10
T225A TBA	0.01	0.76	4.5	9
S229A TBA	0.011	0.40	4.5	8
E221A TBA	0.20	0.70	4.0	11
E221Q TBA	0.21	0.64	4.0	7
E221D TBA	0.15	1	4.0	12
T225A TBA	0.01	0.76	4.0	8
S229A TBA	0.01	0.65	4.0	8
E221A TEA	1.1	1	4.5	10
E221Q TEA	0.91	1	4.5	7
E221D TEA	0.65	1	4.5	7
WT Lidoc.	0.18	1	4.5	16
WT Cd^{2+}	7.9	1	4.0	10
E221A Cd^{2+}	n.d.	n.d.	4.0	8
T225A Cd^{2+}	17.0	1	4.0	7
S229A Cd^{2+}	9.8	1	4.0	6

Supplementary Table 1 Electrophysiology. IC_{50} values (at -80mV) were obtained from a fit of the averaged normalized currents to a single site adsorption isotherm (for n=1), or to a hill equation (with coefficient n for n<1). The number of independent measurements and the pH of the extracellular solution are indicated.

Nature Structural & Molecular Biology: doi:10.1038/nsmb.1933

was recorded at -80 mV, the average of at least 12 independent measurements and their standard deviation are shown. (**d**) Dose-response curves of TBSb and (**e**) TEAs block recorded from GLIC expressed in *Xenopus laevis* oocytes by 2-electrode voltage clamp at an extracellular pH of 4.5. The averages of currents from 7 (TBSb) and 5 (TEAs) oocytes and their standard deviations are shown. Measurements at different membrane potentials (ranging from -120 to -40 mV in 20 mV steps) are colored as indicated with a fit to a single site binding isotherm shown in the same color. (**f**) Voltage dependence of TEAs and TBSb block. The voltage dependence of TEA and TBA are shown for comparison. (**g**) Distribution of anomalous difference electron densities of QA analogues bound to GLIC. The electron densities (ρ) were sampled in the transmembrane region along the pore axis and normalized to their maximum value. The hydrophobic core of the membrane is indicated (grey box). The Cα positions of pore residues are marked. (**h**) Structure of the pore region of GLIC in complex with tetramethylarsonium (TMAs). The orange mesh shows the anomalous difference electron density calculated at 4.0 Å and contoured at 5σ.

	IC_{50}^{-80} / mM	n	pH	Nr
WT TBA	0.07	1	4.0	15
WT TBA	0.14	1	4.5	22
WT TBA	0.13	1	5.0	15
WT TEA	0.24	1	4.5	12
WT TMA	29.0	1	4.5	12
WT TBSb	0.0067	1	4.5	7
WT TEAs	0.20	1	4.5	5
WT TPA	0.008	1	4.5	13
E221A TBA	0.32	0.78	4.5	6
E221Q TBA	0.25	0.65	4.5	6
E221D TBA	0.24	1	4.5	10
T225A TBA	0.01	0.76	4.5	9
S229A TBA	0.011	0.40	4.5	8
E221A TBA	0.20	0.70	4.0	11
E221Q TBA	0.21	0.64	4.0	7
E221D TBA	0.15	1	4.0	12
T225A TBA	0.01	0.76	4.0	8
S229A TBA	0.01	0.65	4.0	8
E221A TEA	1.1	1	4.5	10
E221Q TEA	0.91	1	4.5	7
E221D TEA	0.65	1	4.5	7
WT Lidoc.	0.18	1	4.5	16
WT Cd^{2+}	7.9	1	4.0	10
E221A Cd^{2+}	n.d.	n.d.	4.0	8
T225A Cd^{2+}	17.0	1	4.0	7
S229A Cd^{2+}	9.8	1	4.0	6

Supplementary Table 1 Electrophysiology. IC_{50} values (at -80mV) were obtained from a fit of the averaged normalized currents to a single site adsorption isotherm (for n=1), or to a hill equation (with coefficient n for n<1). The number of independent measurements and the pH of the extracellular solution are indicated.

Nature Structural & Molecular Biology: doi:10.1038/nsmb.1933

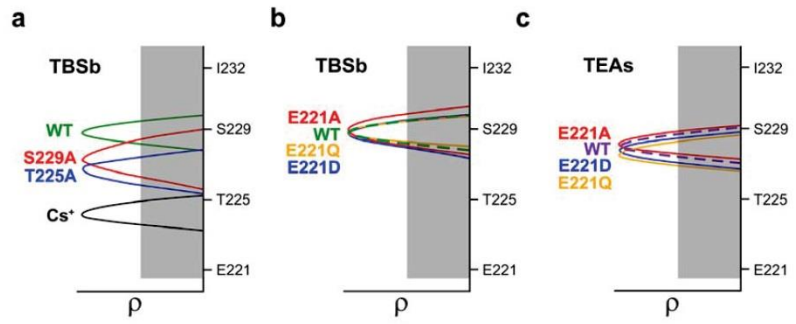

Supplementary Figure 3 Binding of QA compounds to GLIC mutants. The labeling is as in Supplementary Fig. 3g. (**a**) Distribution of anomalous difference electron densities of TBSb bound to the pore mutants S229A and T225A. The positions of TBSb and Cs^+ bound to WT are shown for comparison. (**b**) Distribution of anomalous difference electron densities of TBSb bound to mutants of Glu221. The position of TBSb bound to WT is shown for comparison (dashed line). (**c**) Distribution of anomalous difference electron densities of TEAs bound to mutants of Glu221. The position of TEAs bound to WT is shown for comparison (dashed line).

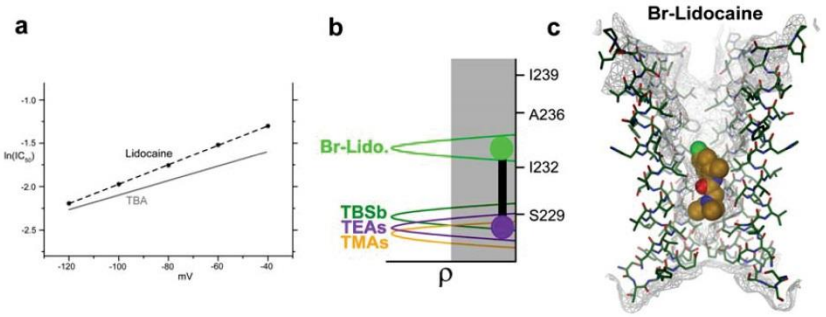

Supplementary Figure 4 Lidocaine block. (**a**) Voltage dependence of lidocaine block suggesting that the inhibitor binds at an electrical distance $z\delta = 0.27$. The voltage dependence of TBA is shown for comparison. (**b**) Distribution of anomalous difference electron densities of Br-lidocaine bound to GLIC. The positions of QA analogues are shown for comparison. The electron density for Br-lidocaine corresponds to the bromide atom attached to the aromatic ring. The extended binding region of the blocker is indicated by two connected circles. (**c**) Structure of the pore region of GLIC in complex with Br-lidocaine. A structure of the inhibitor modeled into the pore is shown in space-filling representation.

Nature Structural & Molecular Biology: doi:10.1038/nsmb.1933

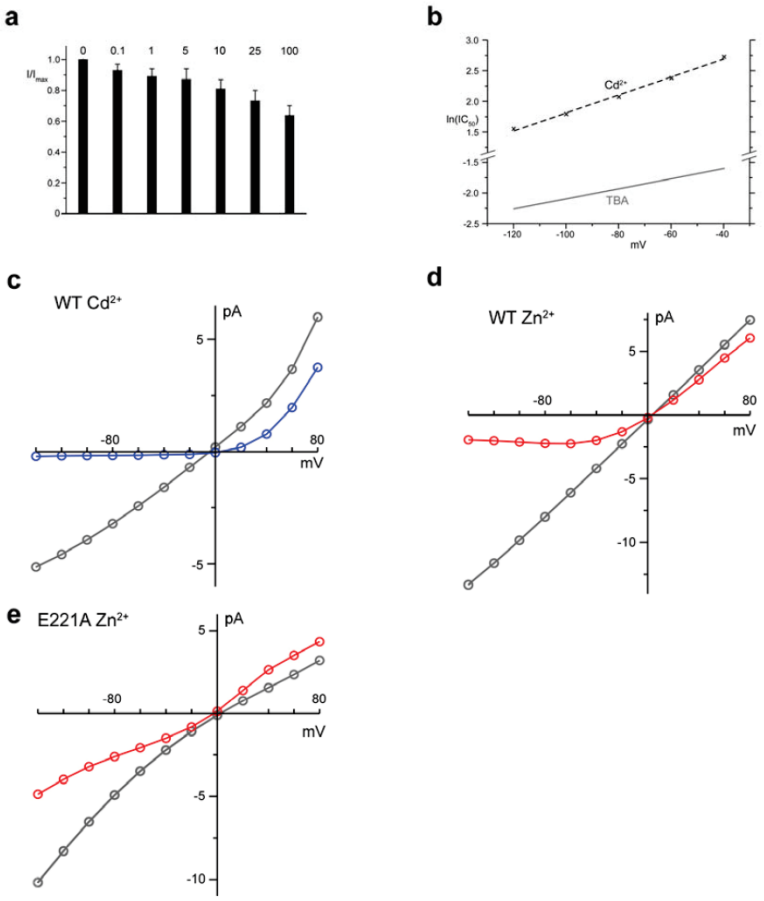

Supplementary Figure 5 Transition metal ion block of GLIC. (**a**) Fraction of the initial currents recovered after subsequent steps of incubation with Cd^{2+} at increasing concentrations. Cd^{2+} concentrations (mM) are indicated above. The currents were measured at -80mV after re-equilibration with bath solution at pH 4.0. The average of 10 measurements and their standard deviations are shown. (**b**) Voltage dependence of Cd^{2+} block suggesting that the divalent ion binds at an electrical distance of $z\delta$ = 0.17. (**c**) Representative current-voltage relationship of GLIC recorded from an extracellular solution (pH 4.0) containing 75 mM Cd^{2+} (blue). The currents after reequilibration in solutions without Cd^{2+} are shown in grey. Representative current-voltage relationship of GLIC (**d**) and the pore mutant E221A (**e**) recorded from an extracellular solution (pH 4.0) containing 200 mM Zn^{2+} (blue). The currents after reequilibration in solutions without Zn^{2+} are shown in grey.

Nature Structural & Molecular Biology: doi:10.1038/nsmb.1933

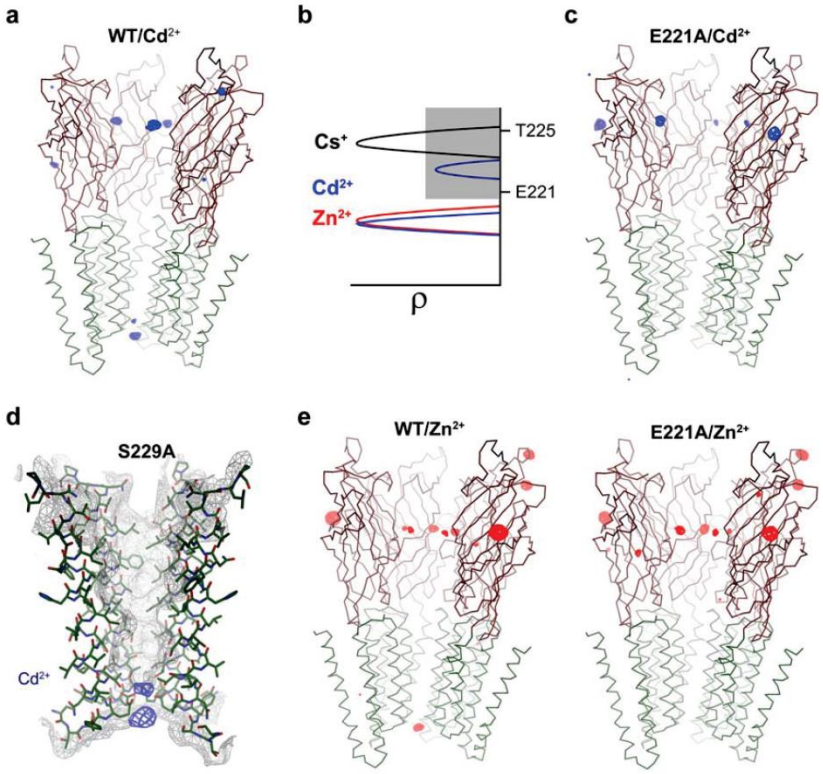

Supplementary Figure 6 Transition metal binding to GLIC. (**a**) Cα representation of GLIC in complex with Cd^{2+}. The extracellular domain is colored red, the pore domain green. The front subunit is removed for clarity. The anomalous difference electron density of Cd^{2+} was calculated at 4.0 Å and contoured at 5 σ and is shown as blue mesh. (**b**) Distribution of anomalous difference electron densities of Cd^{2+} in the pore region. Cd^{2+} ions bind to two sites indicated as blue peaks. The positions of Zn^{2+} and Cs^{+} are shown for comparison. (**c**) Cα representation of the pore mutant E221A in complex Cd^{2+}. The anomalous difference electron density of Cd^{2+} was calculated at 4.0 Å and contoured at 5 σ and is shown as blue mesh. (**d**) Structure of the pore region of S229A in complex with Cd^{2+}. The anomalous difference electron density of Cd^{2+} was calculated at 4.5 Å and contoured at 5 σ and is shown as blue mesh. (**e**) Cα representation of GLIC in complex Zn^{2+}. The anomalous difference electron density of Zn^{2+} was calculated at 4.0 Å and contoured at 4.5 σ and is shown as red mesh. (**f**) Cα representation of E221A in complex Zn^{2+}. The anomalous difference electron density of Zn^{2+} was calculated at 4.5 Å and contoured at 4.5 σ and is shown as red mesh.

Nature Structural & Molecular Biology: doi:10.1038/nsmb.1933

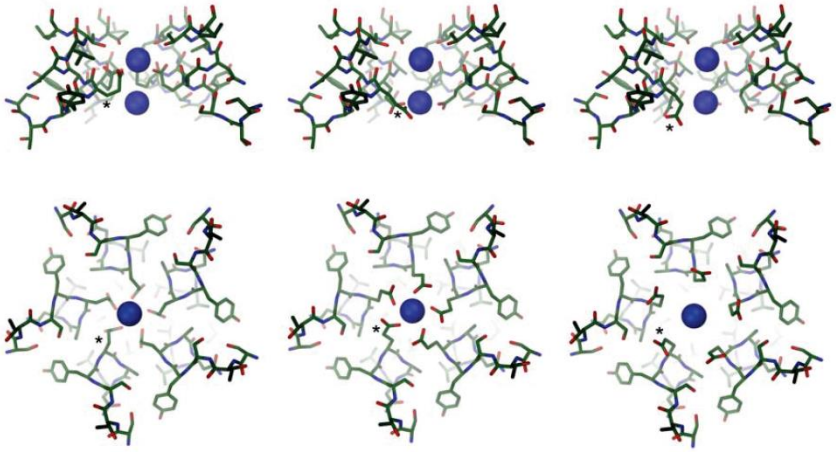

Supplementary Figure 7 Role of Glu221 in Cd^{2+} binding. Model of the binding region of Cd^{2+} ions in the pore of GLIC. Three possible side-chain conformations of Glu221 are shown in views from within the membrane (top) and from the intracellular side (bottom). Cd^{2+} ions are shown in blue. Glu221 of one subunit is labeled (*). Left: conformation as observed in the crystal structure of GLIC crystallized at pH 4.0 and determined 3.1 Å resolution (PDB code 3EHZ). Center: conformation where the Glu side chains interact with the ions in the intracellular binding site. Right: The carboxylate side chains of Glu221 are oriented away from the pore and are not in direct interaction with the ions.

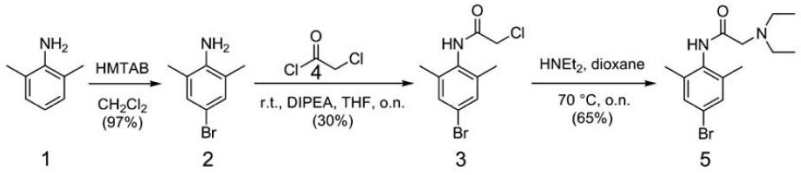

Supplementary Figure 8. The synthesis of a brominated Br-lidocaine synthesis version of lidocaine from 2,6-dimethylaniline (**1**) is illustrated. (**1**) is first selectively brominated in the 4 position, using the hexamethylenetetramine-bromine complex (HMTAB) to give 4-Bromo-2,6-dimethylaniline (**2**). This highly substituted aniline is next converted to amide (**3**), the immediate precursor of lidocaine, by treatment with the bifunctional reagent 2-chloroacetylchloride (**4**) in the presence of Huenigs base. The reaction of amide (**3**) with diethylamine completes the synthetic sequence. (**1, 2, 3, 5**) were purified by flash chromatography on a SiO_2 matrix and analyzed by standard spectroscopic techniques.

Nature Structural & Molecular Biology: doi:10.1038/nsmb.1933

2.2 Signal transduction at the domain interface of pentameric ligand-gated ion channels

Before a pLGIC can be blocked with open pore blockers, the channel first needs to be activated. The activation within the pLGIC family is initiated by the binding of a ligand to a conserved site in the extracellular domain. The following conformational rearrangements in this part of the protein are transduced through interactions in the interface to the transmembrane part of the protein to activate a selective ion permeable pore. Several studies have focused on this activation process. A study where a functional chimera of the prokaryotic extracellular domain of GLIC and the eukaryotic pore domain of GlyR were constructed showed that this chimera was only functional if the β1 - β2 turn of the pore domain and the α2 - α3 loops of the extracellular domain were from the same homologue (*61*). This study indicated that these two loops form an interaction network which is important for channel activation. Further studies have led to the identification of several key residues in the interface region of the nAChR, which were proposed to be part of the 'principal pathway of gating' (*45*) and the 'cys-loop' pathway (*46*). The residues of these pathways are highly conserved within the family and are located on four loops in close vicinity of the interface between the extracellular- and the pore domain. The loops harboring these residues include the β1 - β2, the cys-, the β8 - β9, the β10 - α1 and the α2 - α3 loop (*46*).

With the appearance of high resolution structures (*6, 33, 49, 50*) from family members of the pLGIC, insights into the structural relationship between conserved residues could be obtained. But due to the ambiguity to assign the structures to a specific state within the activation process and the complexity of structure function relationships, the detailed mechanisms of gating remained unclear.

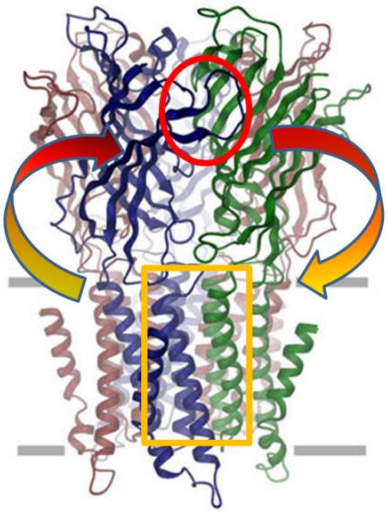

Figure 19: Side view of the pLGIC ELIC. Highlighted in red is the ligand binding domain and in orange the pore domain. It is apparent that ligand binding must induce a structural rearrangement over a large distance to trigger the opening of the pore.

In this study, I aimed to characterize the interactions at the domain interface responsible for the transduction of conformational changes between both folded entities of the prokaryotic homologues ELIC and GLIC. My study has revealed a conserved cluster of residues, which play a key role in the transduction of signals and is in overall agreement with the published data on the prokaryotic and eukaryotic homologues.

2.2.1 Alanine scanning mutagenesis of the domain interface

To investigate the role of interactions in the interface between the extracellular and the transmembrane domain of pentameric ligand gated ion channels, I have mutated residues that make contacts between these domains and certain residues that are in close proximity to the interface in ELIC and GLIC to alanine. My mutagenesis study has also included conserved residues forming a branched salt bridge in GLIC, which are only partly present in ELIC. This salt bridge was previously identified to display a strong effect on gating in the nAChR and was thus assigned to contribute to the 'principle pathway of gating' (*45*). The interacting regions were grouped, according to their location in the protein (i.e. β1 - β2 turn, β6 - β7 loop (cys-loop), β8 - β9 loop, α2 - α3 loop and the residues of the β10 - α1 linker region, Figure 20).

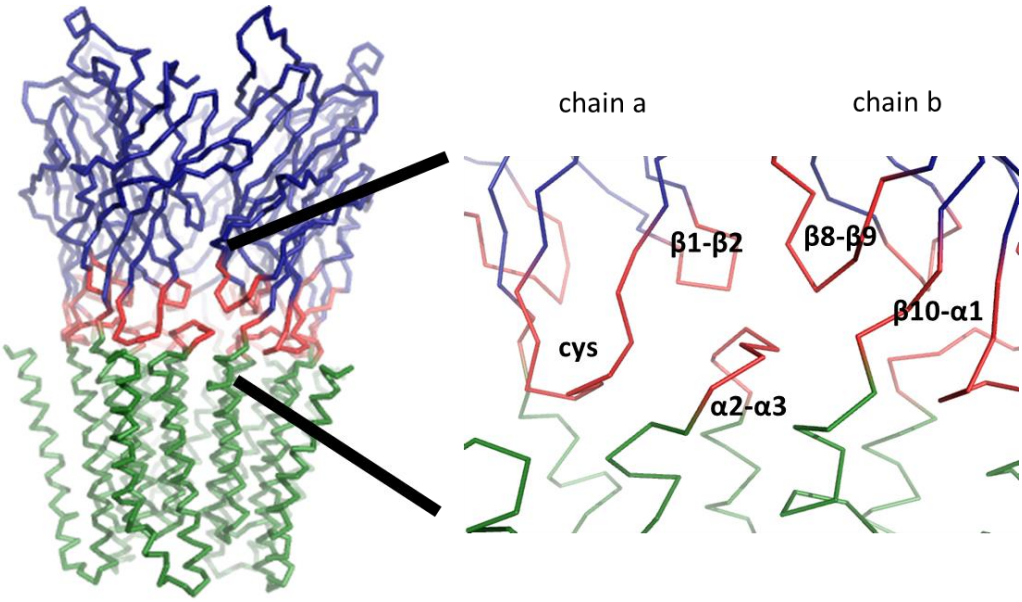

Figure 20: [left] Ribbon representation of GLIC (PDB code 3EHZ). The extracellular domain is colored in blue, the pore domain in green and the residues at the domain interface, which were investigated in the mutagenesis study, in red. [right] A closer look into the interface region between the pore and the extracellular domain of two adjacent subunits, the investigated loops were labeled accordingly.

A multiple sequence alignment of prokaryotic and eukaryotic pLGICs (Figure 21) illustrates that, despite the low overall sequence identiy (below 30%), residues of the domain interface are highly conserved. For example the motif of **D**X**R**X**ZPFD**X**Q** (single letter code; Z = any aromatic residue) in the β6 - β7 loop, (the cys-loop), and the arginine of the β10 - α1 linker are conserved throughout the family (red boxes in Figure 21).

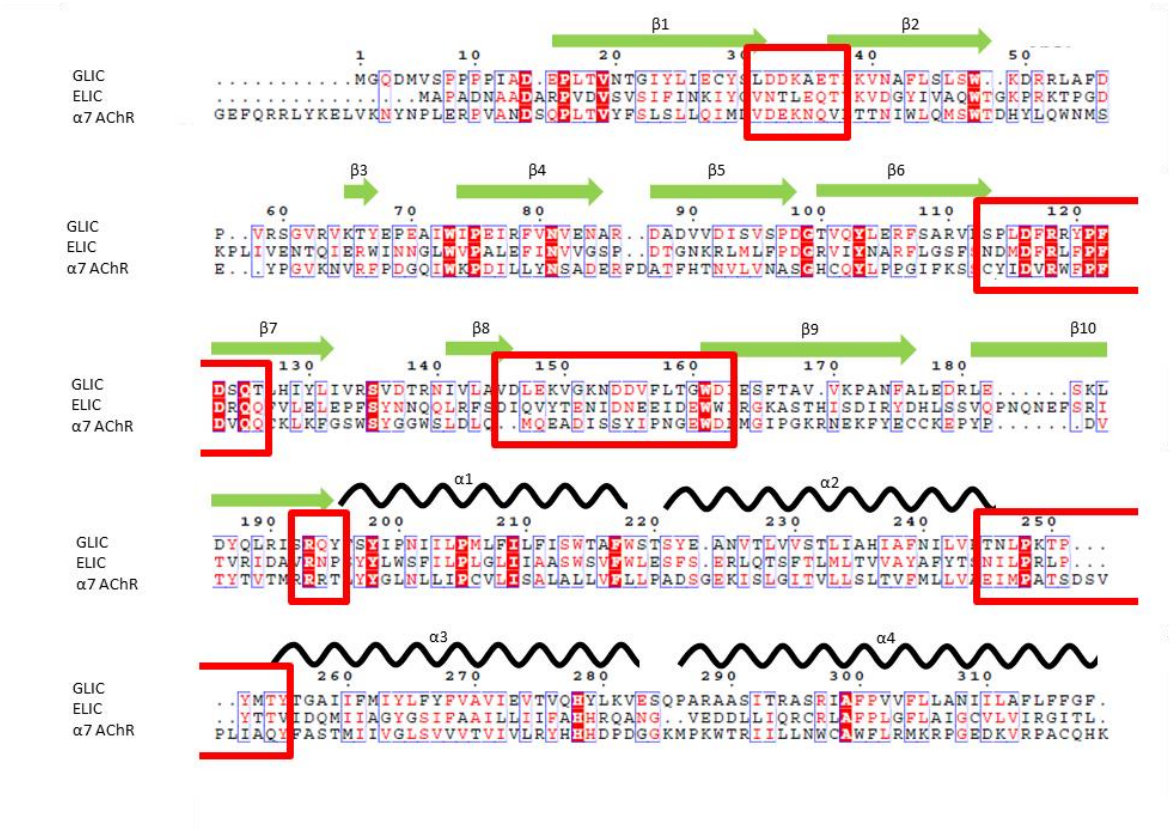

Figure 21: Sequence alignment of the prokaryotic homologues GLIC (top), ELIC (middle) and the eukaryotic mouse α7 nicotinic Acetylcholine Receptor (α7 nAChR). All proteins are from the cation selective branch of the pLGIC family. The red boxes indicate the interface region on which this study has focused. The conservation within the sequence is indicated as follows: In red boxes and white font (X) are the residues which are conserved in all three homologues. In red letters (X) are the conserved residues in two homologues. In blue boxes are stretches of at least two conserved residues.

Initially, I have made alanine point mutants of interface residues and studied these mutants in *Xenopus laevis* oocytes. For that purposed complementary RNA (cRNA) transcribing the mutant proteins with an N terminal hemagglutinin (HA) fusion tag was injected into the oocytes. The surface expression levels of the tagged channels were detected and quantified by immunolabeling methods (ELISA (*66*)) using an antibody recognizing the HA-tag. The signals for each mutant was subtracted from the background obtained from uninjected oocytes and normalized to the expression signal of WT. For comparison background and WT were quantified with every round of measurements. In this analysis most mutants showed robust surface expression in both ELIC and GLIC and only for few positions the surface expression was strongly decreased (smaller than two and a half times over the background, Figure 22 for GLIC (top) and for ELIC (bottom)).

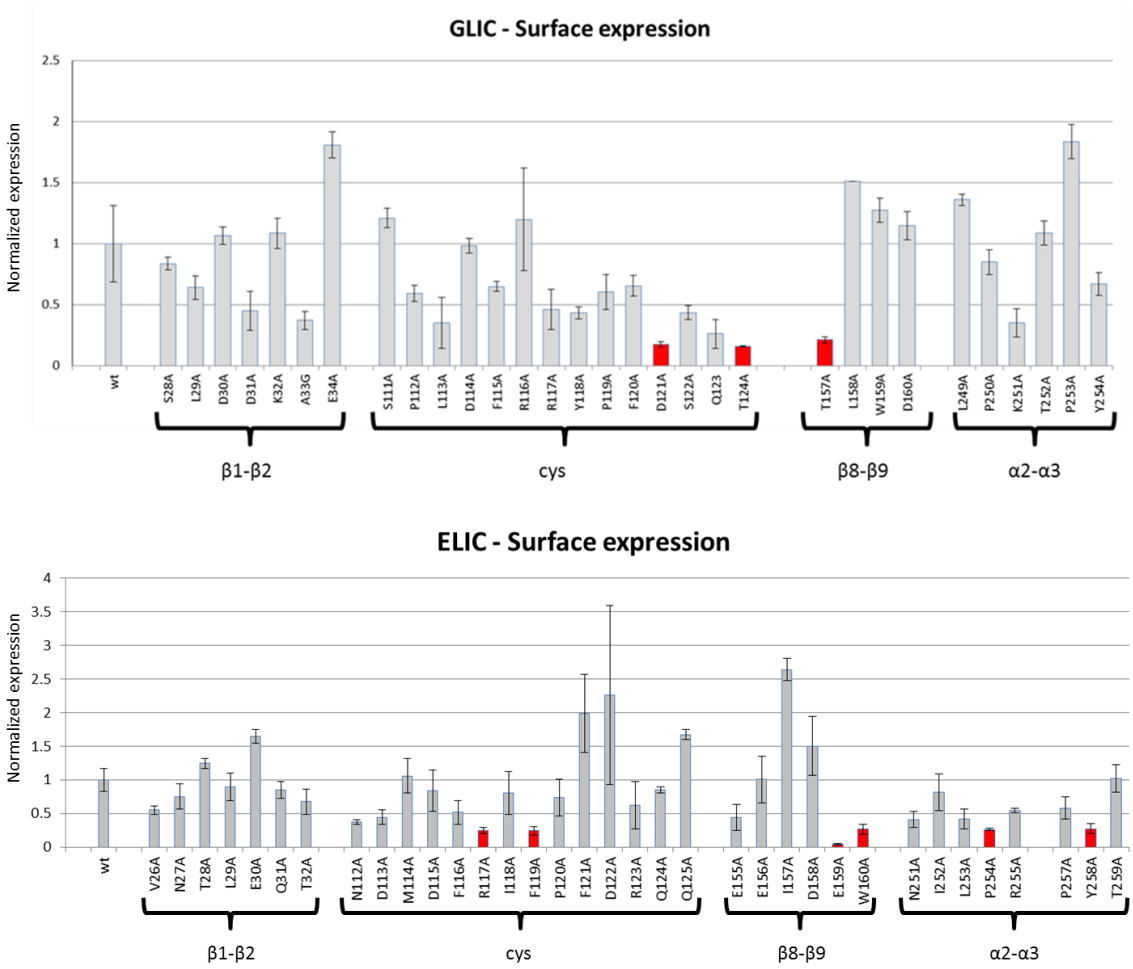

Figure 22: Surface expression of different mutants of GLIC (top) and ELIC (bottom). The signals were normalized to WT (left). Averages are from at least three independent measurements, with the standard error (SEM) shown in black bars. The majority of the mutants show robust expression levels. Mutants that are weakly expressed (<=2.5x background signal of an empty oocyte) are labeled in red.

In GLIC, the low expressing mutants were: D121A, T124A and T157A (Figure 22 top). Interestingly the D121, of the cys-loop, concerns a conserved residue involved in the proposed 'principal pathway of gating'. The role of T124, of the cys-loop, is not obvious, as it does not have any direct interaction partner and its side chain is pointing into the solvent away from the protein. The T157 of the β8 - β9 loop does also not have a direct interaction partner, but it is in close vicinity of the β1 - β2 turn (Figure 23 left), which might be important.

In ELIC the mutant E159A showed only weak signal and was therefore considered to be non-expressing. This mutant is located in the β8 - β9 loop and points towards the internal vestibule of the extracellular domain where it faces the α2 - α3, the β10 - α1 and the β2 - β3 loops and could thus play role in the activation process.

Low expression in mutants of ELIC was found at following positions: R117A, F119A, W160A, P254A and Y258A (Figure 22 bottom). In most cases the location of the residue provides a possible cause for the decreased expression. R117 of the cys-loop is pointing away from the extracellular domain into the solvent and has thus no obvious importance in subunit-subunit or any other protein interaction. F119 is a conserved hydrophobic residue in the cys-loop, which points into a hydrophobic core between the β1 - β2 and the cys-loop,

which might be very important for protein stability. W160 is a conserved hydrophobic residue of the β8 - β9 loop which points towards the β10 - α1 linker and the cys-loop. P254 is a conserved residue of the only pore loop, the α2 - α3, in the interface region, which has been proposed to be important in channel opening (*5*, *46*). And the Y258 is a conserved residue in the α2 - α3 loop, which point towards the hydrophobic core of the β1 - β2 and the cys-loop (Figure 23 right).

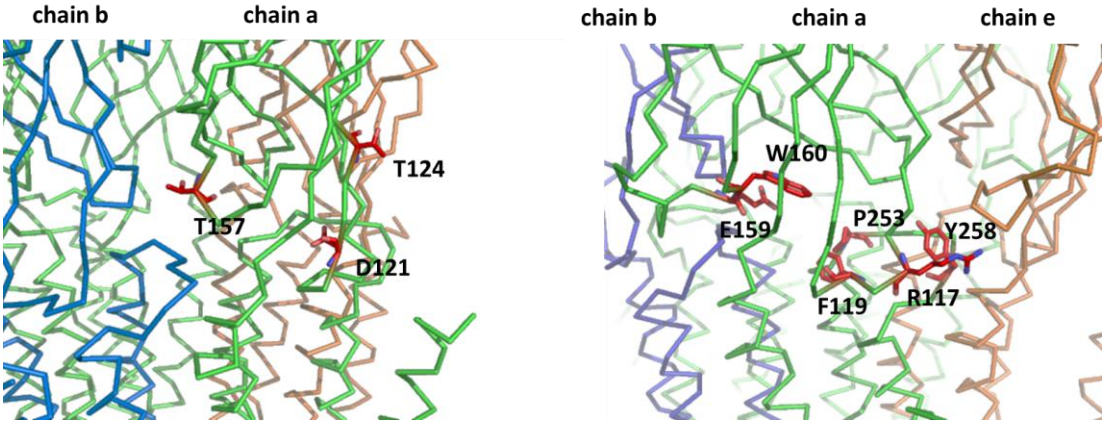

Figure 23: Position of the low expressing alanine mutants in GLIC (left) and ELIC (right). The channels (GLIC and ELIC) are shown in ribbon representation, the mutants are labeled and shown as sticks (red).

After analyzing the expression of mutants on the surface of the oocytes, experiments were performed to test their ability to activate and thus to from a functional channel. For this reason oocytes were again injected with cRNA encoding the mutated channel fused to an N-terminal HA-tag and additionally studied by two-electrode voltage clamp (2EVC) experiments. For this the oocytes were clamped at a holding potential of -50 mV, while the evoked current over the membrane after the application of high concentrations of the agonist was measured. The agonist concentrations (5 mM and 25 mM cysteamine for ELIC and pH 4 and pH 3.5 for GLIC) were chosen to also activate mutants which require higher concentrations of the ligand for compared to the WT channel (Figure 24). After the 2EVC recording, the surface expression of the channel on the same oocyte was detected. These experiments gave an overview about which mutants are still able to activate and for those not being able to activate to see whether they are present in the membrane of the oocyte.

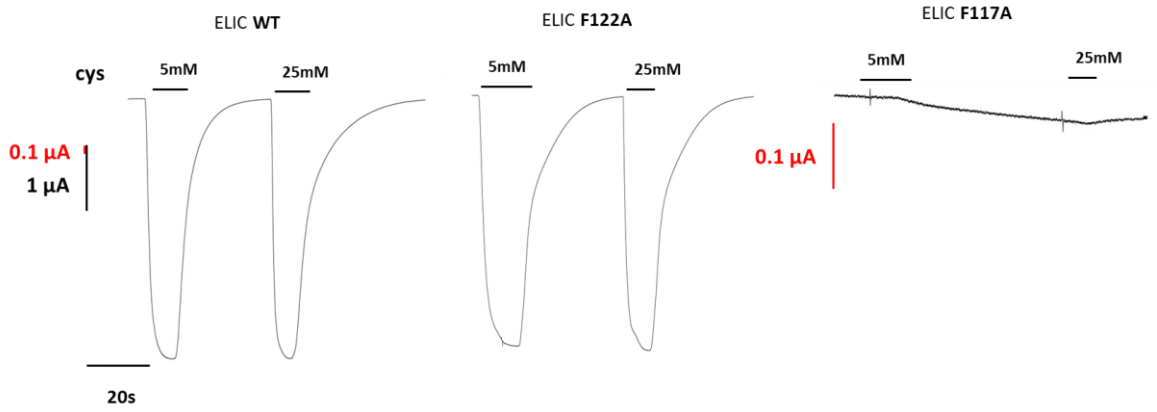

Figure 24: 2EVC activation experiment of ELIC mutants. The holding potential was -60mV. To analyze whether the mutated channels expressed on the surface of the oocytes can still be activated, two different concentrations (5 mM and 25 mM) of the agonist cysteamine (cys) were applied and the evoked current over the membrane were recorded. Two mutants (F122A and the F117A) are shown as an example. While the mutant F122A still activates, the mutant F117A does not even show residual currents despite its robust surface expression and was therefore labelled as 'loss of function'.

While most mutations showed activation similar to the WT channel, few mutations showed no or only residual response upon agonist application (Figure 24 and Table 1), despite being expressed on the surface of the oocyte. As these 'loss of function' mutants are not in the vicinity of the ligand binding domain, the signal transduction from ligand binding to the pore opening might be interrupted.

loop	GLIC	ELIC
β1 - β2	D31A	
cys	F115A	F116A
	R117A	
	Y118A	F119A
	P119A	P120A
	F120A	
	D121A	D122A
α2 - α3	L249A	L253A
	T252A	L256A
	Y254A	Y258A

Table 1: 'Loss of function' mutants in both homologues, which show no or only slightly above residual currents upon agonist application. The mutants are grouped according to their location in the protein. Equivalent positions in ELIC and GLIC are in the same row of the table. This data indicate a similar behavior between the two proteins in seven out of ten positions.

No mutation was identified where the channel has shown large basal activity. In most positions ELIC and GLIC had a similar phenotype, but there are some residues where differences between the two homologues could be observed. The mutation D31A in GLIC, for example, does not activate anymore, while the mutation of the equivalent position in ELIC, a threonine, can still be activated. In both homologues most residues which lead to

an inactive channel were found in the cys-loop and the loop connecting helices α2 and α3 in the pore region (Table 1 and Figure 23).

For the cys-loop the conserved 'loss of function' positions are residues which either change the flexibility of the loop (ELIC Pro120, GLIC Pro119), bulky hydrophobic residues (ELIC Phe116, GLIC Phe115 and ELIC Phe119, GLIC Tyr118) or charged residues (ELIC Asp122, GLIC Asp121). The hydrophobic residues point into a tightly packed hydrophobic core between the cys-loop and the β1 - β2 turn. The charged Asp residue is part of the 'principal pathway of gating', where it forms a conserved salt bridge with an Arg of the β10 - α1 linker.

In the α2 - α3 loop, three residues could be found which are pointing towards the same hydrophobic core of the cys-loop and the β1 - β2 turn: The (ELIC Leu253, GLIC Leu249), the (ELIC Tyr258, GLIC Tyr258) and a non-conserved residue (ELIC Leu256, GLIC Thr252).

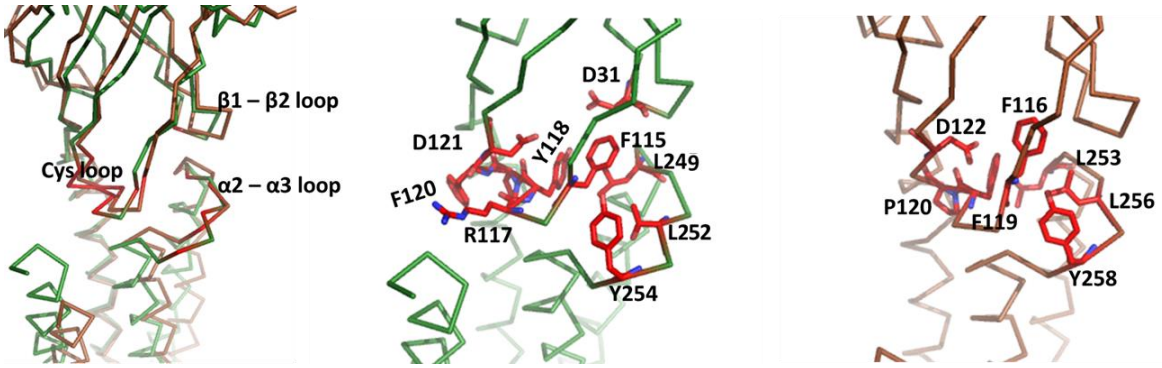

Figure 25: Position of 'loss of function' mutant. (left) Superposition of ELIC (brown) and GLIC (green) in ribbon representation with the interface loops labeled accordingly. The positions of the 'loss of function' mutants are highlighted in red. (middle) Ribbon representation of GLIC (green) with the 'loss of function' mutants shown as sticks (red) and labeled accordingly. (right) Ribbon representation of ELIC (brown) with the 'loss of function' mutants shown as sticks (red) and labeled accordingly.

Overall the experiments showed a similar activation pattern for mutations in both homologues. This behavior is particularly pronounced for the 'loss of function mutants' thus underlining that these positions may be critical for the transduction of conformational changes between the two domains. Furthermore, the results underline the high structural and functional conservation in these loops, which indicates a similar gating mechanism of the two proteins that is likely conserved within the entire family (Figure 21 and Table 1).

2.2.2 Characterization of non-activating mutants in the domain interface

The 'loss of function' mutants where subsequently investigated whether they are still able to fold properly. For this purpose, the proteins were expressed in *E. coli* with a cleavable N-terminal expression and purification tag (*33, 40, 49, 50*). Equivalent amounts of cells were used for purification of each mutant. After extraction in the detergent n-dodecyl-β-D-maltoside (DDM) and affinity purification on Ni-NTA, the N-terminal tags of the proteins were cleaved and removed by an additional Ni-NTA purification step. Subsequently each

mutant was subjected to size exclusion chromatography. The protein was detected by recording of its tryptophan fluorescence (excitation: 280 nm, emission: 320 nm). The peak height of each mutant at the corresponding elution volume was then compared to the peak height of the WT protein (Figure 26). Most mutants could be expressed, purified and were stable in detergent solution, thus indicating proper folding.

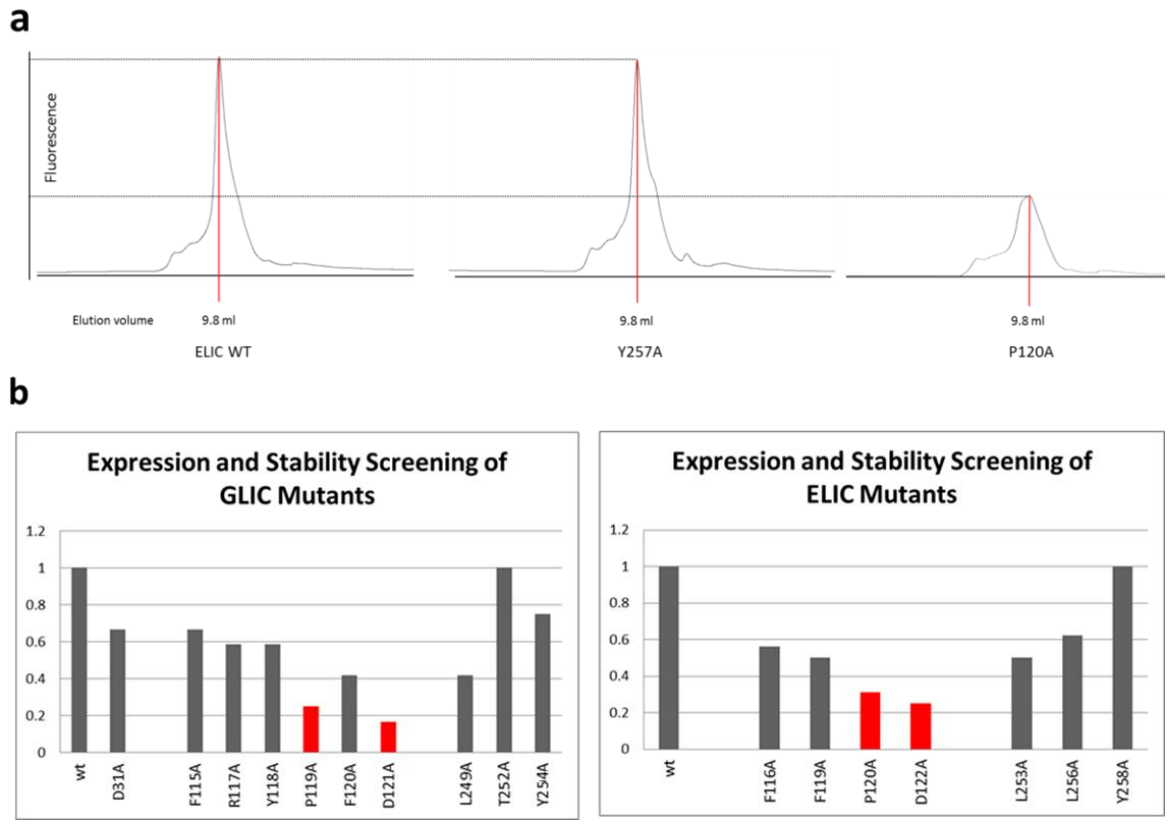

Figure 26: (a) Expression and stability test of ELIC mutants. In this picture the behavior of two mutants (Y258A and P120A) is illustrated. The curves show the recoded Trp fluorescence of each protein during their elution from a G3000SWXL gel-filtration column. For each mutant the peak height at the elution volume (red line at 9.8 ml) was used for analysis. (b) Table of all investigated mutants of GLIC (left) and ELIC (right). The mutants, which showed significant decrease in expression and stability, were highlighted in red.

From the entire set of positions only two mutants replacing a conserved proline and aspartate in the cys-loop showed significant lower expression and stability in both homologues (Figure 26 b).

Structural studies were undertaken in order to investigate whether these 'loss of function' mutants might reveal their inability to activate on a structural level. In ELIC, the mutants F119A of the cys-loop and L256A of the α2 - α3 loop did not show any crystals in initial attempts. For the F116A of the cys-loop and the Y258A of the α2 - α3 loop data sets were collected, which both allowed structure determination at 3.5 Å and 3.2 Å respectively. In both cases, the protein crystallized in the same non-conducting conformation that has been observed in all currently determined ELIC structures (*49, 58, 67-69*). This emphasizes the stability of this state in detergent solution. Small differences in loop conformations in the vicinity of the mutations indicate a local rearrangement of protein interactions. In the F116A mutant, the adjacent β1 - β2 turn moved into the position, which was previously occupied by the bulky phenylalanine (Figure 27). This small change could nevertheless

explain the loss of function, since the β1 - β2 turn moves further away from the α2 - α3 pore loop. The interactions between the β1 - β2 and the α2 - α3 loop have been indicated in several studies as important determinant of channel activation (*5*, *6*, *46*, *57*, *62*, *70*).

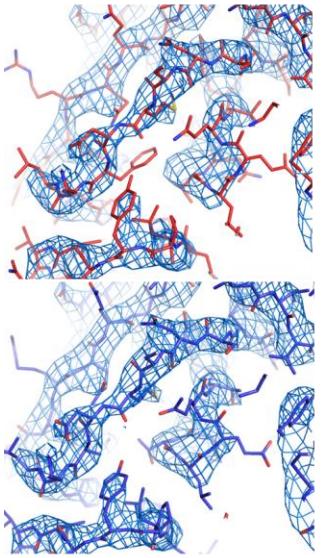

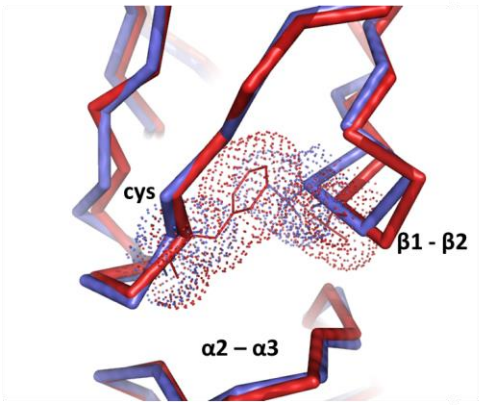

	ELIC F116A
Data collection	
Space group	P21
Cell dimensions	
a, *b*, *c* (Å)	105.0, 266.7, 110.7
α, *β*, *γ* (°)	90.0, 110.2, 90.0
Resolution (Å)	50–3.5
R_{merge}*	16 (60)
$I / \sigma I$ *	9.8 (2)
Completeness (%) *	98.8 (98)
Redundancy *	3.0 (2.7)
Refinement	
Resolution (Å)	30–3.5
No. reflections	78813
R_{work}/ R_{free}	23.5/ 27.1
No. atoms	
Protein	24,960
Ligand/ion	
B-factors	
Protein	113.9
Ligand/ion	
R.m.s. deviations	7.87
Bond lengths (Å)	0.003
Bond angles (°)	0.69

*Values in parentheses are for highest-resolution shell.

Figure 27: [left top] 2Fo-Fc Electron density (blue mesh, contoured at 1.5 σ) of the refined ELIC mutant F116A mutant superimposed on the model of WT (PDB 2VLO, red). The electron density clearly indicates the loss of the Phe side chain whereas the rest of the cys-loop remains unchanged. The adjacent β1 - β2 turn does not fit into the density of WT. [left bottom] The refined model of F116A accounts for the conformational change of the β1 - β2 loop. [right] Superposition of the ELIC WT (red) and the F116A (blue) mutation in ribbon representation. The mutated amino acid is shown in sticks and its van der Waals Radii as dotted spheres. It is visible that upon mutation the β1 - β2 turn moves into the space previously occupied by the F116, while the cys-loop remains unchanged.

For the mutant Y258A, in the α2 - α3 loop, a different picture was obtained. There, both loops, the α2 - α3 and the β8 - β9 loop, which in WT are in close proximity have moved apart from one another (Figure 28). The changes in this mutant emphasize the interaction of the pore-domain loop with the β8 - β9 loop and it suggests that upon interruption of this interaction, the channel loses its ability to open. Both structures emphasize that the interface contains a tight network of interactions where even slight changes lead to drastic effects.

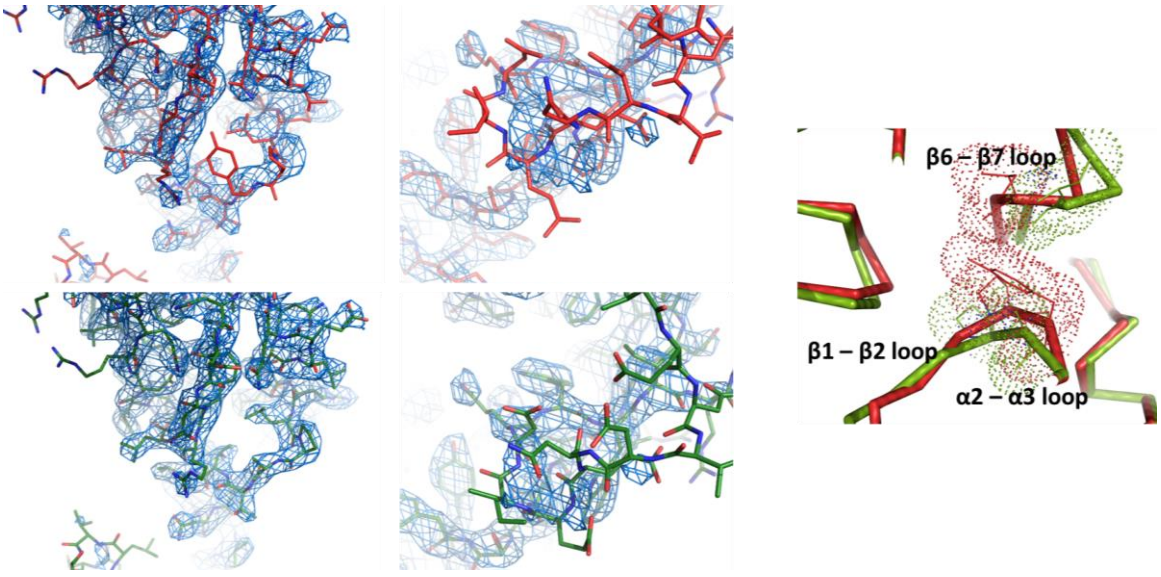

Figure 28: [left top] 2Fo-Fc electron density (blue mesh, contoured at 1.5σ) of the Y257A mutant around the α2 - α3 loop superimposed on ELIC WT (2VLO, red). The loss of the side chain of Tyr258 t in the density is apparent. The poor fit of the loop indicates a local structural rearrangement. [left bottom] Refined model of Y258A (green). [middle top] Conformational changes around the β8 - β9 loop. WT does not interpret the density correctly, while in the refined Y258A structure the fit has improved (middle bottom). [right] Superposition of ELIC WT (red) and the mutation Y258A (green) in ribbon representation. The mutated amino acid is shown in sticks and its van der Waals Radii as dotted spheres. The α2 - α3 loop and the β8 - β9 loop slightly move away from one another, as if a connection was broken.

	ELIC Y258A
Data collection	
Space group	P21
Cell dimensions	
a, *b*, *c* (Å)	105.0, 266.4, 110.0
α, *β*, *γ* (°)	90.0, 110.4, 90.0
Resolution (Å)	50–3.2
R_{merge}*	8.3 (67.5)
$I / \sigma I$ *	11.2 (2.2)
Completeness (%) *	99.9 (98.8)
Redundancy *	3.9 (3.2)
Refinement	
Resolution (Å)	30–3.2
No. reflections	93222
$R_{work/}$ R_{free}	22.8/ 27.5
No. atoms	
Protein	24,950
Ligand/ion	
B-factors	
Protein	83.2
Ligand/ion	
R.m.s. deviations	10.9
Bond lengths (Å)	0.01
Bond angles (°)	1.36

*Values in parentheses are for highest-resolution shell.

Table 6: Data collection and refinement statistics for the ELIC mutant Y258A.

Despite broad screening of conditions, no crystals diffracting to high resolution were obtained for the corresponding mutants in GLIC.

The structural data in ELIC demonstrate that the mutations, despite their severe phenotype on channel activation, have only a local effect on the protein conformation. To exclude that the two non-activating mutations in ELIC have compromised the ability of the protein to bind its ligand, we have studied agonist and antagonist binding by isothermal titration calorimetry (ITC). For this purpose we have purified the protein at a similar scale as used for structural studies. In an ITC experiment the heat exchanged in response to the addition of a ligand to the purified channel is measured. The measurement is corrected by the heat exchange upon addition of the ligand to the buffer not containing any protein. The integrated heat per injection of ligand is plotted against the molar ratio of the protein to the ligand and fitted to a single-site binding isotherm which allows the quantification of the binding affinity (K_D).

The single-site binding isotherm and only a part of the titration curve were used to account for the limitations of the data due to the low binding affinities, which are in the mM range. For such a low affinities the protein concentrations needed for an accurate characterization of binding are beyond reach.

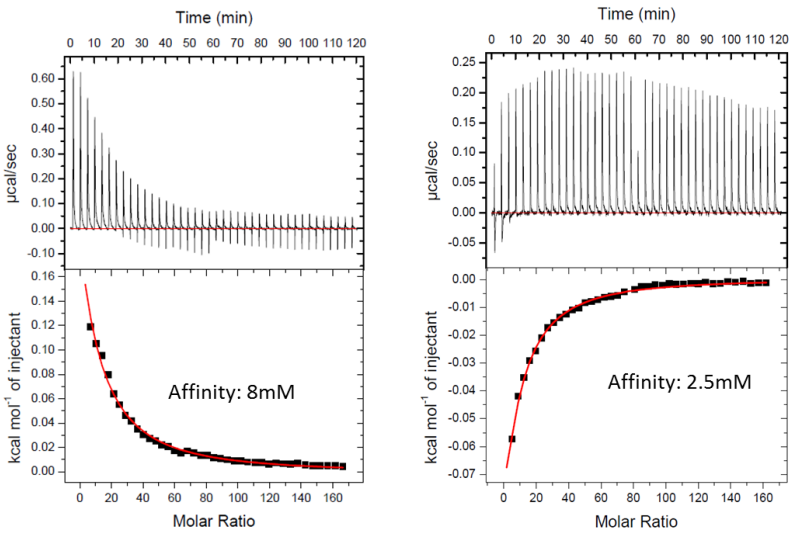

Figure 29: ITC experiment characterizing the binding of the agonist propylamine (left) and the antagonist acetylcholine (right) to ELIC WT. The exchanged heat upon addition of small aliquots of agonist or antagonist was measured (top). The (corrected) integrated values were plotted against the molar ratio between ligand and protein and fitted to a single-site bindinge isotherm (bottom).

To increase the signal of the ITC measurement, the calorimetry experiments were carried out in the background of the mutant R91A of the ligand binding site. This mutant has previously been shown to increase the binding affinity for the agonists cysteamine and propylamine (*58*) and the competitive antagonist acetylcholine (*67*).

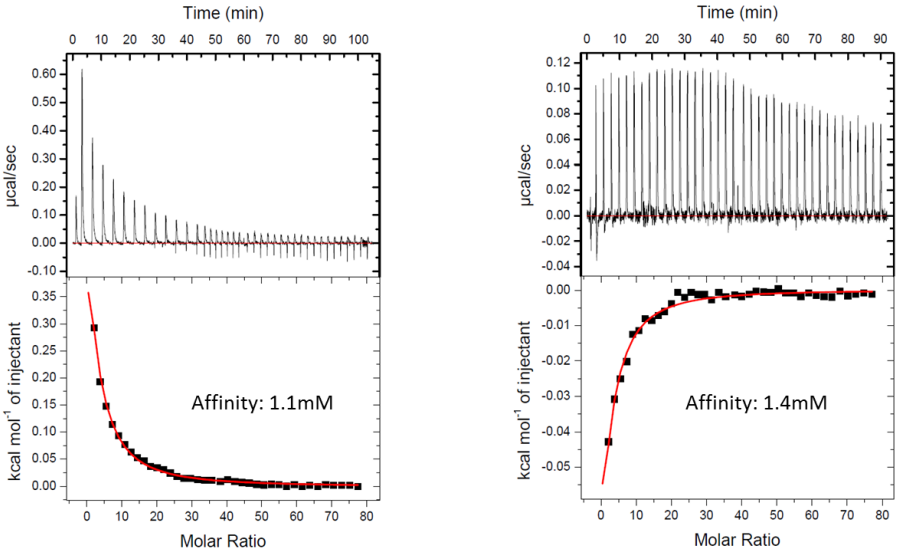

Figure 30: ITC binding experiment on propylamine (left) and acetylcholine binding (right) to the ELIC mutant R91A. The heat exchanged by addition of aliquots of the respective substances are shown (top). The corrected integrated binding energy plotted against the molar ration between ligand and protein and fitted with a single-binding site isotherm is shown on the bottom.

The results of the ITC experiment can then be compared to results obtained from 2EVC dose response experiments. In these experiments the oocyte is exposed to increasing amounts of agonist concentrations (Figure 31). The evoked currents, normalized to the maximally evoked current, is then plotted against the agonist concentration and then fitted

to a Hill-function. The concentration, which evokes half maximal currents is termed EC_{50}. The fit shows a high cooperativity for ligand activation in both homologues.

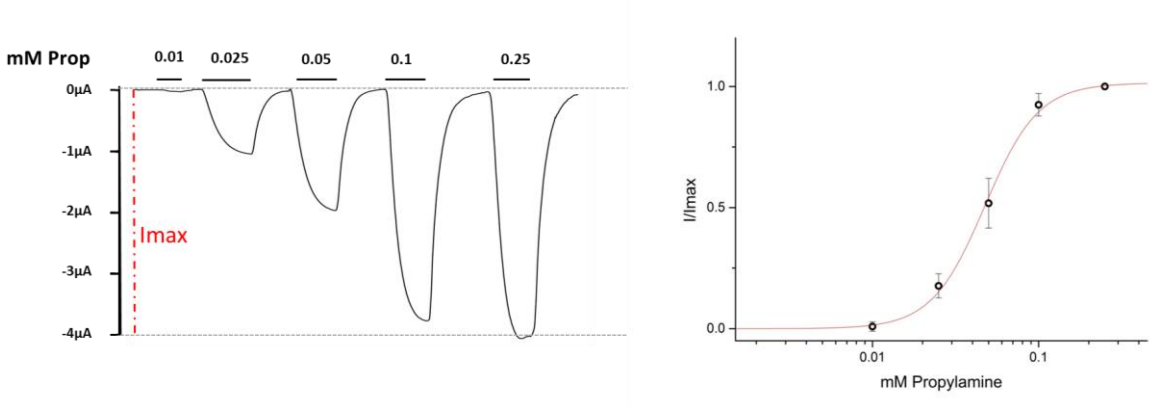

Figure 31: The current response of ELIC R91A upon application and washout of propylamine was recorded at -60 mV with the two-electrode voltage clamp technique. The application of propylamine at the respective concentration is indicated above (black bar). The relative open probability (I/Imax) plotted as a function of the ligand concentration is shown below. The currents were normalized to the maximum at saturating ligand concentration (i.e., 0.25 mM). Each data point comes from the average of 5 oocytes, their standard deviations are shown in black bars. The solid red line shows a fit to a Hill equation with a coefficient of 2.71, with an EC_{50} of 0.05 mM.

In the ITC experiment of the mutant R91A the agonist propylamine binds with a binding affinity (K_D) of 1.1 mM, while the EC_{50} of the 2EVC studies is 0.05 mM (Figure 31). Therefore, the EC_{50} is 20 times lower than the K_D measured by ITC. This difference arise from the fact how both quantities are related to one another and reflect the initial binding of the ligand and the induced conformational change ('Activation of pLGICs' 1.3). The weak affinity measured in the ITC experiment suggests that the protein in detergent solution has an efficacy of around 19 (for WT and R91A, EC_{50} from 2EVC measurements in oocytes), which is rather low then the proposed 130 from electrophysiological experiments for the WT channel in HEK cells (*71*).

The K_D of the competitive antagonist acetylcholine can then directly be measured in 2EVC experiments. In these experiments the displacement of the dose response curve of the agonist upon increasing concentration of antagonist is measured, which can be analyzed with the Schild plot to obtain the K_D for the inhibitor. For the antagonist acetylcholine in the 2EVC experiment a K_D of 0.2 mM was measured (*67*). Also the binding affinity of the antagonist is not in the same order of magnitude as the measured K_D (2.6 mM) of the ITC experiment. The differences in equivalent quantities obtained by measurements with two different techniques underlines that the energetics of binding are different in a lipid or detergent environment. Despite these discrepancies, ITC is still a valuable method to characterize ligand interactions of the non-activatable mutants. When characterized by this method in the background of the R91A mutant both non-activatable mutants, F116A and Y258A, show a similar K_D for the agonist propylamine antagonist acetylcholine as the R91A mutant (Figure 32) , which indicates that the mutations do not alter the binding of the ligand, but are disrupting channel activation.

a

	PA	Ach
	Affinity [mM]	Affinity [mM]
wt	8	2.5
R91A	1.1	1.4
F116A/R91A	0.8	1.8
Y258A/R91A	0.92	1.6

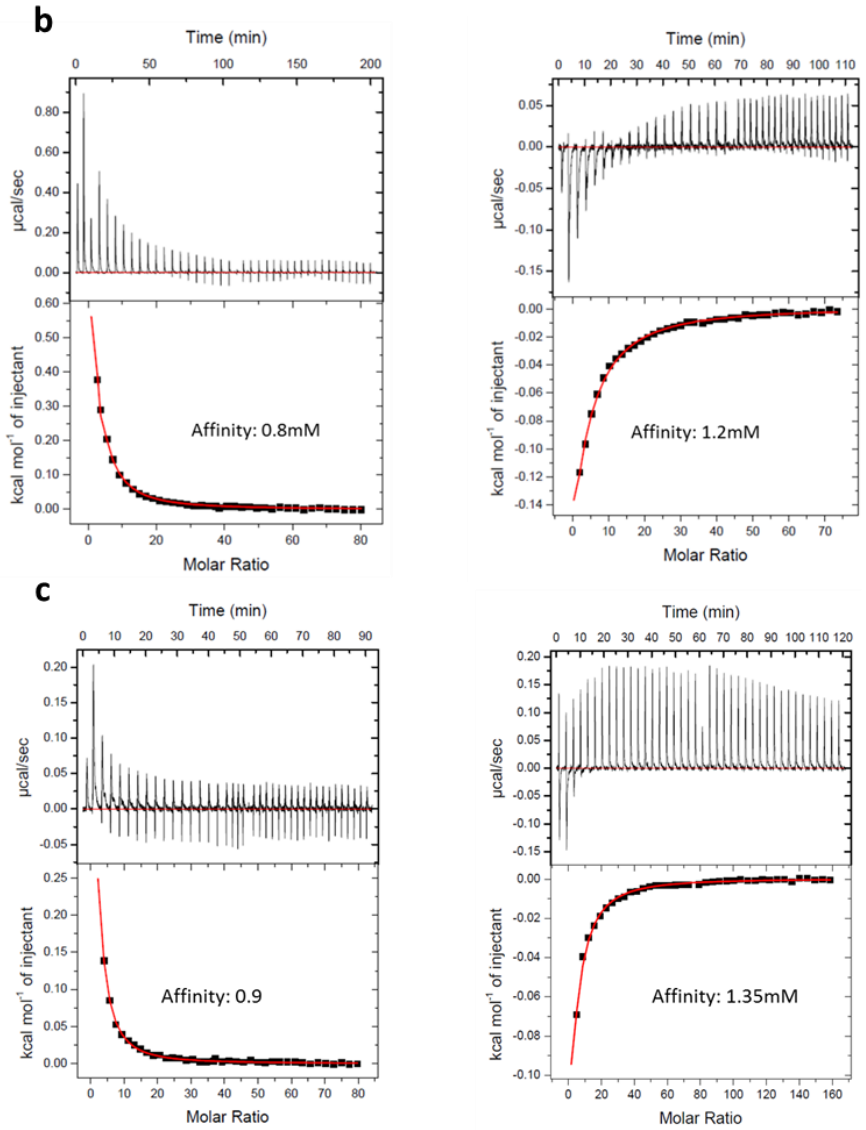

Figure 32: (a) Propylamine (left) and the acetylcholine binding (right) to the ELIC double mutants R91A/F116A (b) and R91A/Y258A (c) as quantified by ITC. Analysis is as in Fig. 29.

2.2.3 Conserved branched salt bridge

Similar to the phenylalanine of the 'loss of function' mutant in the cys-loop, the mutation of an equally conserved aspartate residue in the same region (Asp122 in ELIC and Asp121 in GLIC) results in a complete loss of function in both homologues. Only a conservative mutation to glutamate can restore channel function in both homologues (Figure 33 for ELIC (left) and for GLIC (right)). This residue is located one layer of amino acids above the interface and forms a salt bridge with a conserved arginine residue (GLIC Arg191, ELIC Arg199) at the end of β-strand 10 at the boundary to the α1 helix of the pore domain. The mutation of this residue to alanine did not show any ligand-induced currents in 2EVC experiments whereas the conservative mutation to lysine can restore channel function in both homologues (Figure 33 for ELIC (left) and for GLIC (right)).

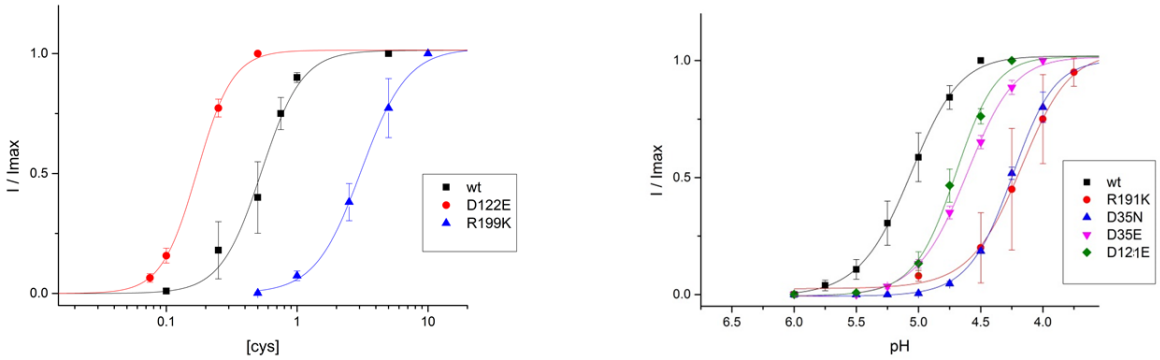

Figure 33: Dose response curves of ELIC (left) and GLIC (right) mutants from at least 5 oocytes, the standard deviation is shown in bars in the color of the corresponding mutant. (left) In ELIC the only mutations of the two residues D122 and R198, which can restore channel activation are the conservative mutations D122E (red) and R199K (blue). WT (black) is shown as a reference. (right) In GLIC the only mutations of the residues D31, D122 and R198 which can restore channel activation are D35N (blue), D35E (pink), D121E (green) and R191K (red). WT (black) is shown as a reference.

In GLIC Arg191 also interacts with Asp31 on the β-strand 2, a position that is conserved in many cys-loop receptor subunits, but not in ELIC where the respective residue is a threonine (or GluCl where it is a valine). Although in GLIC D31A is expressed on the surface of the oocytes (Figure 22), this mutation prevents channel activation (Table 1). Only the mutation of this residue to asparagine or glutamate can restore the function of the channel (Figure 33 right).

When mutating Thr28 in ELIC to aspartate, the residue present in most family members, the EC_{50} of channel activation shifts to a 20 time lower agonist concentration (Figure 35). To investigate whether a similar shift in binding affinity is observed in detergent solution ITC experiments were performed. However, due to its poor stability the mutant T28D could not be purified in the background of the R91A mutation. Therefore in this experiment only the single mutant T28D was measured. As observed in electrophysiology experiments also the ITC experiments of the mutant show a higher binding affinity. In this case the measured K_D for the agonist proylamine was 90 µM (Figure 34), which is ~100 times lower than the K_D of WT (K_D 8 mM, Figure 29). Remarkably in 2EVC experiments the T28D mutant led only to 20-fold reduction of the EC_{50} (Figure 35). In contrast to the agonist the K_D of the

antagonist acetylcholine changed only marginal in comparison to WT (2 mM T28D vs. 2.5 mM WT; see Figure 34).

a

	PA	Ach
	Affinity [mM]	Affinity [mM]
wt	8	2.5
T28D	0.09	2

b

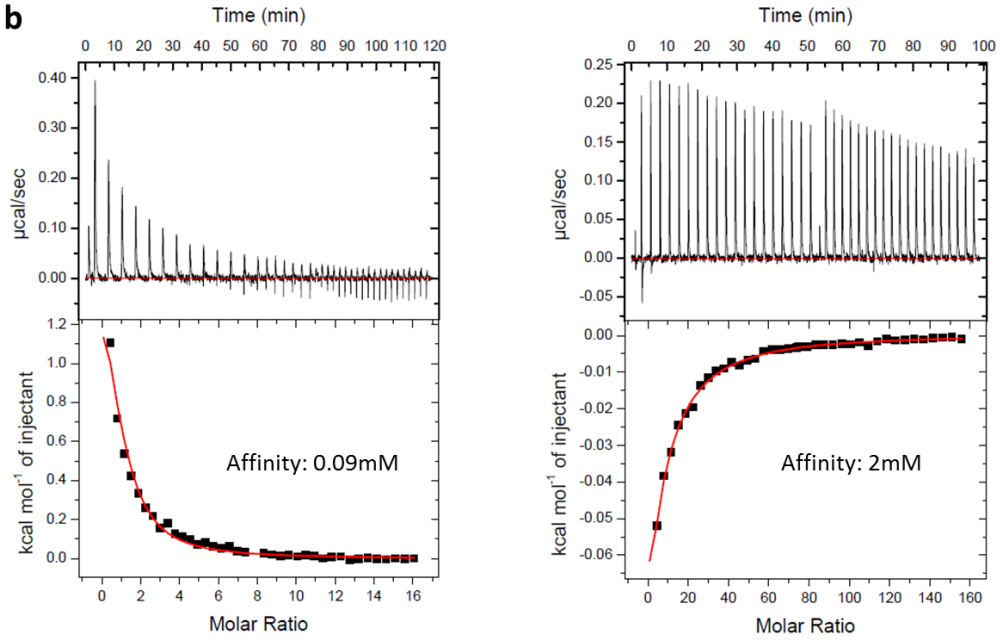

Figure 34: Propylamine (left) and the acetylcholine binding (right) to the ELIC double mutant T28D as quantified by ITC. (a) Summary of results. (b) Thermograms (top) and integrated thermogram peaks and fit (bottom). Analysis is as in Fig. 29.

The results indicate that the mutated channel may have improved properties to change its conformation in detergent solution. This assumption is based on the fact that the antagonist binding in WT and the T28D mutant does not induce any conformational change leading to channel activation, as seen in the ITC experiments (K_D for WT and T28D mutant are in the same range). For the agonist on the other hand a much higher K_D in the ITC experiments is measured for the mutant. Thus showing that the underlying changes upon agonist binding are to a certain degree accessible to this mutant.

Additional mutations to analyze the importance of this position for binding showed that corresponding mutations in ELIC have a weaker effect than in GLIC. While in GLIC, D31A leads to a loss of function in ELIC, the equivalent mutation T28A is still functional, but increases the EC_{50} by a factor of 10. The mutations of Thr28 to aspartate or asparagine led to a shift of the EC_{50} to higher affinity, while the mutation to glutamate, a larger and side

chain, has shifted the EC_{50} to a lower affinity (Figure 35). This suggested that the interaction is not only based on the coulumbic interactions, but also on the size of the residue, with the larger glutamate disturbing the interaction.
In ELIC the reversal of the charges (T28R and R199D) restores the current response upon agonist application, thus emphasizing the importance of this interaction for the transduction of conformational changes during channel activation.

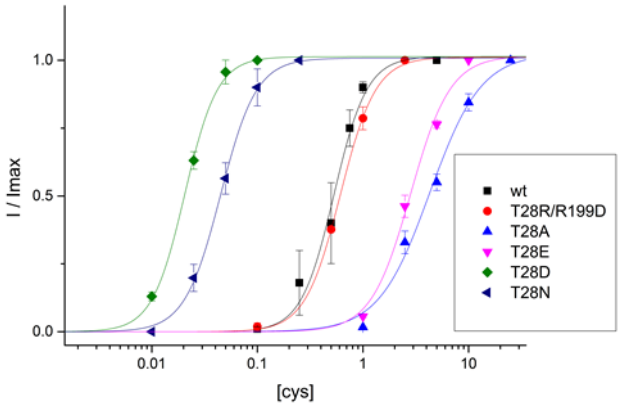

Figure 35: Dose response curves of Thr28 mutants of ELIC mutants from at least 5 oocytes, the standard deviation is shown in bars, which is part of the 'principal pathway of gating'. The experiments show a clear indication for a very strong interaction between the Arg191 and the residue present in position 28, which is dependent on the charge and the size of the respective side chain.

2.2.4 Mutagenesis of the contact region between the β1 - β2 turn and the α2 - α3 loop.

A substantial part of the domain interface is formed by the interaction of the backbone of the residue at the tip of the β1 - β2 turn with the ring of a strictly conserved proline residue in the α2 - α3 loop. This interaction is observed in the open structures of GLIC and GluCl, but not in the non-conducting structure of ELIC, where this contact is broken (*5*, *6*, *49*, *50*). It was suggested that this interaction may play an important role in the activation cycle (*5*). To investigate the proposed role of this interaction for channel activation I have studied mutations on this conserved proline by X-ray crystallography and electrophysiology. The results show that the mutation of this proline to alanine does still lead to channel activation in both proteins, with a slightly changed EC_{50} (Figure 40). In line with the small effect in functional experiments, the crystal structure of the P250A mutant in GLIC, which was determined at 3.2 Å (for statistics see Figure 36) only shows minor deviations in comparison to the respective WT (Figure 36).

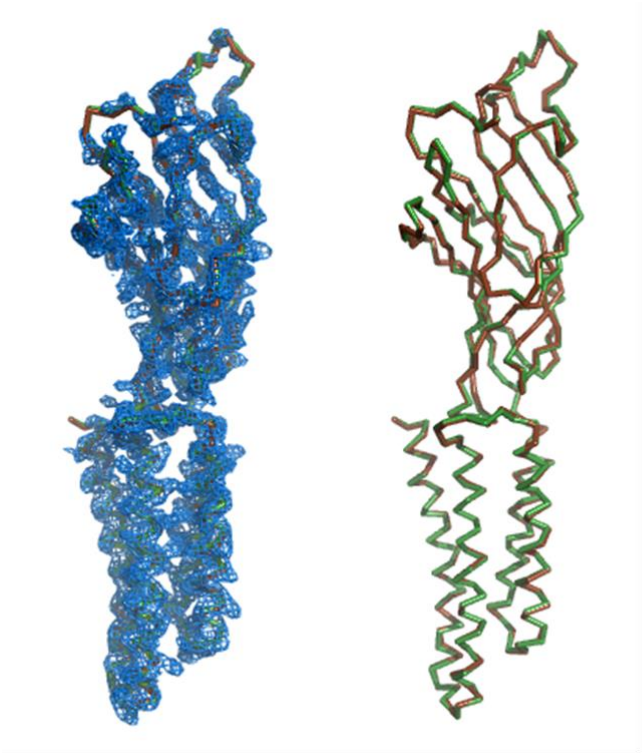

	GLIC P250A
Data collection	
Space group	C2
Cell dimensions	
a, *b*, *c* (Å)	177.7, 134.0, 160.6
α, *β*, *γ* (°)	90.0, 101.1, 90.0
Resolution (Å)	50–3.3
R_{merge}*	14.3 (53.3)
$I / \sigma I$ *	7.3 (2.2)
Completeness (%) *	99.3 (98.4)
Redundancy *	3.2 (1.7)
Refinement	
Resolution (Å)	30–3.3
No. reflections	60451
R_{work}/ R_{free}	23.1/ 25.8
No. atoms	
Protein	12,595
Ligand/ion	
B-factors	
Protein	81.4
Ligand/ion	
R.m.s. deviations	
Bond lengths (Å)	0.027
Bond angles (°)	1.52

*Values in parentheses are for highest-resolution shell.

Figure 36: [left] 2Fo-Fc electron density (blue mesh, contoured at 1.5σ) of the P250A mutant superimposed models of WT and the refined structure of the mutant. [middle] superposition of the WT (green) and the P250A (orange). There are no strong differences between the two models observed, thus indicating that both structures adopt a very similar conformation. (right) Data collection and refinement statistics for the GLIC mutant P250A.

To remove any potential side chain interaction to the ligand-binding domain, the proline was in both channels mutated to the shortest and most flexible amino acid glycine. In ELIC the mutation P254G has only a comparably small effect on the structure, which overall shows the frequently observed non-conducting conformation with a small reorganization of the well-structured α2 - α3 loop (Figure 36).

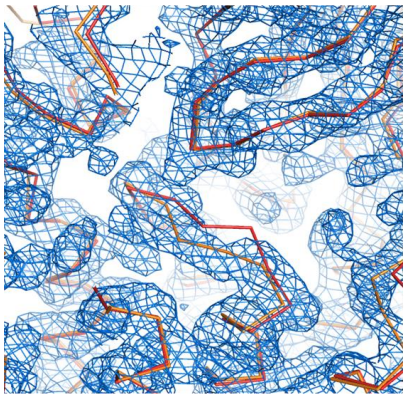

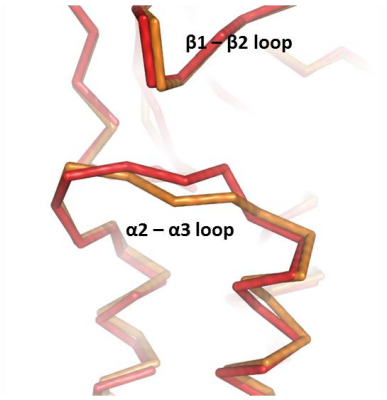

	ELIC P254G
Data collection	
Space group	P21
Cell dimensions	
a, *b*, *c* (Å)	105.0, 266.7, 110.7
α, *β*, *γ* (°)	90.0, 110.2, 90.0
Resolution (Å)	50–3.3
R_{merge}*	16 (60)
$I / \sigma I$ *	10.2 (2)
Completeness (%) *	99.9 (98.8)
Redundancy *	2.9 (2.7)
Refinement	
Resolution (Å)	30–3.3
No. reflections	86714
R_{work}/ R_{free}	22.6/ 26.3
No. atoms	
Protein	24,980
Ligand/ion	
B-factors	
Protein	89.8
Ligand/ion	
R.m.s. deviations	
Bond lengths (Å)	0.016
Bond angles (°)	1.89

*Values in parentheses are for highest-resolution shell.

Figure 37: (left) 2Fo-Fc electron density (blue mesh, contoured at 1.5 σ) of the P254G mutant superimposed on the models of WT (red) and the P254G mutant (orange) in ribbon representation. The α2 - α3 loop of the mutant undergoes a structural rearrangement. (middle) Superposition of one subunit of the WT structure (PDB code 2VLO) in red and the mutant P254G in orange. The overall structural elements are identical, only a change in the α2 - α3 loop is apparent. (right) Data collection and refinement statistics for the ELIC mutant P254G.

The equivalent mutation P250G in GLIC resulted in large rearrangements of the pore when compared to the WT structure. The structure was determined at 3.3 Å and shows a molecule with small differences for most of the protein except for the α2 - α3 loop and the pore-lining helix α2, which both have undergone major conformational changes. The introduced flexibility by replacing the least flexible with the most flexible amino-acid has resulted in the rearrangement of the α2 - α3 loop and the unfolding of the C-terminal part of the helix α2. The remainder of the helix collapsed towards the pore axis.

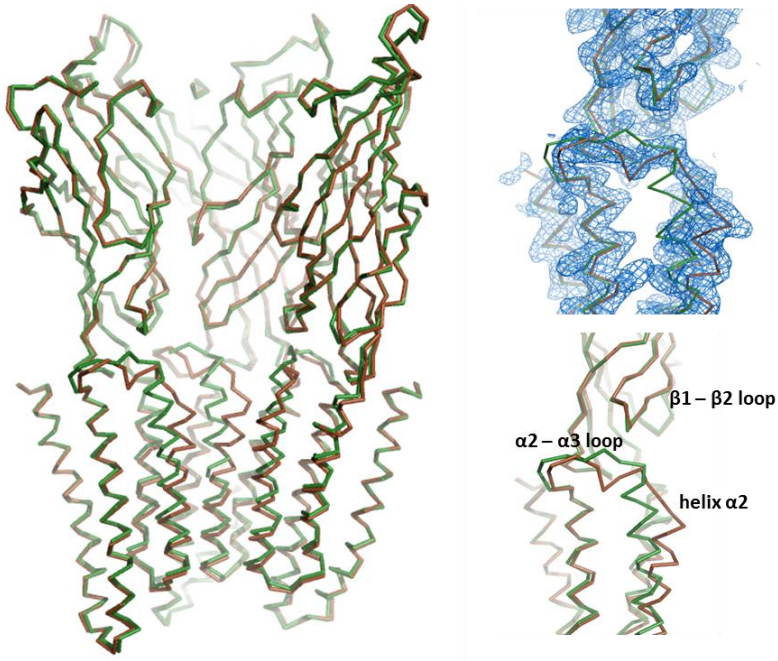

	GLIC P250G
Data collection	
Space group	C2
Cell dimensions	
a, *b*, *c* (Å)	178.9, 133.3, 160.0
α, *β*, *γ* (°)	90.0, 101.7, 90.0
Resolution (Å)	50–3.2
R_{merge}*	20 (72)
$I / \sigma I$ *	7.0 (2.3)
Completeness (%) *	87.9 (82.5)
Redundancy *	3.2 (2.2)
Refinement	
Resolution (Å)	30–3.2
No. reflections	73819
R_{work}/ R_{free}	26.2/ 29.8
No. atoms	
Protein	12,590
Ligand/ion	
B-factors	
Protein	83.3
Ligand/ion	
R.m.s. deviations	
Bond lengths (Å)	0.01
Bond angles (°)	1.54

*Values in parentheses are for highest-resolution shell.

Figure 38: [left] Superposition of GLIC WT (PDB code 3EHZ) in green and the P250G mutant in brown. The front subunits are removed to allow the view into the pore region. Although the largest part of the structure is unchanged, the pore lining α2 helix and the α2 - α3 loop have undergone a large conformational change. (middle top) 2Fo-Fc the electron density (blue mesh, contoured at 1.5 σ) of the P250G mutant superimposed on a subunit of WT and the P250G mutant. The rearrangement of the α2 - α3 loop and the α2 helix is apparent. (middle bottom) Side view of a superposition of a single subunit of WT and the P250G mutant. (right) Data collection and refinement statistics for the GLIC mutant P250G.

This collapse has maximized the hydrophobic interactions of residues at the extracellular part of the helix leading to a pore, which is most probably impermeable to ions.

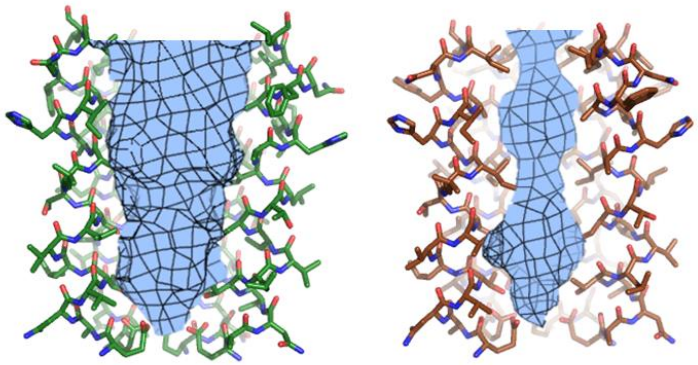

Figure 39: Pore lining helices α2 of WT (left, green) and the P250G mutant (right, brown). The blue mesh shows the water accessible surface of both pore regions.

In contrast to the extracellular half of the pore-forming helix, the conformation of its intracellular half is unchanged compared to the WT structure. Remarkably, this conformation is very similar to the previously reported structures of GLIC obtained by different methods (*62, 63*). In one study cysteine residues were introduced into the interface of the β1 - β2 and the α2 - α3 loop. Upon crosslinking, GLIC adopted a distorted conformation in this region, which closely resembles the structure of the P250G mutant. This distortion was assigned to a locally closed conformation of the ion conduction path. In the second study the structures of two non-activating mutants in the α2 - α3 loop, i.e. T252A and Y254A, were described. The same functional phenotypes for these mutants were also identified in the present study.
Remarkably, despite the strong impact of the mutation on the respective structure, the proline to glycine mutants of both homologues can still be activated.

When studied by 2EVC, the GLIC mutant P250G was activated with an EC_{50} that was shifted by 0.5 pH units towards higher proton concentration (Figure 40). To compare the surface expression and the maximally evoked currents for the mutant and WT, the current of each oocyte in response to saturating agonist concentrations was first measured by 2EVC and subsequently related to the ELISA signal quantifying the relative expression levels. Despite the strong surface expression of the mutant, the amplitude of the maximally evoked current was by a factor of three lower than typically observed for WT (Figure 40), which indicates differences in either the conduction or gating properties of the P250G mutant.

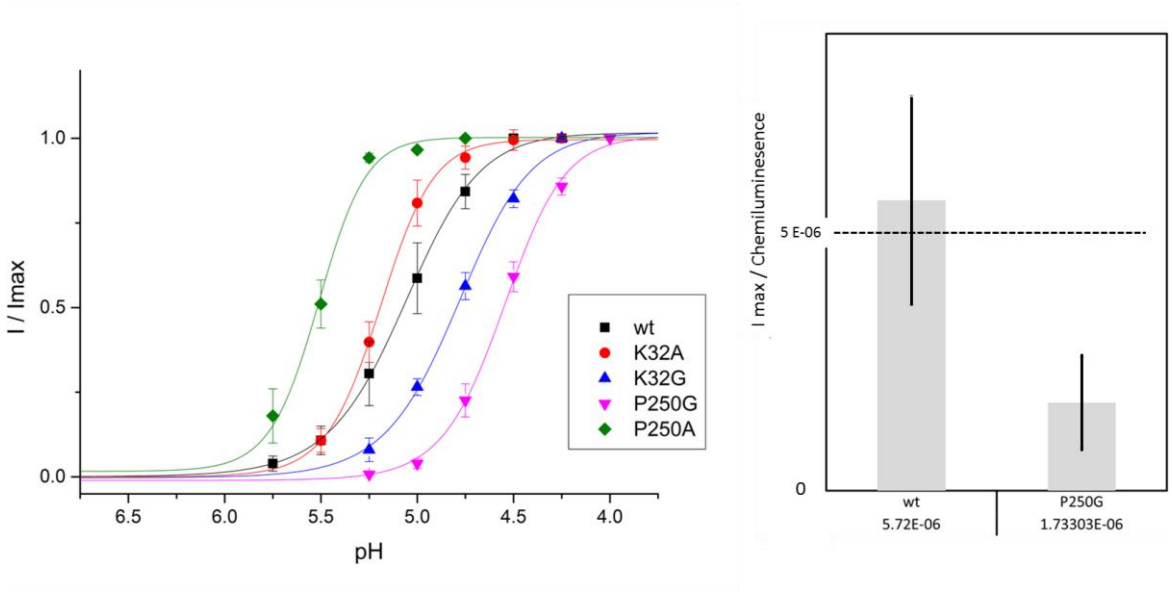

Figure 40 [left] GLIC dose response curves of the α2 - α3 and β1 - β2 loop mutants from at least 5 oocytes, the standard deviation is shown in bars. The tip mutant K32A has a similar EC_{50} than the WT, while the Glycine substitution at the same position leads to a higher EC_{50}. The α2 - α3 loop mutants at the position Pro250 show that the alanine mutant opens at lower proton concentrations than WT, whereas the Glycine mutation is shifted towards higher proton concentrations. [right] Maximally evoked currents of the GLIC P250G mutant and WT relative to the surface expression of the channels. The current density of the mutant P250G is significantly less than for the WT channel.

For ELIC, the mutation at the same position (P254G) is activated with similar EC_{50} as WT (Figure 42). Despite the apparent similarity in the potency of the agonist an unfamiliar phenotype was observed in the macroscopic 2EVC recordings. In these recordings the currents did not decrease with similar time dependence upon washout of the ligands as in WT. Sustained currents that slowly decreased were instead observed for a prolonged amount of time. (Figure 41).

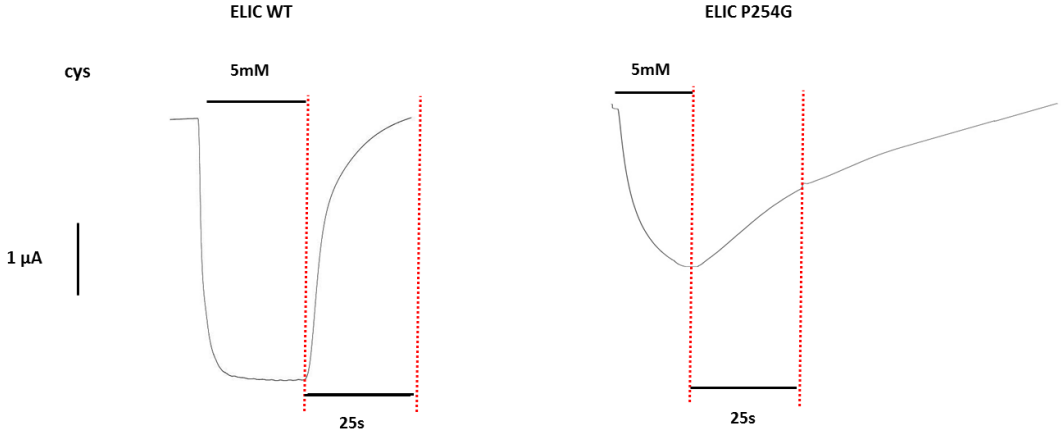

Figure 41: Channel activation and deactivation measured by 2EVC at a holding potential of -60mV. Both WT (left) and the mutant P254G (right) were exposed to 5 mM of the agonist cysteamine. Once the current maximum for this concentration was reached the agonist was washed out by diffusion with agonist-free solution. The WT shows a rapid decay of currents, whereas in the mutant the closing rate appears strongly reduced.

In contrast to the equivalent mutant of GLIC, the P254G mutant in ELIC showed higher maximal currents per surface expressed channels than WT (Figure 42).

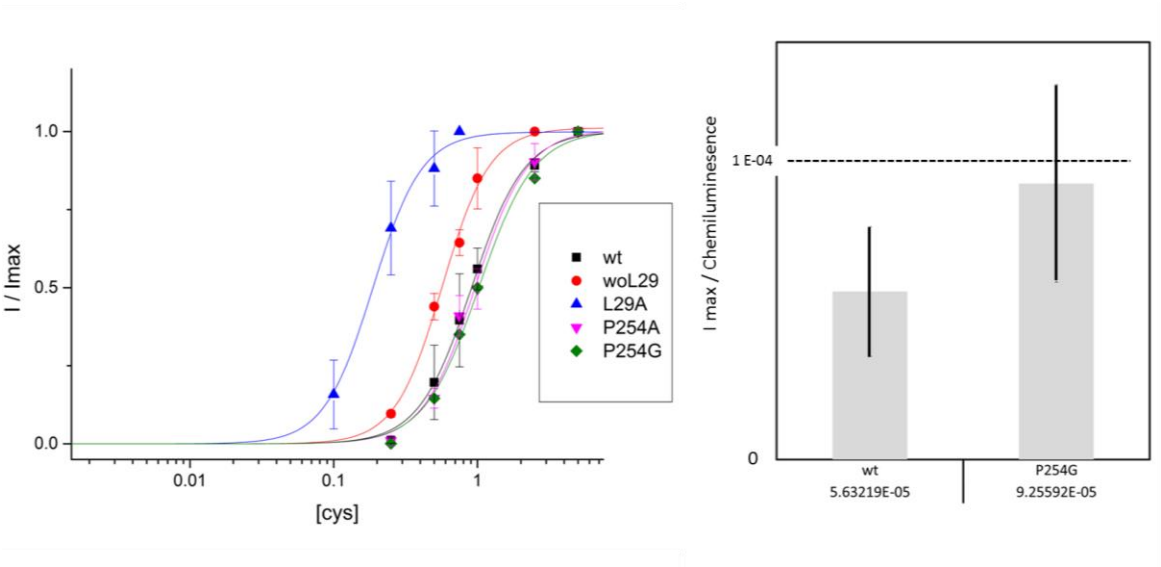

Figure 42: [left] ELIC dose response curves of the α2 - α3 and β1 - β2 loop mutants from at least 5 oocytes, the standard deviation is shown in bars. The tip mutant L29A has a lower EC_{50} than the WT, while the deletion of the residue (woL29) leads to a similar EC_{50}. The α2 - α3 loop mutants at the position Pro254 show that the alanine and glycine substitutions open at similar concentrations as WT. [right] Maximally evoked currents of ELIC mutants and WT normalized to the surface expression quantified immunolabeling. The mutant P254G shows a tendency for higher surface densities than the WT channel.

A maximally evoked current higher than the WT channel has previously only been observed upon addition of positive allosteric modulators (PAM), which abolish or slow down desensitization (*72*).

The cause for the unusually slow deactivation was revealed after a closer inspection on the structure of the P254G mutant. Next to the distortion of the α2 - α3 loop, the electron density showed that the side chain of the close by Arg255 has changed its conformation observed in WT and instead points away from the pore into the region of the β8 - β9 loop of an adjacent subunit. On this loop it interacts with a glutamate residue at position 159 (Figure 43). This interaction, which is was not observed in the WT underlines the slowed deactivation of this mutant. Remarkably E159A was previously identified not to be expressed (4 ± 2 % surface signal compared to WT expression, Figure 26). Which indicates its importance for the folding of the protein.

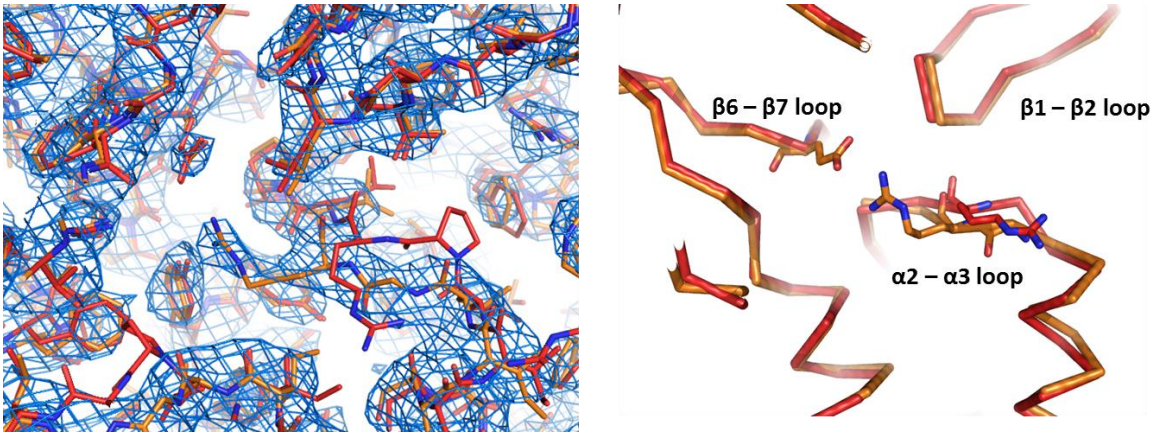

Figure 43: [left] 2Fo-Fc electron density (blue mesh, contoured at 1.5σ) of the P254G mutant superimposed on the model of WT (red) and the P254G mutant (orange). The Arg at position 255 has changed its conformation as visible in the electron density and now faces the β8-β9 loop. [right] Superposition of WT and P254G model. The residues E159 and R255 are shown as sticks.

For the double mutant P254G/R255A, the macroscopic 2EVC measurements showed WT-like closing and a ligand dependence of channel activation that shifted towards lower agonist concentration (Figure 44). Also the single mutant of R255A behaved similar as WT in macroscopic 2EVC measurements (Figure 44). These results confirm the role of this positively charged Arg255 residue in the unusual deactivation phenotype of the P254G mutant.

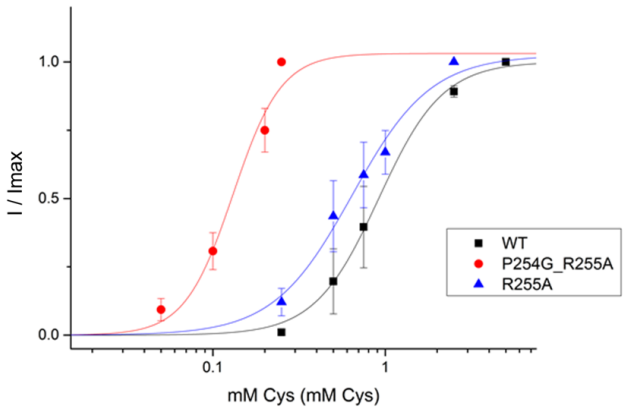

Figure 44: Dose response relationships of ELIC mutants of the α2 - α3 loop as measured by 2EVC mutants from at least 5 oocytes, the standard deviation for each data point is shown in bars in the corresponding color.

Despite the strong conservation of the proline residue in the α2 - α3 loop and the observed interaction with the extracellular domain in the open state of the channel, the mutation of the position to glycine do still promote channel activation in both ELIC and GLIC.
To further probe the importance of the interaction between the β1 - β2 turn to the α2 - α3 loop, additional mutants were constructed. The β1 - β2 loop was shortened by removal of the interacting residue in GLIC (i.e. Lys32) and the corresponding position in ELIC (i.e. Leu29). The deletion mutants woK32 in GLIC and woL29 in ELIC where then characterized with respect to surface expression and dose dependence of channel opening.

In GLIC, this mutant showed severely reduced channel activity with a midpoint of activation that is shifted to higher proton concentration (Figure 45).

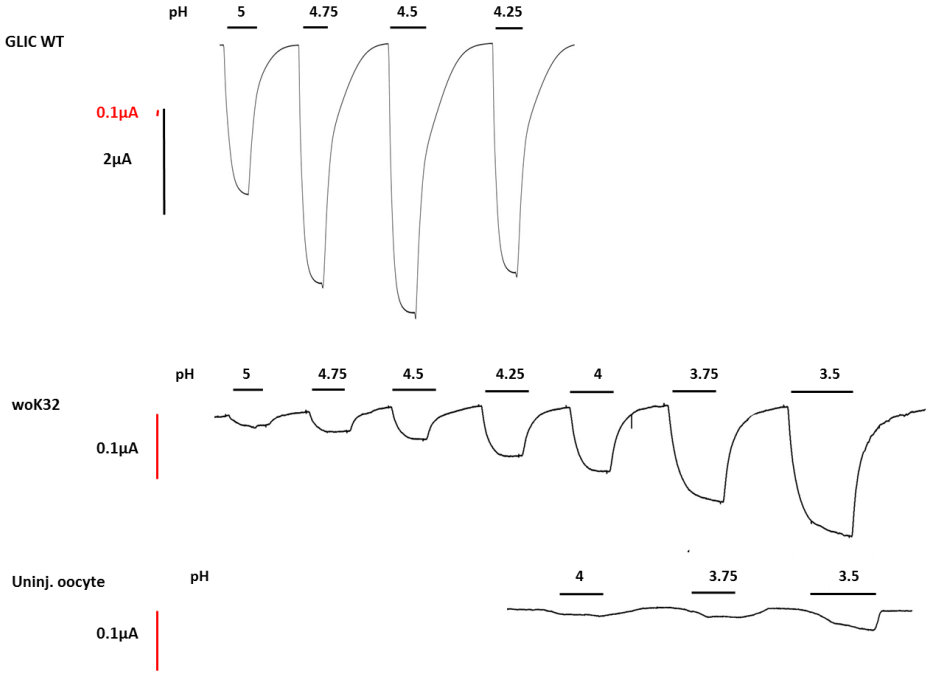

Figure 45: 2EVC dose response experiment. GLIC WT, the mutant woK32 and an uninjected oocyte were exposed to different proton concentrations. While the WT channel shows robust currents with a maximum around pH 4.5 (top), currents in the woK32 mutant (middle) increase even at higher proton concentration (pH3.5). The currents in this mutant are low (please note the different scale for the recordings), but significant above an uninjected, oocyte (bottom). The comparison was made with oocytes which show similar expression levels of the channel.

The equivalent mutation in ELIC exhibited a slightly lower EC_{50} as the WT channel, with reduced maximal current response (Figure 42). Collectively the results on the interaction of the β1 - β2 loop of the extracellular domain with the α2 - α3 loop of the pore domain suggest that this interaction contributes to channel activation, but it appears not to be as crucial as suggested by the X-ray structures.

3 Discussion

Pentameric ligand-gated ion channels (pLGICs) have been studied extensively for decades. In the beginning, these studies were limited to functional investigations of eukaryotic family members by biochemical and electrophysiological methods. The identification of prokaryotic homologues and the availability of their structures at high resolution, opened the door for detailed structure-function experiments. Nevertheless it remained a difficult task to deduce a molecular mechanism that relates the available functional data measured on eukaryotic proteins to the structural features of their prokaryotic homologues. Only in the last few years functional data became available for prokaryotic pLGICs of known structure.

In recent studies the first step of the activation mechanism, the binding of the ligand to a site in the extracellular domain has been described in the context of the full-length protein (*6, 18, 69*). The structural data in general agreed with previous made in the AChBP, which resembles the extracellular domain of the nAChR, and which so far was used as a model to describe agonist and antagonist binding.

The next step of the activation process requires the conformational change in the extracellular domain upon ligand binding to be transmitted to the pore region, where it leads to channel opening. The underlying mechanism of this step is still under debate. One reason for the controversial discussion of the activation mechanism is that any structural information on different conformations of the channels have been obtained from different homologues and that most of the functional data, were obtained from family members with non or limited structural information.

To investigate whether the potential open conformation of GLIC seen in the crystal structure does indeed resemble a conductive state, known inhibitors of the nAChR were used to investigate the pore properties. These inhibitors bind to the open pore from the outside and thereby block the ion flow through the channel of nAChRs. This study revealed the structural basis of open channel block in the pLGIC family and confirmed the hypothesis that the structure of GLIC shows an open conformation.

In the second part of the thesis I have studied the proposed pathway of activation of pLGIC family in the two prokaryotic homologues ELIC and GLIC. These studies confirmed the importance of stretches of conserved residues in the domain interface region of the extracellular and pore domain for the transduction of conformational changes.

3.1 Modulation of pLGICs

3.1.1 Open pore block

With a known structure of its potential open state the prokaryotic pLGIC GLIC became an ideal model to study the effect of open pore blockers. The study revealed that the same set of molecules inhibiting the currents in nAChR also act on GLIC by a similar mechanism. These pore blockers include quaternary ammonium compounds, local anesthetics and divalent transition metal ions. By a combination of electrophysiological and structural studies two distinct interaction modes of the open pore blockers with the pore could be revealed.

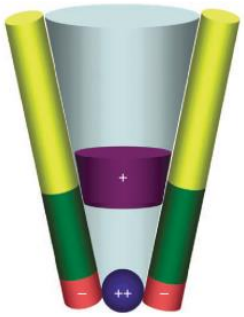

Figure 46: Schematic representation of the interaction of the funnel shaped open pore with the open pore blockers of GLIC. The pore lining helix α2 (cylinder) is color coded depending of the properties of the pore facing residues (yellow: hydrophobic; green: polar; red: charged). Two distinct binding areas could be distinguished: The bulky monovalent quaternary ammonium compounds and local anesthetics block the channel at the boundary between the hydrophobic and polar part, whereas the divalent transition metal ions directly interact with the negatively charged residues at the intracellular end of the pore.

One area of interaction is located at the boundary between the hydrophobic and polar parts of the funnel-shaped pore. The studies showed that bulky monovalent open pore blockers are attracted to the channel by their net charge, but that they are too big to pass the channel constriction. The exact binding position is dependent on the size of the molecules, with smaller blockers binding deeper in the pore. Similar observations were previously made for open pore blockers of the nAChR (*20*). Our study also demonstrated that the mutation of the conserved negatively charged ring, which in nAChR was termed the 'intermediate ring of charge', has an effect on the binding affinity of the blocker, but not on its location within the pore. Thus it can be concluded that the size and not the electrostatic interactions with the only charged area in the pore is determining their binding position. This finding also underlines the significance of the 'intermediate ring of charge' to attract cations to the channel, but it also shows that these residues are not the only factor for cation selectivity (*54*, *73*).

For the second binding site a different mode of interaction was observed. In this case the divalent transition metal ion Cd^{2+} binds to the conserved glutamate residue at the intracellular pore exit. The mutation of this position to the uncharged and smaller residue alanine removes the block and also abolishes binding, as confirmed in the crystal structure of the mutant. The comparably low binding affinity of the impermeant Cd^{2+} applied form

the extracellular side suggests that the block is not due to tight interactions with this site, but instead due to a high energy barrier in the translocation path. A tight interaction of divalent ions with this conserved ring of negative charges has as well been described for the nAChR (*74*, *75*) and was also observed for the conduction of the permeant ion Zn^{2+} in GLIC. In summary it can thus be concluded that the studies on open channel block in GLIC agree well with the published data on other family members (*20*, *76-78*). The agreement of electrophysiological and structural data of this specific homologue also suggests that the structure of GLIC, indeed closely resembles an open state of the channel.

In the course of the study of open pore blockers it was observed that the divalent ions Zn^{2+} and Cd^{2+} do not only bind in the pore region, but also in the extracellular domain of GLIC. Despite the fact that during the investigation of pore block the potential functional importance of these additional binding sites was neglected, they are not necessarily unimportant. Divalent ions have been shown to modulate pLGICs not only in the pore region. In nAChRs modulatory effects of divalent ions have been studied in detail. In these channels certain divalent ions had an activating effect at low concentrations and an inhibitory effect at higher concentration (*79*). It was postulated that the positive effect originates from an interaction in the extracellular domain, whereas the high concentration of the ion leads to pore bock. Additionally divalent ions have been known to interact with certain residues in the vestibule of the extracellular domain, which in addition to charged residues in the pore region contribute to ion selectivity of the channel (Figure 47 and (*80*)). The residues within the extracellular domain that were identified as important determinants of charge selectivity are located at the extracellular entrance (i.e. E64 in ELIC and E72 in GLIC) and the center of the extracellular vestibule (i.e. D86 in ELIC and D89 in GLIC). With respect to distance and geometry, these residue are in prominent positions to influence the electrostatics of the vestibule and thus to function as selectivity screen in the extracellular lumen.

	Diameter Å	SD
ELIC (2VL0)		
EC D86*	19.7	0.07
EC E64*	20.2	0.05
TM E229	16.3	0.17

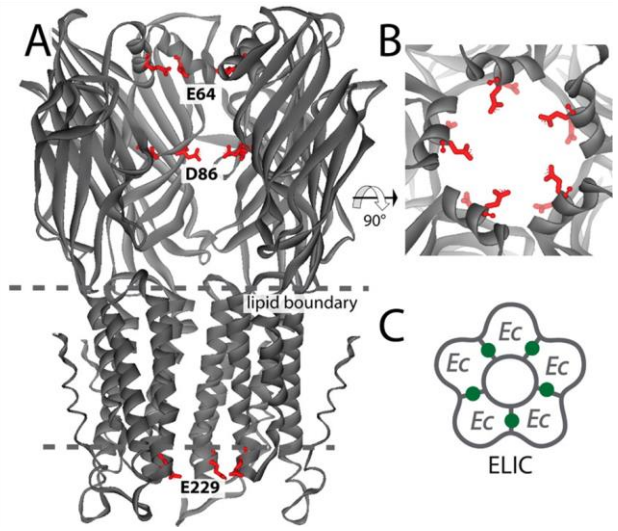

Figure 47: Residues important for ion selectivity in ELIC. (left) Table of diameter distances (calculated from α-carbon distances) including SD values (from five different measurements) of residues important for ion selectivity in ELIC. (*A*) Ribbon representation of ELIC viewed from within the membrane with the front subunit removed. Residues predicted to be important for ion selectivity are shown in red. (*B*) Top view of the first ring of residues (E64) involved in the ion selectivity. (*C*) Homopentamer ELIC with five binding sites for ions, showing the ion selectivity sites (Adapted from Hansen et al. (*80*)).

In a study by Zimmermann and colleagues, in which I have participated, the effects of divalent ions on permeation and gating in ELIC were investigated (*67*). In this study, three different binding sites for divalent cations were identified. The three sites were named according to their location in the channel as S_{in}, S_{out} and S_{pore}. Whereas the site S_{out} was linked to the allosteric inhibition of ELIC by divalent cations, the other two sites, S_{in} and $S_{pore,}$ did not participate in any modulatory effect.

By comparing these binding sites with the sites coordinating divalent ions in GLIC, it was remarkable to see that one site in the extracellular domain occupied by Zn^{2+} was at the equivalent position as S_{in} in ELIC (D68, Figure 47 and Figure 48). This is a location which has previously been shown to be important for charge selectivity and conductance, thus emphasizing the conservation of functional mechanisms within the family.

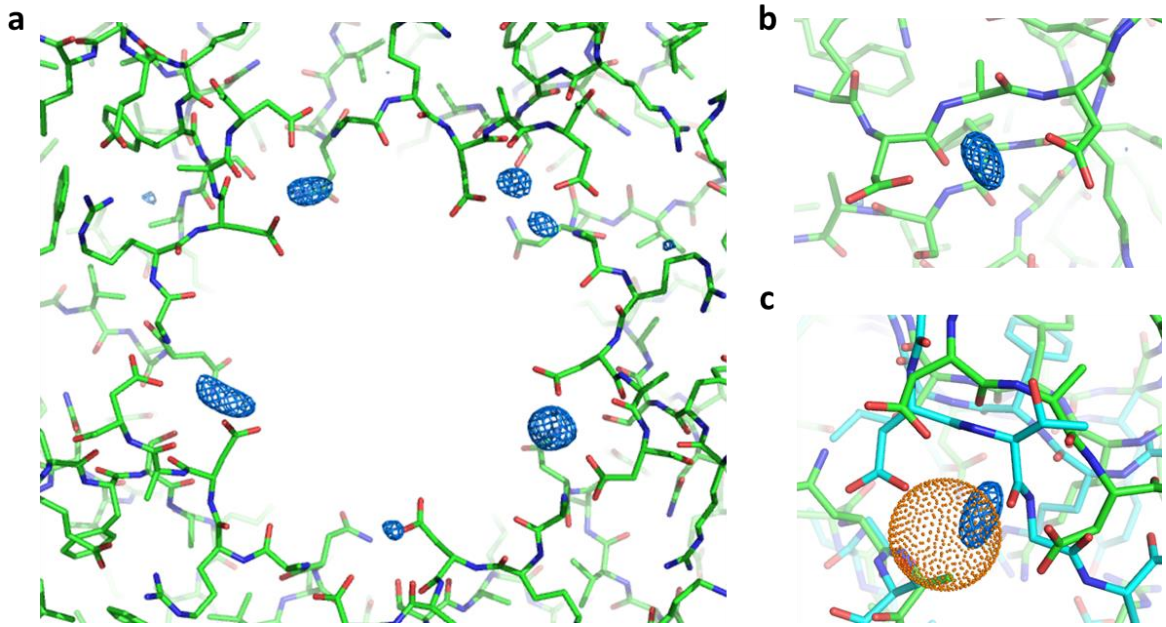

Figure 48: (a) Top view of the anomalous difference electron densities of Zn^{2+} (blue mesh, contoured at 4σ) in GLIC WT (green; PDB code 3EHZ), in all five subunits the Zn^{2+} ion is present. (b) Close view of the binding site of Zn^{2+} in one subunit, it is coordinated by two Aspartate residues (i.e. Asp 86 and Asp 88). (c) Superposition of the ELIC WT (light blue; PDB code: 2YN6) crystallized with Ba^{2+} (Van der Waals radius of the barium ion in orange dots) with GLIC WT (green) with the anomalous signal of Zn^{2+} (blue mesh) at the position of the S_{in} site, an extracellular ion selectivity site. The binding sites of both divalent ions are very close, differences arise from local differences in the structure.

3.2 An insight into gating

Before a pLGIC can be blocked by open pore blockers, the channel first needs to be activated. The activation within the pLGIC family is initiated by the binding of a ligand to a conserved site in the extracellular domain. The following conformational rearrangements in this part of the protein are transduced through interactions in the interface to the transmembrane part of the protein to activate a selective ion permeable pore.
During my PhD studies I have investigated how mutations at or close to the interface between the extracellular and the pore domain are affecting gating in the two prokaryotic pLGICs ELIC and GLIC. I was able to identify residues in a region of high conservation in the cys- and the α2 - α3 loop, which, upon mutation, lost their ability to open the channel.

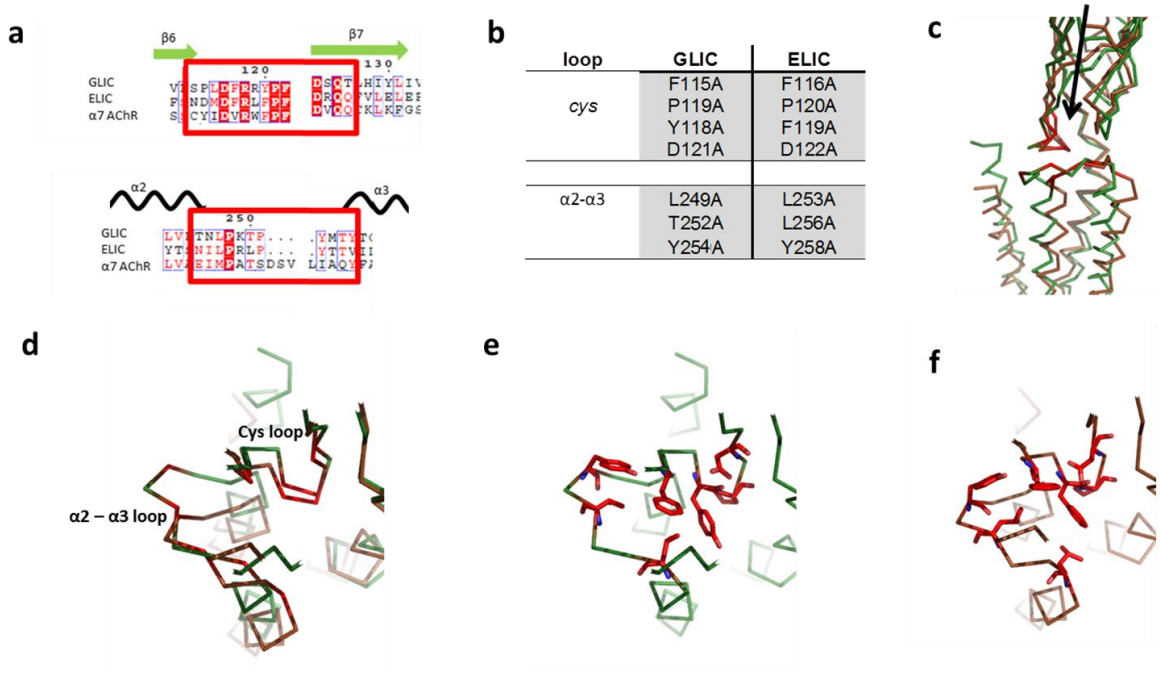

Figure 49: 'loss of function mutants'. (a) Sequence alignment of the cys-loop and the α2 - α3 loop (the color coding for the conservation is the same is in Figure 21). (b) List of residues which upon mutation to alanine show a 'loss of function' phenotype. (c) Superposition of GLIC (green) and ELIC (brown) the location of the loss of function mutants are indicated in red. The black arrow indicates the direction of view for panels (d-f). (d) Close-up of the interface between the α2 - α3 loop and the cys-loop. (d) Cα trace of GLIC with its 'loss of function mutants' shown in red. (f) Cα trace of ELIC with its 'loss of function mutants' shown in red.

An interesting feature of these conserved 'loss of function' (lof) mutants is that, except for two residues, they are in both structures (ELIC and GLIC) part of a hydrophobic interface between the pore and the extracellular domain. This interface must play an important role during the activation cycle. Two residues not involved in this interface are a conserved proline and a conserved aspartate of the cys-loop. The proline likely plays a structural role in rigidifying the loop, whereas the aspartate is part of a conserved salt bridge of the 'principal pathway of gating' (*45*). In this proposed pathway of activation a network of interactions connects the cys-loop with the β1 - β2 loop via a conserved arginine at the transition between the extracellular domain and the pore.

Previously an equivalent hydrophobic network as the one identified in our study has been proposed by Sine and coworkers (*46*) to influence gating in the nAChR and termed the 'cys-loop pathway'.
Also there a hydrophobic core of the cys- and the α2 - α3 loop was shown to exert a large effect on activation. The residues identified in nAChR were two phenylalanines (F135 and F137) of the cys-loop and a tyrosine (Y277) and a leucin (L273) of the α2 - α3 loop. Even though in the structure of the nAChR they are at different positions than their equivalent residues in ELIC or GLIC a similar functional effect was observed. A reason for the discrepancy in structural details could arise from the fact that the nAChR cryo - EM structure ((*42, 44*)) was not determined at sufficiently high resolution to allow the correct assignment of residues. Despite the fact that in their study Sine and colleagues have used comparably conservative mutations, their results as well emphasize the importance of this hydrophobic core at the interface for channel activation, which is in agreement with my findings. In my studies I could show that certain 'loss of function' mutants, despite their drastic effect on channel opening, were still able to bind the agonist in a similar manner as WT. This underlines that these mutations did not interfere with ligand binding, but with gating.
Two of the 'loss of function' mutants of the α2 - α3 loop of GLIC have recently been characterized in GLIC by X-ray crystallography and electrophysiology (*63*). Despite the same effect on gating, the structures of the equivalent mutants, Tyr254 in GLIC determined by Gonzalez-Guiterrez et. al. and the mutant at the corresponding position from ELIC (i.e. Tyr258), which was determined in this study, are not directly comparable. In the Y254A mutant of GLIC the channel was crystallized at low pH and shows a similar conformation as the 'locally closed structure' determined by the Corringer group or the P250G structure in our study. Whereas most of the structure is in a similar conformation, the α2 - α3 loop and the pore forming helix α2 have rearranged leading to an occluded pore, which would be in agreement with the 'loss of function' phenotype of the channel. ELIC in contrast showed its common non-conductive conformation also for the 'loss of function' mutants. Only local changes in the α2 - α3 and the β8 - β9 loop indicate a potential interaction between those two loops in the activation mechanism. No change in the β8 - β9 loop was observed in any GLIC 'loss of function' mutant structures and it therefore remains to be shown whether these differences come from different activation mechanisms of the two homologues. A remarkable structural feature concerns the structural stability of the α3 helix in GLIC, which is found in the same position in all currently published structures. This indicates that this helix might not change its position in the activation cycle, different to a mechanism proposed earlier by comparison of the ELIC and GLIC structures (*5*). These findings it led to an alternative mechanism for activation, where the α2 helix locally unwinds at the extracellular side to close the pore (*62*). Data supporting this mechanism were recently also obtained from a low resolution structure of GLIC crystallized at high pH, which showed similar features in the pore region (unpublished data).
The occlusion of the pore 'loss of function' mutants in GLIC (*63*) was also observed during our studies. The P250G mutant from GLIC shows a similar conformational change of the pore region. Interestingly though, I have demonstrated in electrophysiology experiments, that this mutant can still be activated.

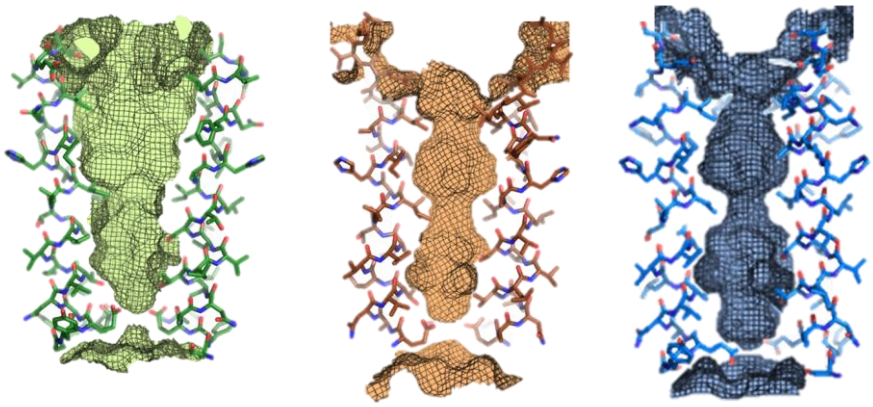

Figure 50: Representation of the water accessible surface (calculated with Hollow (*81*)) in the pore region for GLIC WT (green, left), and the GLIC mutants P250G (brown, middle) and Y254A (blue, right). Helices α-2 are shown as stick with the front subunit being removed for clarity, the water accessible surface is shown as colored mesh. Both mutants show an occluded pore conformation which is impermeable for ions. The pore diameter of the P250G mutant (middle) is similar and even slightly smaller than in the loss of function mutant Y254A (blue).

Although the mutant can be activated, I have observed that the P250G mutant has a lower maximally evoked current at saturating ligand concentration when compared to WT. This finding indicates that the occluded, non-conductive, conformation is in equilibrium with the activated state of the channel and thus cause a smaller macroscopic currents. It is hard to say whether this locally collapsed state is indeed part of the activation mechanism or just a detergent / mutation artefact. Because this state has not been seen in the homologue ELIC. In ELIC the equivalent mutation (i.e. P254G) causes a slightly different phenotype. This mutant is as well still able to active the channel, but while in GLIC the channel showed a smaller maximally evoked current in comparison to WT, in ELIC the maximum current was higher. At the same time the channel was shown to be open for a prolonged period of time even after the removal of its ligand. The structural data of this mutant showed a possible explanation for this unusual phenotype. Despite the fact that the overall structure of the ELIC mutant P254G showed the same non-conductive conformation seen in all other structures, a local rearrangement in the α2 - α3 loop has led to an ionic interaction between Arg255 of the α2 - α3 loop with a Glu159 of the β8 - β9 loop. I could show that this interaction is responsible for the higher stability of the open state. A sequence alignment showed that the residues of this salt bridge are not conserved within the family, thus suggesting that the observed phenomenon may be unique to the homologue ELIC.
Most of the structural data obtained for GLIC is in agreement with the proposed opening mechanism where the interaction between the backbone of the residue at the tip of the β1 - β2 loop to a conserved proline in the α2 - α3 is critical for the stability of the open state (*5*). This interaction during gating will from now on be referred to as ‘tip’ pathway.

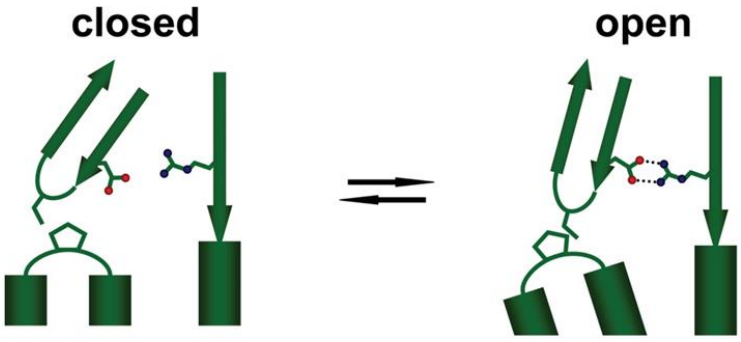

Figure 51: Schematic representation of a proposed opening mechanism. The conserved proline residue of the α2 - α3 pore loop is pushed and hold in an open position by the tip of the extracellular β1 - β2 loop (Adapted from (*5*)).

The mutation of this rigid proline residue to the most flexible amino acid glycine leads to a loss of this contact and therefore a collapsed pore. In the two published 'loss of function' mutant structures, the α2 - α3 loop adopts a different conformation, which leads to a loss of contact between these two loops and to a similar pore conformation. Nevertheless the functional phenotype of P250G is not in full agreement with this mechanism, as the mutant is still able to activate.
Similarly, the removal of the backbone interaction partner by shortening of the β1 - β2 loop through deletion of a lysine residue (woK32), shows a dramatic reduction of channel activity, but not a complete loss of function. The same effect was seen in ELIC, where despite the deletion of the equivalent residue Leu29 (woL29) the channel is still activated by its ligand, although with a reduced activity. Both tip deletion mutants did still respond to their ligand with reduced maximal activity, which indicates that the signal transduction for gating is perturbed, but not completely interrupted.
My results thus exclude the 'tip' pathway as the main determinant for gating.

This conserved proline in the α2 - α3 loop has previously been investigated in the nAChR, but due to the absence of detailed structural information a potential interaction with the β1 - β2 loop was not detected. Therefore a different hypothesis has been proposed for the importance of this conserved residue. In nAChR (Auerbach and colleagues ((*47*))) and in 5-HT3 receptors (Lummis and colleagues ((*82*))) it was suggested that the proline undergoes a cis–trans isomerization during activation. The mutation to alanine would thus allow the loop to affect the equilibrium of the isomerization which is reflected and in a lower agonist concentration required for activation. A similar effect in the EC_{50} was seen for the equivalent mutation in in GLIC, but not in ELIC where the EC_{50} of the mutant does not change significantly in comparison to WT.
Auerbach proposes that in the nAChR the conformational changes in the extracellular domain following ligand binding (a process called C - capping) is perturbing the potential salt bridge between the Arg of the β10 - α1 linker and the Glu of the β1 - β2 loop (Asp31 in GLIC and Thr28 in ELIC), which was previously assigned to be part of the 'principal pathway of gating' by Sine and colleagues (*45*). It could be shown that for the nAChR the exchange to various combinations of residues (i.e. A/L, H/A, N/L, K/L, H/R, A/R, N/R and Q/R) did still lead to channel activation. Therefore the salt bridge, even though present in

the structures of the nAChR (*42*) and GLIC (*33, 50*), is likely not one of the main determinants for gating (*47*). This conclusion cannot be extended to GLIC, where the disruption of this ionic interaction does not show any channel activation. This indicates that for GLIC this interaction is necessary for pore opening. The behavior of ELIC is less pronounced than in GLIC and somewhat resembles the nAChR. In ELIC the residue present in the β1 of WT is a Thr, whose mutation to Asp strongly enhances channel activation, whereas the mutation to Ala results in a weaker, but still ligand-dependent activity. These findings are in agreement with the previous findings in nAChR (*47*), showing that this interaction, although important, is not essential for activation. At this point it could be speculated that the D31A mutation in GLIC might also still be activated but at a much lower pH which is not accessible in a cellular system. Since the mutations in ELIC would indicate a much more dramatic effect.

In summary, in my experiments I could show that there is not only one key interaction that is important for gating, but it is instead a network of several different pathways which, when acting in concert, trigger the opening of the pore. The various pathways include the 'tip' pathway, the hydrophobic network of the 'cys-loop' pathway and the 'principal pathway of gating', which all have also been shown to be important in the mammalian nAChR. It thus appears likely that, despite some protein specific differences, the overall mechanism of activation is very well conserved within the family. Lessons learned from prokaryotic pLGICs are thus relevant for the entire family.

4 Outlook

Although, with recent data on prokaryotic pLGICs, our understanding of channel function has increased until now there are no high resolution crystal structures of a single pLGIC in different functional states available. Knowledge of such structures will be a prerequisite for the comprehension of the gating mechanism. . Therefore an important future task will be to get more information and if possible structures of different states of the protein. The newly discovered positive allosteric modulators for ELIC are an interesting tool for such experiments and should be considered further in combination with the information obtained from mutagenesis studies to stabilize and crystallize an open conformation of ELIC. The experiments addressing the gating mechanism have so far revealed few very interesting mutants, whose functional properties were only superficially characterized by 2EVC. Macroscopic and single-channel patch–clamp experiments would extend the study and reveal the underlying change in the kinetics and single channel behavior of the mutant. These additional data could provide deeper insight into the gating mechanism.

Another major task will be a detailed analysis of the conformational properties of the protein in detergent solution and the comparison of channels embedded in a lipid environment by Electron Microscopy and EPR spectroscopy to obtain insight into the entire ensemble of conformations of the protein in their native environment.

5 Methods

5.1 Cloning

All vectors used in this thesis (Figure 52) were modified by Dr. I Zimmermann to be compatible with the FX cloning system.

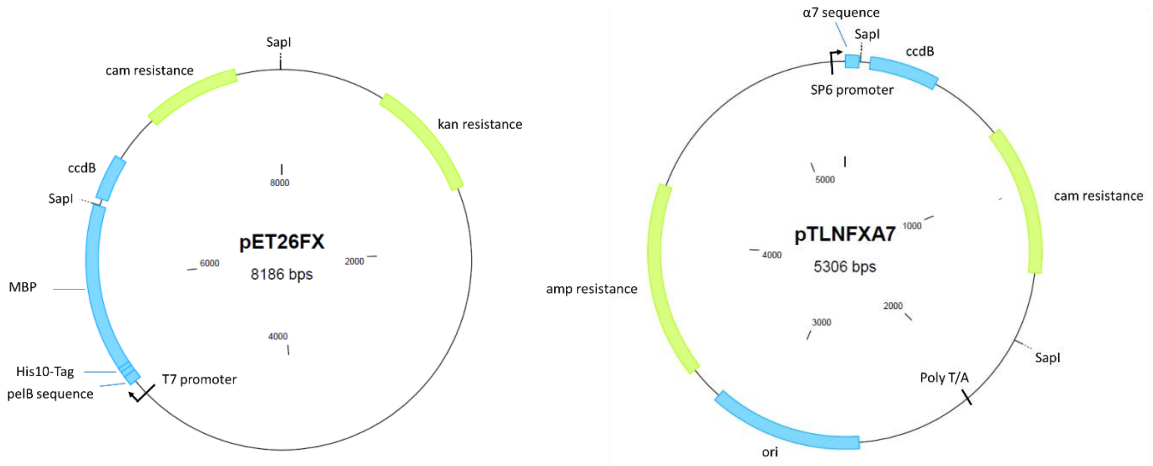

Figure 52: FX-compatible vectors used in this thesis. Both vectors (left and right) contain a SapI cleavable ccdB site. This site is important for FX cloning, since this gen is lethal to *E. coli* MC1061 used for cloning. (left) Expression vector in *E. coli*. This vector fuses the pLGICs with a cleavable N-terminal signal sequence (pelB), a deca histidine tag and a MBP fusion protein. (right) Vector used for expression in *Xenopus laevis* oocytes. This vector contains the SP6 RNA polymerase promoter and adds a N-terminal chicken α7 signal sequence to the protein.

The PCR technique was used to amplify genes for FX cloning. FX primers were designed to introduce SapI restriction sites on either side of the gene. The primers were generated using an algorithm on the online FX platform (www.fxcloning.org) and obtained from Microsynth (www.microsynth.ch). The respective genes were amplified with a standard PCR protocol using Phusion Polymerase (NEB). The amplified DNA was applied on a 1% agarose gel and separated by electrophoresis. The band corresponding to the amplified gene was isolated from the gel and purified with the High Pure PCR Product Purification Kit (Roche).

6 µl of the purified gene containing SapI sites were mixed with 1 µl of the desired FX-compatible vector, 1 µl of SapI restriction enzyme, 1 µl of T4 DNA ligase, 1 µl ATP (10 mM) and 1 µl 10X Ligase buffer. The mixture was incubated for 1.5 h at 37 ºC and inactivated for 20 min at 65 ºC. Following a transformation into *E. coli*, the cells were applied on LB-agar plates containing an antibiotic for selection (Ampicillin –pTLNA7; Kanamycin pet26) and incubated ON at 37 ºC. To confirm the sequence of the incorporated gene the constructs were sequenced (www.microsynth.ch). After successful FX-cloning of the pLGICs the vectors were named pet26 and pTLNA7, not to confuse with the pet26FX and pTLNA7FX, which still included the suicide cassette (ccdB).

Mutations were inserted with the QuikChange®Site-Directed Mutagenesis protocol (Stratagene). Primers were designed using the PrimerX online platform (http://www.bioinformatics.org/primerx/cgi-bin/DNA_1.cgi) to insert the desired mutations into the gene. Then the primers (Microsynth) were added at a concentration of 0.25 µM to the QuickChange mixture containing 5 µl of 10× reaction buffer, 1 µl (5–50ng) of dsDNA template, 1 µl of dNTP mix (10 mM each), 31.5 µl ddH_2O and 1 µl of PfuTurbo DNA polymerase (2.5 U/µl).

5.2 Electrophysiology

5.2.1 Expression in Xenopus oocytes

For expression in *Xenopus laevis* oocytes, constructs of ELIC and GLIC in the pTLNA7 vector were used (Figure 52). After linearization of the plasmid DNA by MluI, capped complementary RNA (cRNA) was transcribed with the Message Machine kit (Ambion) using the SP6 RNA polymerase and purified with the RNeasy kit (Qiagen). Depending on the expression level of the respective mutant, 50 nl of RNA at a concentration ranging between 10 and 400 ng/µl was injected into defolliculated oocytes. For expression oocytes were incubated in barth solution (88 mM NaCl, 1 mM KCl, 1 mM $CaCl_2$, 0.33 mM $Ca(NO_3)_2$, 0.82 mM $MgSO_4$, 10 mM Na-Hepes (pH 7.4) and 50 µg / ml Gentamycin) at 16 °C.

5.2.1.1 Two electrode voltage-clamp recording

Measurements were performed 1–3 days after injection at 20 °C with the two-electrode voltage-clamp technique with an OC-725B amplifier (Warner Instrument Corp). Currents for GLIC were recorded in bath solutions containing 130 mM NaCl, 2 mM KCl, 1.8 mM $CaCl_2$, 5 mM $MgCl_2$. The respective pH values were stabilized by addition of 10 mM HEPES (pH 7.0) or 10 mM of citrate (pH 3.5–pH 5.0). For ELIC the bath solution had to be adapted and contained the following: 130 mM NaCl, 2 mM KCl, 0.5 mM $CaCl_2$ and 10 mM Hepes (pH 7.0). For activation of ELIC the bath solution was supplemented with agonist (propylamine or cysteaime) at concentrations varying from 1 µM up to 50 mM depending on the mutant. For the characterization of channel block of GLIC the bath solution was supplemented with the specified inhibitor concentrations. For recording in solutions containing either Zn^{2+} or Cd^{2+}, citrate was replaced by 10 mM glucuronate. Electrodes were bathed in 1 M KCl solution connected to the bath solution by agar bridges.

5.2.1.2 Oocyte surface expression assay

Xenopus oocytes were injected and maintained as described above. The amount of cRNA had to be adapted for each mutant and varied from 5 ng/µl for ELIC WT to 450 ng/µl for certain mutants. Surface assays were performed 2–4 days after injection. For surface labeling, oocytes were blocked for 30 min in ND96 (93.5 mM NaCl, 2 mM KCl, 1.8 mM $CaCl_2$, 2 mM $MgCl_2$ and 10 mM Hepes (pH 7.4)) with 1% bovine serum albumin (BSA) at 4°C, labeled with 1 µg/ml rat monoclonal anti-HA antibody (3F10 (Roche), in 1% BSA for

90 - 120 min at 4°C), washed 4x 10 min at 4 °C, and incubated with 0.16 µg/ml horseradish peroxidase–(HRP) coupled secondary antibody (HRP-conjugated goat anti-rat F(Ab)2 fragments (Jackson), in 1% BSA for 30–60 min at 4°C). Cells were extensively washed (1% BSA, 5x10 min, 4 °C) and transferred to ND96 solution without BSA. Individual oocytes were placed in 50 µl Power Signal ELISA (Pierce) and incubated at room temperature for 1 min. Chemiluminescence was quantitated using Perkin 96 Flat Bottom white polystyrol plate with a Tecan infinite M-10000 plate reader.

5.2.1.3 Assay to quantify the maximal evoked currents per surface expressed channels

Xenopus oocytes expressing the respective channels were prepared as described above. The amount of cRNA was chosen based on the results of the surface expression assays and varied from 5 ng/µl to 450 ng/µl. Two-electrode voltage-clamp measurements were recorded 2-3 days after injection at 20 °C (OC-725B, Warner Instrument Corp.) as described above. Required agonist concentrations for the recording of maximally evoked currents was obtained from previous dose-repose measurements of each mutant. After the measurement of the maximal currents the oocyte was washed in bath solution (and collected in a 96 well plate). As a control uninjected oocytes and oocytes injected with WT RNA were treated with the same protocol. After recording surface expression was assayed as described (5.2.1.2).

5.3 Biochemical and structural methods

5.3.1 Small scale stability screening of mutants

The stability of mutants of ELIC and GLIC that were targeted for structure determination was initially investigated in small-scale expression cultures. pet26 vectors containing the respective constructs were transformed into BL21(DE3) cells and grown in terrific broth (TB) medium (12 g peptone, 24 g tryptone, 4 ml glycerol, 50 mg kanamycin, 2.31 g KH_2PO_4 and 12.54 g K_2HPO_4 per liter). For small scale experiments, the cells were grown in 5 mL TB at 37ºC to an OD_{600} between1.6 and 1.8 and subsequently cooled to 19 °C. Protein expression was induced with 0.2 mM IPTG for 12–13 hours at 19 °C. The overnight cultures were collected and resuspended in purification buffer A (50 mM K_2PO_4 pH 8.0, 150 mM NaCl) with addition of 1 mM phenylmethyl sulfonyl fluoride (PMSF), 20 mg/ml DNaseI, 1 mg/ml lysozyme, 1 mg/ml pepstatin and 1 mg/ml leupeptin. The cells were lysed on a FastPrep-24, solubilised for 1 h in 0.9 mM DDM, centrifuged at 10’500 g for 15 min to remove the cells debris and incubated for 30min with 1 ml Ni-NTA beads. The Ni-NTA resin was subsequently loaded on a gravity flow column and the eluate was monitored by recording of the AU_{280}. Beads were washed with buffer A containing 15 mM and 55 mM imidazole until baseline was reached. The protein was subsequently eluted with buffer A containing 300 mM imidazole in a final volume of ~25 ml. To remove the His10-tag and the MBP, the eluted fusion protein was digested for 2 h at 4 °C by addition of 3C precision protease in a 1:20 w/w ratio of protease to fusion protein. During the 2 h incubation the solution was dialyzed against a buffer containing 10 mM K-Phosphate (pH 8.0), 150 mM NaCl and detergent at a concentration of 1.2 CMC to remove the imidazole. After cutting,

the solution was passed over the same Ni-NTA column used for purification to remove the MBP/His_{10}-tag and the His-tagged 3C protease. After the elution of the 2nd Ni-NTA column the samples were centrifuged for 10min at 100'000g (Beckman). 70 µl of each sample was transferred on a NUNC 96-well plate and subjected to FSEC. For that purpose50 µl aliquots were applied to a TOSOH BIOSCIENCE G3000SWXL gel-filtration column, mounted on an Agilent HPLC. Samples were eluted at 1 ml/min, in buffer A and the Trp-fluorescence was recorded on a fluorescence detector with an excitation wavelength of 280 nm and an emission of 320 nm). For analysis the respective peak heights and elution volumes of the mutants were compared to WT.

5.3.2 Large scale Expression and membrane purification

Constructs of GLIC and ELIC were expressed in *E. coli* as a fusion to the C terminus of maltose binding protein (MBP) that was preceded by an *E. coli* pelB signal sequence and a decahistidine (His_{10}) tag. For this purpose the constructs were cloned into the pet26FX vector using the FX-cloning method. The plasmids were transformed into BL21 (DE3) cells and grown in terrific broth (TB) medium. For ELIC 16 0.6 l shaker flasks, and for GLIC 32 0.6l flasks were used. Cells were grown at 37 ºC to an OD_{600} of 1.6 to 1.8 and subsequently cooled to 19 °C. Protein expression was induced with 0.2 mM IPTG for and proceeded for 12–13 hours at 19 °C.
Cells were harvested by centrifugation for 10 min at 5.000 rpm with a Sorvall SLC-6000 rotor. The cell pellet was subsequently resuspended in 50 mM K-Phosphate (pH 8.0), 150 mM NaCl (buffer A) with the addition of 1 mM phenylmethyl sulfonyl fluoride (PMSF), 20 mg/ml DNaseI, 1 mg/ml lysozyme, 1 mg/ml pepstatin and 1 mg/ml leupeptin. Cells were lysed with an Emulsiflex high-pressure homogenizer (Avestin) with three to four passages at ~6000 psi and the lysate was cleared by low-spin centrifugation at 10.500 g for 15 min. Membranes were isolated by ultracentrifugation for 1 h at 45.000 rpm on aTI-70 rotor (Beckmann). For storage membranes were homogenized in 10% sucrose (w/v) in 1 / 10 of the final extraction volume, flash-frozen in liquid nitrogen and stored at -80 °C.

5.3.3 Protein preparation

The frozen membranes were homogenized in buffer A (10 ml buffer/g of membrane) and extracted by addition of 2 % detergent. For crystallization ELIC was extracted with n-undecyl-β-D-maltoside (UDM, Anatrace, Inc.) and purified in buffers containing 3 mM UDM, whereas GLIC was extracted with n-dodecyl-β-D-maltoside (DDM, Anatrace, Inc.) and purified with 0.5 mM DDM in all following buffers. Extraction was carried out for 1.5h at 4 °C and the solution was subsequently centrifuged for 20 min at 17.000 rpm on a Heraeus 3335 rotor. The supernatant was supplemented with 15 mM imidazole to reduce unspecific binding to the IMAC column. Both homologues were purified by affinity-chromatography on Ni-NTA resin (Qiagen). For this purpose the protein was supplemented with 12.5 ml Ni-NTA beads and incubated for 40 min. Afterwards the mixture was loaded on an empty gravity flow column and washed with buffer A containing 15 mM and 55 mM imidazole until OD_{280} reached baseline. The protein was eluted with buffer containing 300 mM imidazole in a final volume of ~25 ml. To remove the His_{10}-tag and the MBP, the

eluted fusion protein was digested for 2 h at 4°C by addition of 3C precision protease in a 1:20 w/w ratio of protease to fusion protein. During these 2 h the solution was dialyzed against a buffer containing 10 mM K-Phosphate (pH 8.0), 150 mM NaCl and detergent at a concentration of 1.2 CMC to remove the imidazole. After cutting, the solution was passed over the same Ni-NTA column used for purification to remove the MBP/His_{10}-tag and the His-tagged 3C protease. The flow-through containing the pLGIC was collected and concentrated using a Vivaspin Centrifugal Filter Unit (Millipore) with a 30 kDa molecular weight cutoff to a volume of ~ 400 µl. The protein was filtered (Millipore 0.22 µm spin filters) and then subjected to gelfiltration on a Superdex S200 column (GE Healthcare) in a buffer containing 10 mM Tris (pH 8.0), 150 mM NaCl and either 3 mM UDM (for ELIC) or 0.5 mM DDM (for GLIC). The chromatogram usually showed two peaks, one at the void volume of the column and a second peak corresponding to a pentameric channel (at 11.2 ml). The second peak was pooled and used for further experiments.

5.3.4 Crystallization and crystal preparation

GLIC and ELIC were crystallized in sitting drops at 4 °C. Crystals were obtained by mixing protein containing additional 0.5 mg / ml *E. coli* polar lipids (Avanti Polar Lipids, Inc.) in a 1:1 ratio with reservoir solution containing between 200-500 mM $(NH_4)_2SO_4$, 50 mM sodium acetate (pH 4.0), 9–13% (w/v) PEG 4000 for GLIC and 200–300 mM $(NH_4)_2SO_4$, 50 mM ADA (pH 6.5), 9–14% (w/v) PEG 4000 for ELIC. For cryoprotection, the crystals were transferred into mother liquor containing 30% (v/v) ethylene glycol and flash-frozen in liquid propane. For structural studies on channel block in GLIC, the complexes were obtained either by cocrystallization or by soaking of native crystals in solutions containing the respective inhibitors (5 mM TBSb (Aldrich), 10 mM TEAs, 30 mM TMAs, 15 mM bromo-lidocaine). For divalent ions, NaCl was replaced by the respective Cl^- salt (100 mM $ZnCl_2$ or 50 mM $CdCl_2$).

5.3.5 Data collection and refinement

All datasets of ELIC and GLIC were collected on frozen crystals on the X06SA beamline at the Swiss Light Source of the Paul Scherrer Institute on a 6M PILATUS detector (Dectris). For block studies a suitable wavelength to maximize the anomalous diffraction of the bound inhibitors was chosen (As, 1.04 Å; Br^-: 0.92 Å; Cd^{2+}: 0.46 Å; Sb^+: 0.4 Å; Zn^{2+}: 1.28 Å). The data were indexed, integrated and scaled with XDS (*83*) and further processed with CCP4 programs (*84*). The crystals for all mutants and complexes were isomorphous to WT (GLIC space group *C*2 (cell dimensions: a = 178.5 Å, b = 133.5 Å, c = 160.5 Å, $\alpha = \gamma = 90°$, $\beta = 106.1°$) and ELIC $P2_1$ (cell dimensions a = 105.5 Å, b = 266.2, Å, c = 110.85 Å, $\alpha = 90.0°$, $\gamma = 90.0°$, $\beta = 109.5°$)). The structures of GLIC (PDB code 3EHZ) and ELIC (PDB code 2VLO) without water molecules served as starting models that were improved by rigid-body refinement in PHENIX (*85*). The electron density was inspected and structural changes, mutations and heavy atoms were introduced in COOT (*86*) and subsequently refined in PHENIX. For datasets exceeding a resolution of 3.6 Å, the structures were additionally subjected to refinement of individual atom positions in PHENIX maintaining global NCS constraints. In later stages, the strict constraints were

loosened (to account for subtle differences between each subunit) and restraint individual B-factors were refined. R_{work} and R_{free} were monitored throughout. R_{free} was calculated from the same 5% set of reflections that were initially selected and omitted in the refinement.
For the calculation of the anomalous difference densities, a high resolution cutoff of $I/\sigma I > 5$ was used throughout. The one-dimensional density profile along the pore was sampled using the program MAPMAN (*84*). The molecular surface was calculated with MSMS (*87*).

5.3.6 Isothermal Titration Calorimetry

The proteins (ELIC WT and its mutants) were purified as described above except that the gelfiltration buffer was exchange for the ITC buffer (25 mM Hepes pH 7.0, 150 mM NaCl, and 0.9 mM UDM). The purified protein was dialyzed overnight at a concentration between 100-250 µM (monomer) against ITC Buffer. Binding of the agonist propylamine and the antagonist acetylcholine to ELIC was measured by isothermal titration calorimetry (ITC) with a MicroCal ITC200 system (GE Healthcare). The syringe was loaded with agonist solution containing a 300x molar excess of propylamine or acetylcholine to the monomer dissolved in ITC buffer for ELIC WT, a 175x excess for the mutant R91A and a 70x excess for the ELIC mutant T28D.The sample cell was loaded with 300 µl of purified ELIC in ITC buffer. Ligand was applied by sequential injections of 2 µl aliquots followed by a 180-240 s equilibration period after each injection. A heat of dilution recorded by injection of the ligand into ITC buffer not containing any protein was subtracted from the measurement. The background corrected data was analyzed by a fit to a single-site binding isotherm (Origin 7.0).

5.3.7 EPR

5.3.7.1 Sample preparation

The mutants of ELIC and GLIC were essentially purified as described before with the following deviation: after the elution from the 2nd Ni-NTA column the protein concentration was measured and a 1:1.5 molar ratio of MTSSL label was added. The protein was subsequently incubated with the label for 3hs or o/n. To get rid of the excessive spin label the mixture was subjected to gel-filtration (in the same buffer as described before). The protein peak corresponding to the pentamer was pooled and concentrated to 10-15 mg/ml. For each construct two aliquots of 50 µl each were used for the EPR experiment. One aliquot was recorded under ligand-free conditions, the second aliquot was mixed with agonist (10 mM propylamine for ELIC and 50 mM Acetate (pH4) for GLIC). For cryo-protection 10% D-glycerol was added as a last step to each sample, before flash freezing it in liquid nitrogen.

5.3.7.2 Continuous Wave (CW) EPR Measurements

EPR spectra were recorded at X-band frequencies (9.3–9.4 GHz) with a Bruker Elexsys 580 spectrometer equipped with a Bruker super-highQ cavity and a continuous flow N_2 cryostat. For room temperature recordings, the microwave power was set to 0.6 milliwatts

and the *B*-field modulation amplitude to 0.1 milli-Tesla. To quantify the labeling efficiency the CW spectra of the sample was compared to a standard (100 µM TEMPOL) measured afterwards on the same spectrometer, which allowed the quantification of the label concentration in the sample and the ratio of label to protein subunit.

5.3.7.3 DEER EPR Measurements and Data Analysis

Q-band DEER measurements with high power excitation were performed using the homebuilt Q-band spectrometer operated from a standard console (Bruker) equipped with a pulsed TWT amplifier with a nominal output power of 150 W (Applied Systems Engineering Inc.). All measurements were performed using the four-pulse DEER experiment. Experimental data were collected at 50 K with observer pulse lengths of 16 ns for $\pi/2$ and 32 ns for π pulses, with the electron double resonance π pulse set to 12 ns. Proton or deuterium modulations were averaged. Data analysis of the DEER traces was performed with the software DeerAnalysis 2008.1.

6 Appendix A

6.1 Abbreviations

2EVC	Two electrode voltage clamp
5HT	5-hydroxytryptamine, or serotonin
Ach	acetylcholine
AChBP	Acetylcholine Binding protein
Ala	Alanine
Asp	Aspartate
Cys	Cysteine
EC_{50}	Conc. of agonist that leads to 50% of the maximally evoked currents
EPR	Electron Paramagnetic Resonance
ELIC	*Erwinia chrysanthemi* Ligand-Gated Ion Channel
GABA	γ-amino butyric acid
GLIC	*Gloeobacter violaceus* Ligand-Gated Ion Channel
Gly	Glycine
Glu	Glutamate
IC_{50}	Conc. of inhibitor that leads to 50% of the maximally evoked current
ITC	Isothermal Titration Calorimetry
Leu	Leucin
LGIC	Ligand-Gated Ion Channel
nAChR	nicotinic acetylcholine recpeptor
pa	propylamine
pLGIC	pentameric Ligand-Gated Ion Channel
SCAM	substituted cysteine accessibility method
Tyr	Tytosine
Val	Valine
WT	wild type

7 Appendix B

7.1 Structural characterization of prokaryotic pLGICs by double echo electron spin resonance (DEER) spectroscopy.

In collaboration with Dr. Polyhach Yevhen (yevhen.polyhach@phys.chem.ethz.ch).

7.1.1 Aim

In the course of the studies on signal transduction across the domain interface of ELIC and GLIC I have crystalized several mutants of the two prokaryotic homologues. Despite the pronounced phenotypes observed in electrophysiological experiments, the structures of the mutants generally showed, apart from local changes, similar conformations. These observations suggested that only a subset of possible conformations of the channels may be accessible in detergent solution. In the membrane protein field the question in how far detergent solubilized proteins reflect the natural behavior of the protein in a lipid environment is a topic of continuous debate (*88-91*).
In this work, I have attempted to characterize the different conformations of the pore region that are accessible in detergent solution and try to relate them to the conformations seen in the know crystal structures. For that purpose I have used DEER measurements, an EPR method which measures distances between introduced spin labels, to determine conformational changes in the transmembrane domain induced by the binding of the ligand.

7.1.2 Results

In order to determine whether the two prokaryotic homologues ELIC and GLIC undergo structural rearrangements in a detergent environment, I performed "double echo electron spin resonance" (DEER) EPR experiments. In such experiments, a methanethiosulfonate spin label (MTSSL, (*92*)) is introduced to the protein. This MTSSL reagent is a highly reactive, thiol-specific label and contains a group with a stable free radical (unpaired valence electron) that can be detected by EPR. The DEER experiment measures the distance between the free radicals, which are covalently linked to the protein via accessible cysteines (Cys).

Initially, a cys-free version of the protein was constructed. For that purpose both natural Cys residues present in either protein were mutated to valine or leucin by site-directed mutagenesis. To confirm that these cys-free mutants of ELIC and GLIC are still functioning, they were analyzed in two electrode voltage clamp (2EVC) experiments (*40*, *58*). For that purpose *Xenopus* oocytes were injected with cRNA coding for the different mutants. After a few days ligand-induced currents were measured at a holding potential of -50 mV. These experiments showed that the cys-free mutants still respond to the ligand in a similar manner as WT (Data not shown).

The next step was to introduce single cys residues by site-directed mutagenesis. For an accurate measurement of an introduced spin label in an EPR system several factors had to be considered. First, the sites need to be accessible for labeling and second, the distance between each spin label should be in a detectable range between 1.5–8 nm. To accurately distinguish conformational changes, distances have to differ by at least 0.15 nm (*93*).

The proposed opening mechanism based on the two available structures was taken as a starting point to select appropriate positions (*5*). In this mechanism the extracellular and the pore domain undergo two distinct conformational changes upon channel activation.

One is a rotation for each extracellular subunit around an axis that is slightly tilted with respect to the channel axis, whereas in the pore domain a rotation is assumed for each subunit around an axis that is perpendicular to the pore. With regards to the transmembrane domain, these changes should only affect helices α2 and α3, whereas the other two α-helices (1 and 4) remain largely unchanged. Based on this model, the structural differences assumed for the pore domain would be in the suitable range for EPR distance measurements (Figure 53). Helix α3 was chosen for labeling due to its better accessibility and since the label distances are in the appropriate range for EPR experiments.

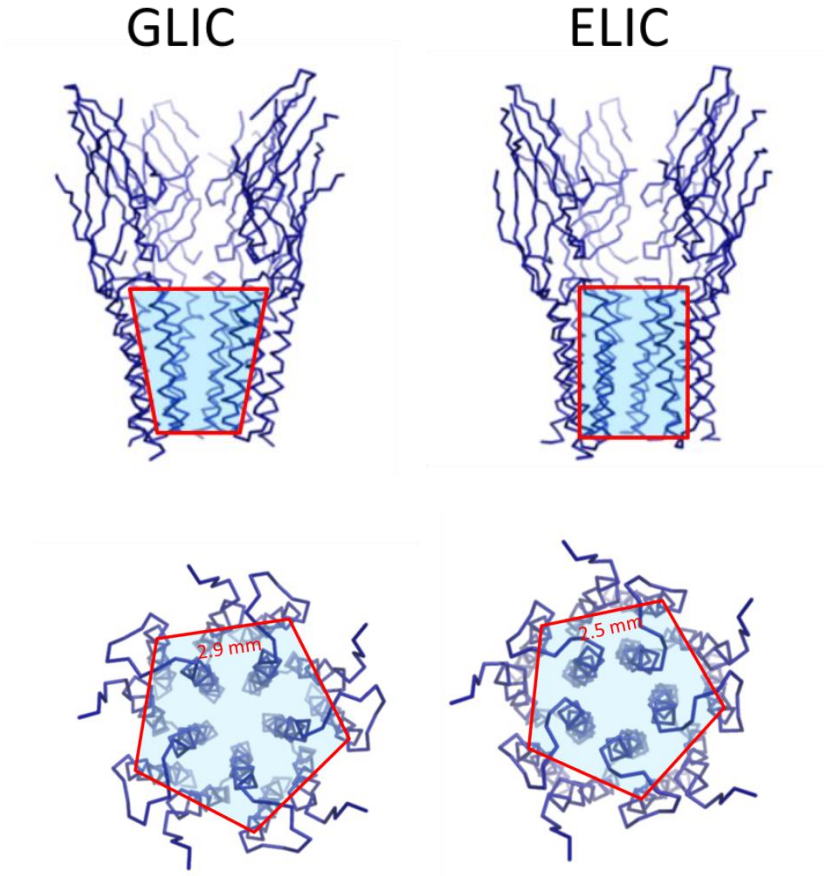

Figure 53: (top) Ribbon representation of the crystal structures of GLIC (left) and ELIC (right). The front subunit has been removed for clarity. Red lines in both structures in the pore domain show the expected movement of helixα-3 upon pore opening. For GLIC these helices are arranged in a funnel-shaped manner, whereas for ELIC they are cylindrical. (bottom) Extracellular view on the TM part of both homologues (GLIC, left, ELIC, right). The dimension of the pentagon differs significantly between the two homologues. In GLIC the α3 helices on the extracellular side are further apart from each other than in ELIC.

To identify appropriate labeling positions in the pore domain, simulations were performed. These simulations take into account the accessibility and flexibility of the spin-label attached to the structure of the protein at a certain position (by using a rotamer library within the MMM program (*94*)). The structure itself was assumed to be immobile in these simulations. An example for such a simulation on GLIC is shown in Figure 54. The simulation of the DEER experiment shows an appropriate distance distribution (bottom right - red) for this site in GLIC that is in a sensible range for DEER experiments. Two distinct sharp distance peaks are observed, one of which had a small shoulder at a short distance range (Figure 54).

These two peaks are due to the fact that there are two possible monomer distances observed within the pentamer, a short distance between two adjacent subunits and a long distance between subunits in 1 - 3 position.

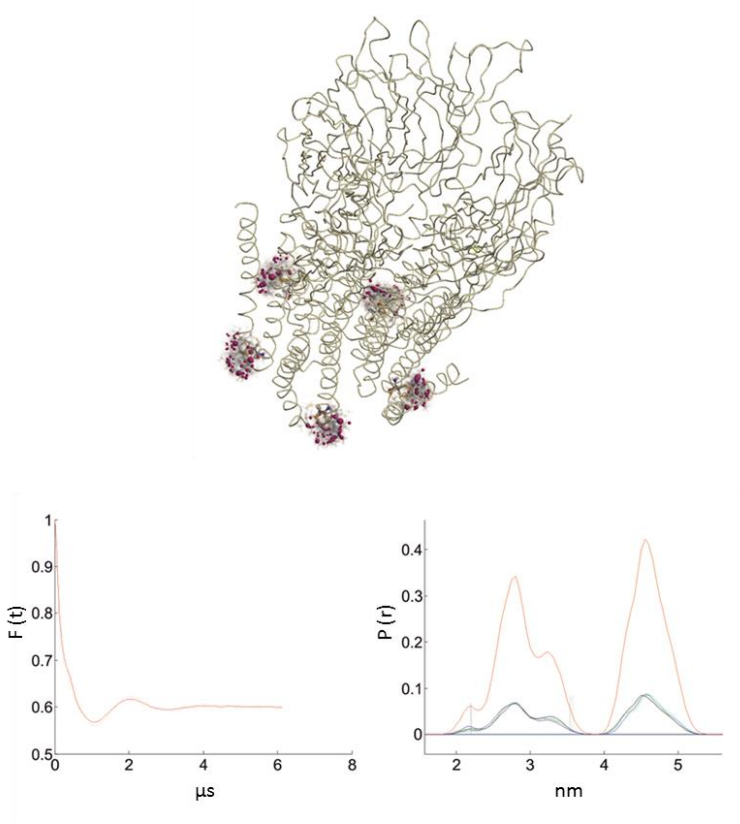

Figure 54: (top) MMM simulation of the accessible rotamers of the spin labelled GLIC mutant L278C. GLIC is shown in ribbon representation (grey). The MTSSL attached to the protein is in yellow. The possible spin location is shown as red spheres. (bottom, left) Background corrected dipolar evolution function (Form factor, F (t) - simulated DEER traces) based on the distance distributions (P (r)) of the rotamer cloud in red. (bottom, right) Corresponding distance distribution P(r) of the DEER trace is shown in red.

To address the question whether the structural rearrangements are as proposed by the model, two positions (on the intra- and extracellular part of α-helix 3) were selected for each homologue. The intracellular position was located at the extracellular start α-helix 3 (i.e. at Phe281 in ELIC and Ala278 in GLIC). The simulated traces and the corresponding distance distributions for this position look significantly different to be distinguishable (Figure 55). In GLIC, the short distance shown in the simulation has its peak height at around 2.8 nm, whereas the long distance would be around 4.6 nm. While in ELIC the corresponding sites would be at a short distance of 3.3 nm and a long distance of 5.2 nm. The distance differences between these two simulations, of 0.5 nm for the short and 0.8 nm for the long distance, would also be in the detectable range for a DEER experiment.

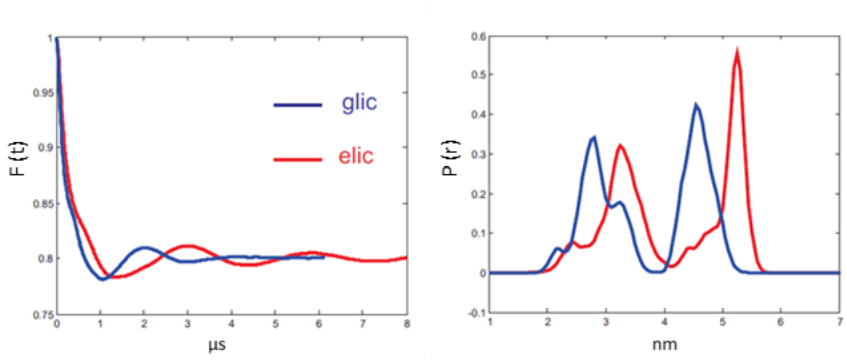

Figure 55: Results of a simulated DEER experiment at the Position ELIC F281C and GLIC L278C based on their respective crystal structure. (left) Simulated DEER signal. The signals show already at short time ranges significant differences. (right) Corresponding distance distribution of the DEER simulation.

On the extracellular side of the pore, residues at the N-terminal end of α helix 3 were selected (i.e. Gly263 for ELIC and Ala256 for GLIC). The distance distribution for the ELIC mutant G263C (red) is broad, indicating a bigger flexibility for the spin label (Figure 56). The short distance has several peaks that are spread between 2.5 nm up to 3.8 nm. The long coupling distances is reflected in a peak around 4.9 nm. For the equivalent position in GLIC (i.e. A256C) the distance distribution is sharper. Two peaks for the short distance (around 3 nm and 3.6 nm) and one peak (5.2 nm) for the long distance are clearly distinguishable.

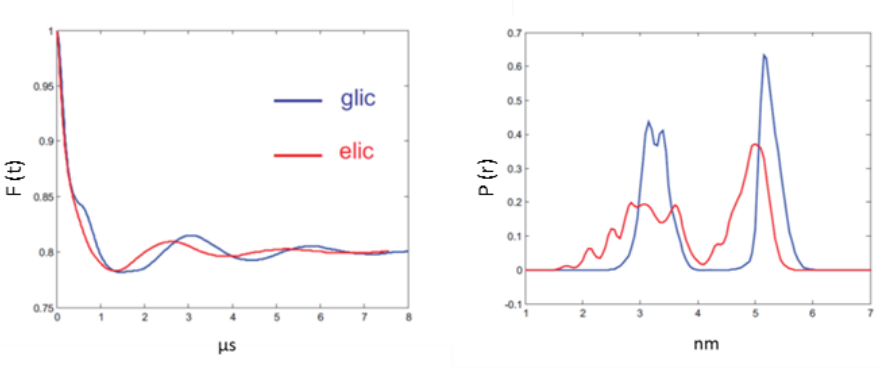

Figure 56: Results of a simulated DEER experiment for the mutants ELIC G263C (red) and GLIC A256C (blue) based on their crystal structure. (left) Simulated DEER signal. The signals show already significant differences at early time points. (right) Corresponding distance distribution of the DEER simulation. .

To exclude that the introduction of the amino acid cysteine would affect the ability of the channel to open, 2EVC experiments were performed. These experiments showed that the introduced Cys did not change the functional properties of the channel (Figure 57).

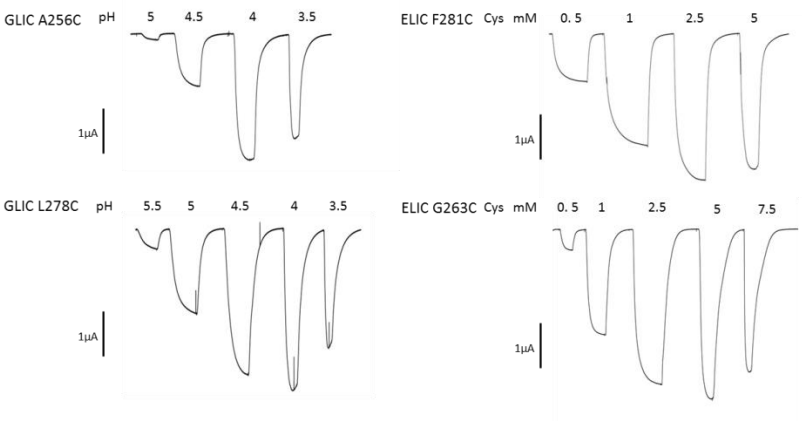

Figure 57: Does response 2EVC traces of the Cysteine mutants in A256C and L278C of GLIC (left) and F281C and G263C of ELIC (right). pH values (for GLIC) concentration of the ligand propylamine (for ELIC) are indicated. The voltage was set to -70 mV.

For the EPR experiments the mutated channels had to be purified in large amounts and subsequently labeled. To investigate whether the introduction of a cysteine might have altered the properties of the different mutants in *E. coli*, their expression was studied in small scale cultures. These experiments showed that for mutants in the extracellular part of the pore the ELIC mutant F281C was stronger expressed than the corresponding mutant L278C in GLIC. An opposite behavior was found for the mutations at the intracellular part, where A256C of GLIC expressed at higher yields than G261C of ELIC (Figure 58).

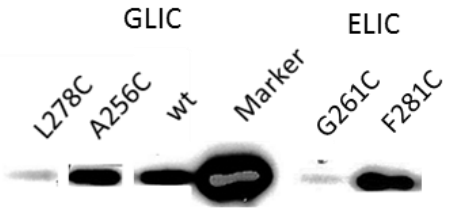

Figure 58: Western Blot analysis of the expression properties of different Cys mutants of ELIC and GLIC expressed in *E. coli* BL21 cells. The His-tagged proteins were detected with an Anti-His Antibody.

For labeling the proteins were expressed in a 9.6 l for ELIC and 19.2 l for GLIC, purified in the detergent DDM and incubated with the spin label. To confirm that the sites are accessible to the spin label (MTSSL) and to quantify the labeling efficiency, a continuous wave (CW) experiment was performed. These experiments showed a complete incorporation of MTSSL at the free cysteines (data not shown) and thus confirmed that the site is accessible. At this point the labeling strategy had to be optimized. This optimization was needed, since a pentamer, if all sites are labeled, would contain five spin labels. In a system, which has more than two direct spin neighbors multi spin interferences may complicate the analysis. In this case each spin is influenced by the decay and interferences of differently behaving spins which results in a complex pattern that is difficult to deconvolute. To overcome this problem, a molar ratio of pentamer to spin label of 1:1.5 was used for labeling. In such a case, on average one pair of labels would be introduced

and thus only a single distance per pentamer would be measured, without mutli spin interference. After CW experiments have confirmed the expected ratio of label to protein, DEER data was recorded to obtain distance distributions. Initial DEER experiments with the labeled mutant F281C-MTSSL of ELIC showed a very fast relaxation time (T_m), which does not permit accurate distance measurements (Figure 59).

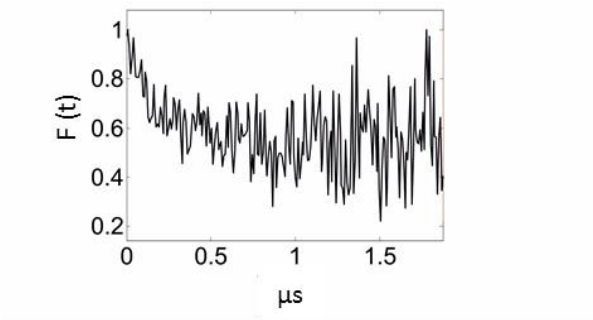

Figure 59: DEER spectrum of the ELIC F281C labeled mutant. The sample is very noisy and that there are no oscillations are visible.

To decrease the spin relaxation, 10 % of deuterated D-glycerol had to be added. Glycerol acts as cryoprotectant and prevents the formation of water crystals upon flash-freezing in liquid nitrogen, which could denature the protein sample. The deuterated form of glycerol is used for technical reasons: Protons (H) have a nuclear spin, which is detectable in NMR experiments. In the DEER experiment, all free valance electrons (radicals) are aligned in the field – which results in a signal whose decay is recorded in the measurement. Electron spins and nuclear spins are excited at different wavelengths, therefore in a DEER experiment the nuclear spins are not excited. However, each spin creates a local magnetic field, which is sensed by all other spins, regardless of their origin. This magnetic field leads to a disturbance of the align spins of the DEER experiment and therefore to a faster decay of the signal. By adding a deuterated compound into the solution the number of nuclear spins in the system, and thus the interference is reduced. The addition of D-glycerol allowed the recording of the signal up to 4 µs, which made it possible to measure distances to maximally 4.5 nm. For accurate distances measurement of additional distances, a longer time span would have to be measured. Therefore in this study, only the short distances of the system were taken into consideration. After optimization of the labeling and the reduction of the noise and the spin relaxation time a DEER spectrum was recorded. For that purpose each cys mutant was purified, labeled, cryo-protected and flash-frozen. For the label at the intracellular side of the pore in ELIC (mutant F281C) the data was of sufficient quality to allow the quantification of the shorter of the two possible distances. The measurement of the protein in the absence of its agonist showed 2 peaks (Figure 60), a big and broad peak for the short distance at a maximum at around 2.9 nm and a smaller peak for the long distance at around 5.8 nm. Similarly two peaks were observed in the presence of the agonist, with one having a maximum at around 3.2 nm and another around 5 nm. Despite the recorded difference in the short distance upon application of the agonist, this difference could also arise from the different phase drifts and noise during the experiment.

Therefore more measurements need to be performed to accurately quantify potential conformational changes upon ligand application.

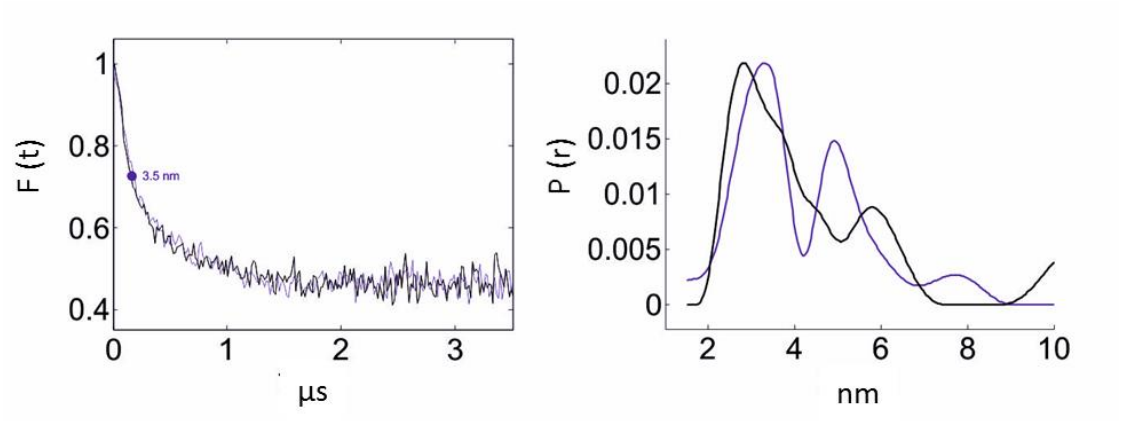

Figure 60: DEER traces of the labeled ELIC mutant F281C. (left) DEER signal (form factors) in the presence (blue) and absence (black) of the ligand. (right) Corresponding distance distribution in the same coloring scheme. From the comparison of the DEER signal it is hard to judge whether the obtained changes in the distance distribution reflect a conformation change or whether they originate from noise.

Analogous experiments were performed for the position A256C at the extracellular part of the pore of GLIC. After optimization of the labeling procedures (CW data not shown), a DEER experiment was recorded. Also, for this mutant of the pH gated channel GLIC, the protein was incubated at two distinct conditions, at high (pH 4) and low proton concentration (pH7). In both cases, a DEER signal could be measured which only allowed the accurate determination of the short distance. The sample that was incubated at neutral pH (Figure 60, blue trace) had two distinct peaks. The short distance had its maximum at around 3.4 nm while the long distance is around 5.5 nm. For the samples that were incubated at low pH the recording showed, despite the high concentration of the ligand which should favor the open state, a very similar pattern to the one observed at neutral pH. The long distances overlapped and in the region of short distances, three overlapping peaks were formed (with maxima at 2.9 nm, 3.8 nm and 4.2 nm). Due to the weak signal, however, the values have to be taken with caution as it is still possible that all three peaks correspond to one distance around 3.3 nm (Figure 61).

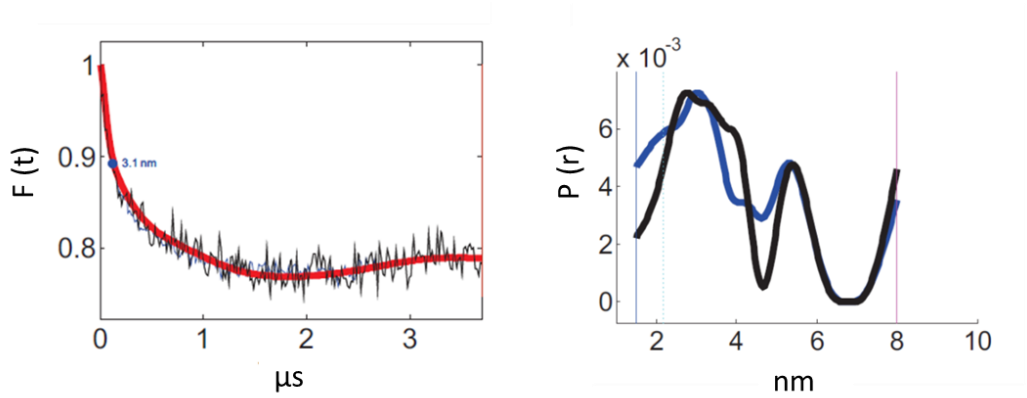

Figure 61: Superposition of the DEER data of the labeled GLIC mutant A256C recorded at pH4 (black) and ph7 (blue) (left) and the corresponding distance distribution (right) The red line on the left panel shows the fit to the data recorded at pH 4..

7.1.3 Discussion

In this study DEER experiments were used to characterize ligand-induced conformational changes in the two prokaryotic homologues ELIC and GLIC and to assess whether such changes could be observed for the detergent solubilized protein. Currently it is not known whether the structural rearrangements underlying pore opening in a lipid environment are also accessible in detergent solution.

For the intracellular part of the transmembrane domain, the ELIC mutant F281C was selected. In the absence of the ligand, the measured signal does not correspond very well to the simulated MMM signal of the spin label added to the respective position of the crystal structure. Whereas the simulated distance was around 3.4 nm, maximum of the broad peak of in the distance distribution measured in the DEER experiment was around 3 nm, which indicates that in solution, the actual distance is smaller than in the crystal environment but bigger than predicted in the simulations of the equivalent position in GLIC. The observed distance distribution thus shows a pore, with dimensions in-between the crystal non-conductive structure of ELIC and the conductive structure of GLIC. It could thus be that the crystal structure shows a conformation that is biased by the crystallization conditions. The smaller distance could easily be obtained by a slight tilting of the α2 and α3 helices without changing the functional state of the protein.

Upon ligand activation, the proposed mechanism would predict a narrowing of the pore, to reach its funnel-like shape. This reduced distance would also be required for the glutamates at the end of the α2 helix to form a selectivity filter (*5, 49*). In my experiments the opposite movement, a potential widening of the pore by 0.3 nm, was observed upon ligand addition. The correspondence of the distances in the presence of the ligand with the crystal structure of ELIC (crystallized in the absence of its ligand), indicates that observed structure may resemble a desensitized state, the stable conformation of the channel in the presence of its agonist. ITC experiments (*67*) in contrast do not support the hypothesis of the detergent extracted protein resembling a desensitized state. There the measured affinity of the channel to its ligand is too weak, since in a desensitized state the binding affinity is expected to be much higher (*13*). The fact that the ligand-bound state in detergent solution can neither be assigned to an activated nor a desensitized state indicates that the protein in detergent solution may behave differently than in the membrane.

In any case more accurate data is required to reach conclusive results. Such experiments may benefit from recent the advances in data acquisition and mutants, which lock the protein in specific states and that would thus allow to more accurately determine structural differences. For the GLIC mutant A256C labeled in the extracellular part of the pore, the experimental and simulated results for the pH 4 condition were very similar. It can thus be concluded that the state seen in the crystal structure is also present in solution. At neutral pH, where the protein is expected to change into a resting state, the same distance distribution was observed. These results indicate that the conformation of the α3 helices seen in ELIC are not found for the homologue GLIC, which could either indicate that there is no structural rearrangement in this position upon pore opening, as proposed in recent studies (*5*), or that this conformation cannot be reached in detergent solution. A novel activation mechanism for GLIC was proposed based on different crystal structures (*62, 95,*

96). In this mechanism, activation underlies a local reorganization of the α2 helix, whereas the α3 helix retains its conformation in both states of the protein. The results of this study are in agreement with this mechanism. It can, however, also not be excluded that the protein in detergent solution may not be able to adopt all conformations accessible in the membrane environment. Recent findings from EPR experiments on the homologue GLIC have indeed shown a different structural behavior in a detergent and a lipid environment (*96*).

In the EPR studies on ELIC and GLIC I was able to observed two different behaviors. In ELIC, where distance changes in the intracellular part of the pore were studied, I have observed, a narrower pore than seen in the crystals structure in the absence of the ligand. Upon ligand binding, this pore appears to widen to the dimensions seen in the crystal structure, which could indicate that in its pore region the crystal structure could resembles a ligand bound, desensitized state.
With regards to GLIC, my findings are not in agreement with an initial model that have proposed a change from an ELIC to a GLIC-like conformation upon ligand activation, but they correspond to the newer finding of activation by local changes the α-helix 2.
These conclusions are very preliminary and still speculative since they all rely on measurements of a single position whereas data of more positions would be required to obtain conclusive insight. It should also be emphasized that the data quality will have to be significantly improved. Finally all experiments should be remeasured after reconstituting of the protein into a lipid environment, such as nanodiscs (*97*) or liposomes. Since experiments in detergent solution might not exactly reflect the conformational behavior of the protein in its lipid environment (*91*).

8 Appendix B

8.1 Modulation of the prokaryotic pLGIC ELIC

8.1.1 Introduction

8.1.1.1 Partial agonists

pLGICs can be activated by a variety of different chemical compounds. Some molecules, which bind to the same binding site as the agonist, at full occupancy only evoke a fraction of the maximum response of the channel. These orthosteric modulators are called partial agonists. In the del-Castillo-Katz model this phenomenon is explained by differences in the efficacy of gating (*8*). Based on analysis of single channel events with different concentrations of full and partial agonists, a new intermediate was proposed, the flipped state. This state was seen to correspond to a conformational rearrangement in the extracellular domain, before pore opening, and could correspond to the C–loop capping seen in AChBP. Additionally, these experiments revealed that the difference of partial and full agonist is not due to the gating step, but rather because of the transition between the resting ligand bound state and the flipped state (*98*).

8.1.1.2 Allosteric modulators

pLGICs are allosteric proteins, which exist in several different conformational states. The distribution between these states is related to their free energy by a Boltzman distribution. Allosteric modulators can bind to one or several of these states and such influence their free energy, which in turn leads to a different population of states and thus a shift in the equilibrium. The binding site of these modulators is not confined to a specific place but can instead be in different parts of the protein. Allosteric modulators influence the apparent affinity of the receptor to the agonist by influencing the equilibrium between the open and closed states once the ligand is bound. This effect can either be positive or negative. Positive modulators are termed allosteric potentiators, while negative ones are called allosteric inhibitors.
As described earlier a change in the EC_{50} does not allow to discriminate whether the effect shifts the genuine affinity of the ligand or the efficacy of pore opening. Therefore further investigations are required to address whether which parameter would be influenced.
Different to competitive inhibitors is that the effect is saturable. (*18*).

Several allosteric modulators of pLGICs have been discovered and characterized. All have distinct binding sites in the in the receptor, distant from the agonist binding site. The chemical composition of these modulators vary highly from small proteins to ions and for the α7 nAChR
PAMs have been considered as potential drugs (*72*).

Calcium ions were the first known allosteric potentiators of α7 nAChR (*99*) responses, followed by the discovery of the antiparasitic agent ivermectin (*100*). Unfortunately, these "first generation" α7 PAMs lack desirable potency, efficacy, and/or selectivity profiles for potential drug targets. For example, ivermectin is non-selective, since it also works on other pLGICs (*6*).

Since the discovery of the first α7 nAChR modulators, small molecular PAMs with diverse potency, efficacy and selectivity profiles have emerged. These discoveries have led to the classification of PAMs into two categories. The PAMs classified as type I, increase the amplitude and therefore the efficacy of an agonist but they do not alter the kinetics of agonist-evoked responses. Type II PAMs appear to slow or reverse α7 nAChR desensitization and therefore show higher currents than obtained from agonist application alone (Figure 62).

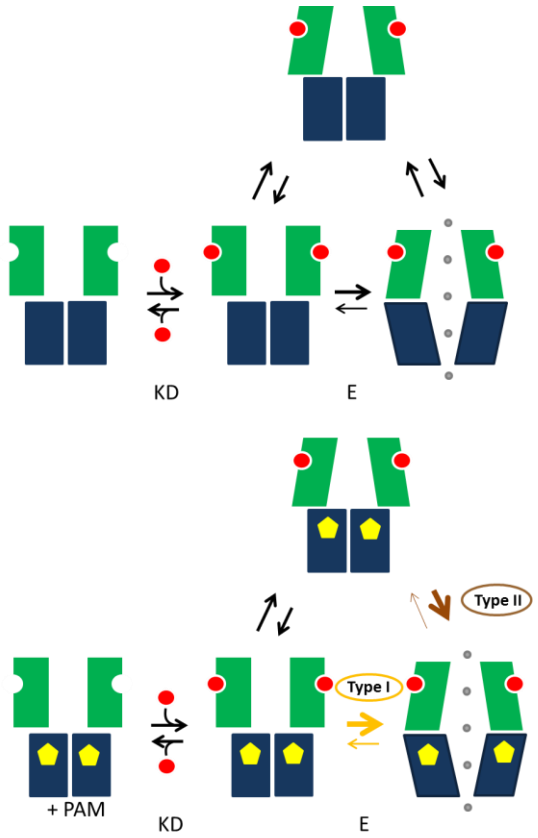

Figure 62: Schematic mechanism of activation and desensitization of pLGICs in the absence and presence of PAMs. In the first step the receptor binds to its ligand. This step is described by the affinity constant K_D. In the second step the bound ligand induces a conformational change in both the extracellular and pore domain characterized by the efficacy (E). In a third step the activated, ligand bound, channel can go into a desensitized, non-conductive, state. The positive allosteric modulators (PAM) bind the channel in the closed, ligand unbound state. In the presence of PAMs two effects can be observed. First (orange) the efficacy of the ligand can be enhanced and secondly (brown) the population of the desensitized state is reduced or even completely abolished (Adapted from doctoral thesis of I. Zimmermann (*18*)).

8.1.2 Results & Discussion

The modulation of pLGIC is complex and goes beyond competitive inhibition, open pore block and the modulation with divalent ions. The previously described negative effect of divalent ions as pore blockers is not their only mode of interaction with pLGICs. They have also been described as positive allosteric modulators (PAM) (*72*). PAMs are able to change the population of states in the presence of the ligand and are thus potentially useful tools for structural studies. The type which shows the biggest potential for structural studies are the type II PAMs, since they are able to reduce or completely abolish the presence of the desensitized state (*72*). This would lead to a decreased conformational diversity in the presence of the ligand and a stabilization of the instable open state. It was previously shown that the use of a PAM played a critical part in the structure determination of the first eukaryotic pLGIC GluCl. There, the known PAM Ivermectin, which binds in the pore region, was used to stabilize the open state of the protein (*6*).

In an attempt to stabilize the homologue ELIC in a conductive conformation, I have investigated whether positive allosteric modulators for this protein exist and they benefit my structural studies.

In an initial approach, I have investigated whether Ivermectin would exert an additional activating effect in either of the two homologues ELIC or GLIC. However, the application, together with the agonist only had a slightly inhibitory effect. Even the introduction of mutants in ELIC and GLIC to closer resemble the binding site of GluCl did not show the desired outcome (data not shown). As Ivermectin did not show the expected effect different known PAMs of the nAChR were tested (Figure 63)

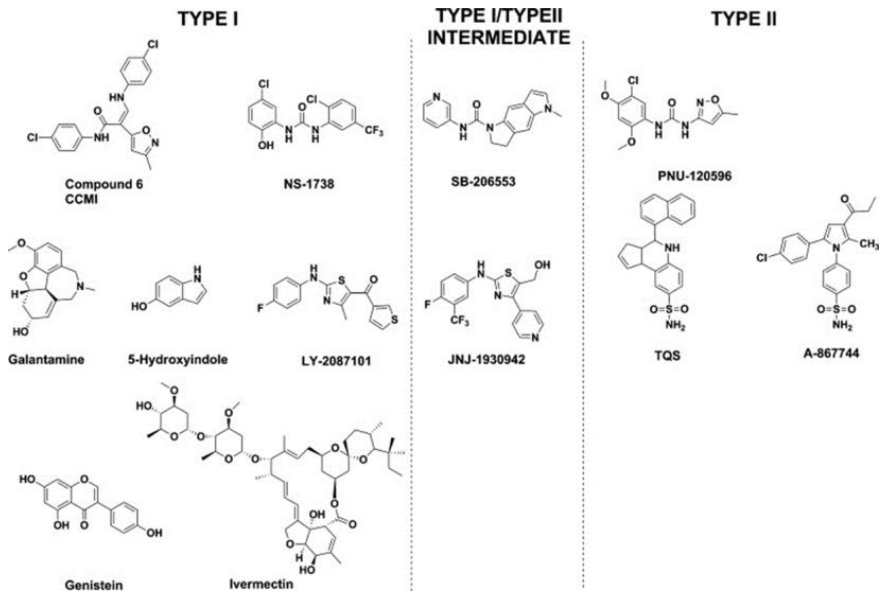

Figure 63: Structures of PAMs activating the α7 nAChR. The molecules are grouped according to their mechanism of action.Type I PAMs increase the amplitude but do not strongly alter the kinetics of α7 nAChR -mediated agonist-evoked responses. Type II PAMs slow or reverse α7 nAChR desensitization. (*72*).

Initial 2EVC experiments in oocytes showed that several of the investigated molecules may act as PAMs (Figure 64). By this assay the type I PAMs CCMI, NS1738 and Ly2087101 and the typ II PAM TQS were found as potential candidates (Figure 64).

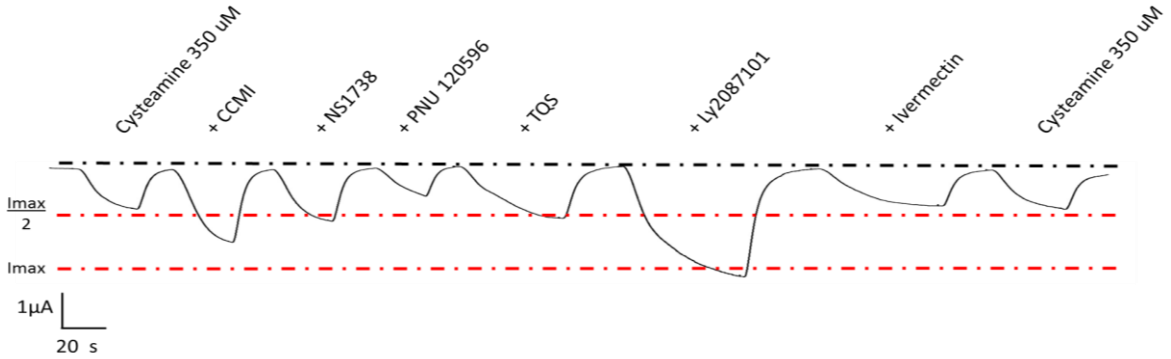

Figure 64: 2EVC experiments investigating the effect of known enhancers of the α7 nAChR on ELIC at a holding potential of -60mV. In addition to the application of cysteamine at its EC_{50} (350uM) different potential enhancers were applied. The concentration for each enhancer was chosen based on their maximal solubility (Tocris AG). All potentiators were easily washed out after application. Some compounds show strong activating effects.

These potentiators showed increased currents upon co-application with the agonist cysteamine at its half maximum activating concentration. The most promising candidate was Ly2087101. When applied together with the ligand at a concentration of 20 µM, currents higher than the I_{max} for cysteamin activation were observed (Figure 65).

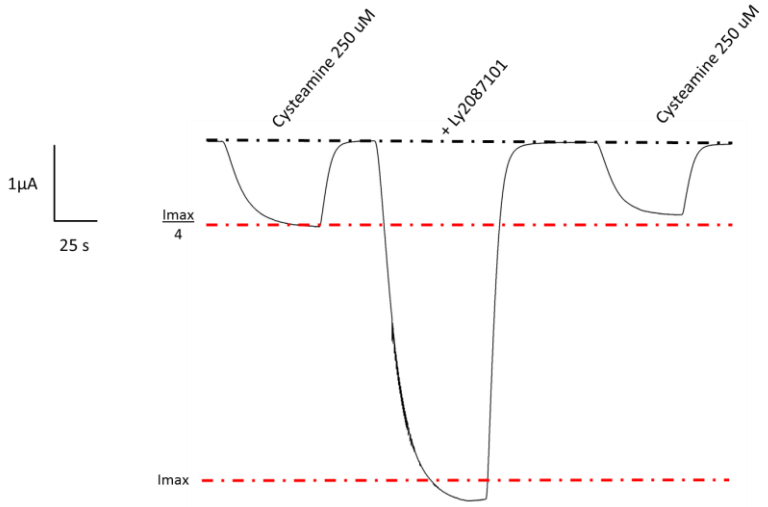

Figure 65: 2EVC experiment of *X. laevis* oocytes expressing ELIC with the PAM Ly2087101 (20 µM) co-applied at the EC25 of the agonist cysteamine at a holding potential at -60mV. The currents reached by the addition of Ly2087101 are more than 4 times higher than observed by the observed EC25 response, indicating that the channel may be even more active than with saturating cysteamine concentrations. This is a common feature for type II PAMs, since they reduce desensitization.

This indicated that Ly2087101 could act as type II PAM in ELIC, although it is known as a type I modulator in the α7 nAChR Receptor. The differences in the mode of modulation could be explained by differences in the interaction with ELIC compared to the α7 nAChR. I used this compound as additive in crystallization experiments, but despite the fact that crystals allowed data collection at 3.2-3.4 Å, the observed conformation was very similar to WT.

Since the use of PAM did not allow the stabilization of an open state in the crystals, I tried to understand which other factors are preventing the homologue ELIC to not undergo the desired conformational changes. Thus far all purification and crystallization experiments of ELIC were performed in Tris buffer. It was therefore surprising to see that Tris itself can modulate the activation of the channel. Electrophysiological experiments showed that the addition of 20 mM Tris to cysteamine applied at its EC_{50} lead to a further increase of the currents by about 10% (Figure 66).

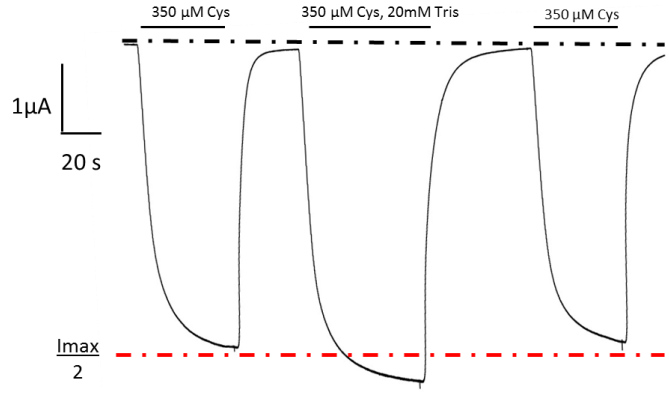

Figure 66: 2EVC experiment at a holding potential of -60mV. The application of Tris Buffer together with cysteamine at its EC_{50} enhances t the currents by around 10%.

In a number of initial ITC experiments, Tris buffer (pH7.5) was used. Only later on to directly compare binding affinity of the agonist and the antagonist of the 2EVC experiments to the ITC experiments the buffer was exchanged to Hepes. When comparing the results in Hepes and Tris, an interesting difference in the binding affinity was found. The binding affinity of the agonist propylamine in the presence of Tris was more than 1.5 times higher than that in Hepes, whereas the binding affinity of acetylcholine was about 2 times lower (Table 2 and Figure 67).

	Buffer:		**Buffer:**	
	25 mM **Hepes** @ pH7		25 mM **Tris** @ pH7	
	150mM NaCl		150mM NaCl	
	UDM (2xCMC)		UDM (2xCMC)	
	Affinity		**Affinity**	
Propylamine	8	mM	5	mM
Acetylcholine	2.5	mM	5	mM

Table 2: ITC binding affinity. Shown is the comparison of the binding of ELIC WT to the agonist propylamine and the antagonist acetylcholine in different buffers (left 25 mM Hepes, right in 25 mM Tris).

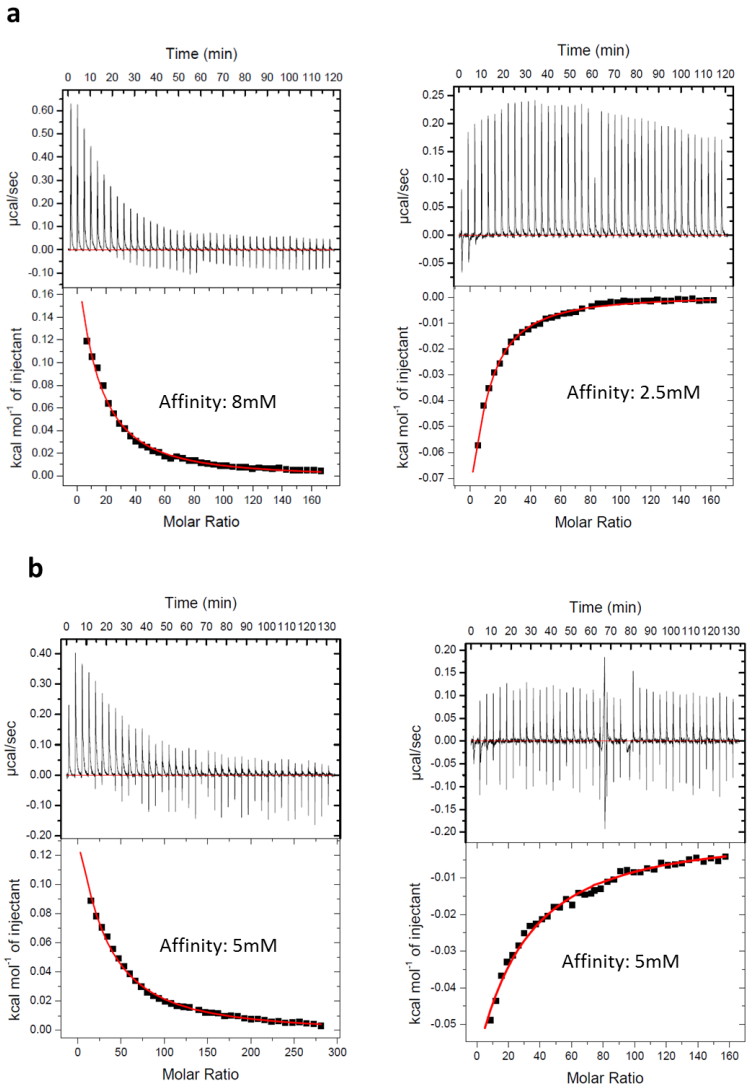

Figure 67: ITC experiment of ELIC WT at different buffer conditions. (a) Tris: ELIC WT against the agonist propylamine (left) and the antagonist acetylcholine (right). (b) Hepes: ELIC WT against the agonist propylamine (left) and the antagonist acetylcholine (right).

Since antagonist binding, unlike the agonist binding, is not cooperative any agonist or allosteric/orthosteric modulator would show a similar phenotype. Despite the fact that no further experiments were performed to show in which way Tris interacts with the channel, its structural similarity to the known partial agonist ethanolamine (Figure 68) is striking.

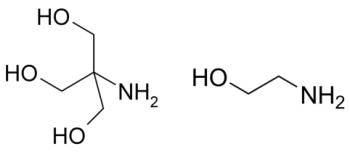

Figure 68: Tris (left) and the partial agonist ethanolamine (right). The structural similarity is apparent thus indicating a potential mode of action of Tris as partial agonist.

The results of my experiments suggest that binding in detergent solution is cooperative for the agonist propylamine and non-cooperative for the antagonist acetylcholine which is in agreement with previous findings by electrophysiology (*18*, *67*, *69*).

9 Appendix C

Curriculum Vitae

Name / First Name: Bertozzi Carlo Lorenzo

Date and place of birth: 5th November 1983 in Zurich

Nationality: Swiss & Italian

Education:

09/2009 - Today: PhD Student in Biochemisty
Institute of Biochemistry, University of Zurich
Mechanistic insight into gating and open channel block in prokaryotic pLGICs

2003 - 2008 Dipl. Nat. ETH Zurich
Institute of Molecular Biology and Biophysics, ETHZ
Investigation of the Interaction between the Signal Recognition Particle and the Ribosome.

1996 - 2003: High School Education
Kantonsschule Graubunden, Kt. Graubunden, Switzerland
*Typus C (*mathematisch-naturwissenschaftlich)

Publications:

Zimmermann I, Marabelli A, Bertozzi C, Sivilotti L and Dutzler R. Inhibition of the Prokaryotic Ligand-Gated Ion Channel ELIC by Divalent Cations, *PLoS Biol,* e1001429 (2012).

Hilf R, Bertozzi C, Zimmermann I, Reiter A, Trauner D, Dutzler R. Structural basis of open channel block in a prokaryotic pentameric ligand-gated ion channel, *Nat Struct Mol Biol, 17, 11,* (2010)

Verel, R., Tomka, I. T., Bertozzi, C., Cadalbert, R., Kammerer, R. A., Steinmetz, M. O., and Meier, B. H. Polymorphism in an Amyloid-Like Fibril-Forming Model Peptide, *Angew Chem Int Ed Engl*., (2008).

10 References

1. R. J. C. Hilf, Doctoral Thesis, Universität Zürich, (2009).
2. G. M. Shepherd, *Neurobiology*. (Oxford University Press, New York, ed. 3, 1994).
3. P. S. Miller, T. G. Smart, Binding, activation and modulation of Cys-loop receptors. *Trends Pharmacol Sci* **31**, 161-174 (2010); published online EpubApr (10.1016/j.tips.2009.12.005).
4. A. J. Thompson, H. A. Lester, S. C. Lummis, The structural basis of function in Cys-loop receptors. *Quarterly reviews of biophysics* **43**, 449-499 (2010); published online EpubNov (10.1017/S0033583510000168).
5. R. J. Hilf, R. Dutzler, A prokaryotic perspective on pentameric ligand-gated ion channel structure. *Curr Opin Struct Biol* **19**, 418-424 (2009); published online EpubAug (10.1016/j.sbi.2009.07.006).
6. R. E. Hibbs, E. Gouaux, Principles of activation and permeation in an anion-selective Cys-loop receptor. *Nature* **474**, 54-60 (2011); published online EpubJun 2 (10.1038/nature10139).
7. D. Gundisch, C. Eibl, Nicotinic acetylcholine receptor ligands, a patent review (2006-2011). *Expert Opin Ther Pat* **21**, 1867-1896 (2011); published online EpubDec (10.1517/13543776.2011.637919).
8. J. a. K. Del Castillo, B., Interaction at the end-plate receptors between different choline derivatives. *Proceedings of the Royal Society of London* **Series B**, 369-381 (1957); published online Epub1957 (
9. D. Colquhoun, Binding, gating, affinity and efficacy: the interpretation of structure-activity relationships for agonists and of the effects of mutating receptors. *Br J Pharmacol* **125**, 924-947 (1998); published online EpubNov (
10. J. MONOD, WYMAN, J., and CHANGEUX, J. P., ON THE NATURE OF ALLOSTERIC TRANSITIONS: A PLAUSIBLE MODEL. *J Mol Biol* **12**, 88-118 (1965).
11. M. B. Jackson, Kinetics of unliganded acetylcholine receptor channel gating. *Biophys J* **49**, 663-672 (1986); published online EpubMar (10.1016/S0006-3495(86)83693-1).
12. A. Bhattacharya, H. Dang, Q. M. Zhu, B. Schnegelsberg, N. Rozengurt, G. Cain, R. Prantil, D. A. Vorp, N. Guy, D. Julius, A. P. Ford, H. A. Lester, D. A. Cockayne, Uropathic observations in mice expressing a constitutively active point mutation in the 5-HT3A receptor subunit. *J Neurosci* **24**, 5537-5548 (2004); published online EpubJun 16 (10.1523/JNEUROSCI.5658-03.2004).
13. B. Katz, S. Thesleff, A study of the desensitization produced by acetylcholine at the motor end-plate. *J Physiol* **138**, 63-80 (1957); published online EpubAug 29 (
14. A. Feltz, A. Trautmann, Desensitization at the frog neuromuscular junction: a biphasic process. *J Physiol* **322**, 257-272 (1982); published online EpubJan (
15. E. L. Ochoa, A. Chattopadhyay, M. G. McNamee, Desensitization of the nicotinic acetylcholine receptor: molecular mechanisms and effect of modulators. *Cell Mol Neurobiol* **9**, 141-178 (1989); published online EpubJun (
16. P. J. Corringer, S. Bertrand, S. Bohler, S. J. Edelstein, J. P. Changeux, D. Bertrand, Critical elements determining diversity in agonist binding and desensitization of neuronal nicotinic acetylcholine receptors. *J Neurosci* **18**, 648-657 (1998); published online EpubJan 15 (
17. A. Keramidas, J. W. Lynch, An outline of desensitization in pentameric ligand-gated ion channel receptors. *Cell Mol Life Sci* **70**, 1241-1253 (2013); published online EpubApr (10.1007/s00018-012-1133-z).
18. I. Zimmermann, Doctoral Thesis, Universität Zürich, (2012).
19. B. Hille, *Ion channels of excitable membranes*. Ion channels of excitable membranes (Sunderland, USA, 2001), vol. 3, pp. 814.
20. J. M. Pascual, A. Karlin, Delimiting the binding site for quaternary ammonium lidocaine derivatives in the acetylcholine receptor channel. *J Gen Physiol* **112**, 611-621 (1998); published online EpubNov (

21. M. Adler, A. C. Oliveira, E. X. Albuquerque, N. A. Mansour, A. T. Eldefrawi, Reaction of tetraethylammonium with the open and closed conformations of the acetylcholine receptor ionic channel complex. *J Gen Physiol* **74**, 129-152 (1979); published online EpubJul (
22. R. J. Leonard, C. G. Labarca, P. Charnet, N. Davidson, H. A. Lester, Evidence that the M2 membrane-spanning region lines the ion channel pore of the nicotinic receptor. *Science* **242**, 1578-1581 (1988); published online EpubDec 16 (
23. A. B. Steinbach, A kinetic model for the action of xylocaine on receptors for acetylcholine. *J Gen Physiol* **52**, 162-180 (1968); published online EpubJul (
24. A. B. Steinbach, Alteration by xylocaine (lidocaine) and its derivatives of the time course of the end plate potential. *J Gen Physiol* **52**, 144-161 (1968); published online EpubJul (
25. E. Neher, J. H. Steinbach, Local anaesthetics transiently block currents through single acetylcholine-receptor channels. *J Physiol* **277**, 153-176 (1978); published online EpubApr (
26. C. M. Armstrong, Time course of TEA(+)-induced anomalous rectification in squid giant axons. *J Gen Physiol* **50**, 491-503 (1966); published online EpubNov (
27. C. M. Armstrong, Interaction of tetraethylammonium ion derivatives with the potassium channels of giant axons. *J Gen Physiol* **58**, 413-437 (1971); published online EpubOct (
28. R. R. Neubig, M. Spedding, T. Kenakin, A. Christopoulos, N. International Union of Pharmacology Committee on Receptor, C. Drug, International Union of Pharmacology Committee on Receptor Nomenclature and Drug Classification. XXXVIII. Update on terms and symbols in quantitative pharmacology. *Pharmacological reviews* **55**, 597-606 (2003); published online EpubDec (10.1124/pr.55.4.4).
29. R. R. Kaldany, A. Karlin, Reaction of quinacrine mustard with the acetylcholine receptor from Torpedo californica. *J Biol Chem* **258**, 6232-6242 (1983); published online EpubMay 25 (
30. J. M. Pascual, A. Karlin, Delimiting the binding site for quaternary ammonium lidocaine derivatives in the acetylcholine receptor channel. *J Gen Physiol* **112**, 611-621 (1998); published online EpubNov (
31. A. Karlin, Emerging structure of the nicotinic acetylcholine receptors. *Nature reviews. Neuroscience* **3**, 102-114 (2002); published online EpubFeb (10.1038/nrn731).
32. S. M. Sine, A. G. Engel, Recent advances in Cys-loop receptor structure and function. *Nature* **440**, 448-455 (2006); published online EpubMar 23 (10.1038/nature04708).
33. R. J. Hilf, R. Dutzler, Structure of a potentially open state of a proton-activated pentameric ligand-gated ion channel. *Nature* **457**, 115-118 (2009); published online EpubJan 1 (10.1038/nature07461).
34. T. J. Nutter, D. J. Adams, Monovalent and divalent cation permeability and block of neuronal nicotinic receptor channels in rat parasympathetic ganglia. *J Gen Physiol* **105**, 701-723 (1995); published online EpubJun (
35. D. J. Adams, T. M. Dwyer, B. Hille, The permeability of endplate channels to monovalent and divalent metal cations. *J Gen Physiol* **75**, 493-510 (1980); published online EpubMay (
36. J. A. Dani, G. Eisenman, Monovalent and divalent cation permeation in acetylcholine receptor channels. Ion transport related to structure. *J Gen Physiol* **89**, 959-983 (1987); published online EpubJun (
37. O. Arunlakshana, H. O. Schild, Some quantitative uses of drug antagonists. *Br J Pharmacol Chemother* **14**, 48-58 (1959); published online EpubMar (
38. T. P. Kenakin, '7TM receptor allostery: putting numbers to shapeshifting proteins. *Trends Pharmacol Sci* **30**, 460-469 (2009); published online EpubSep (10.1016/j.tips.2009.06.007).
39. A. Tasneem, L. M. Iyer, E. Jakobsson, L. Aravind, Identification of the prokaryotic ligand-gated ion channels and their implications for the mechanisms and origins of animal Cys-loop ion channels. *Genome Biol* **6**, R4 (2005)10.1186/gb-2004-6-1-r4).
40. N. Bocquet, L. Prado de Carvalho, J. Cartaud, J. Neyton, C. Le Poupon, A. Taly, T. Grutter, J. P. Changeux, P. J. Corringer, A prokaryotic proton-gated ion channel from the nicotinic

acetylcholine receptor family. *Nature* **445**, 116-119 (2007); published online EpubJan 4 (10.1038/nature05371).
41. K. Brejc, W. J. van Dijk, R. V. Klaassen, M. Schuurmans, J. van Der Oost, A. B. Smit, T. K. Sixma, Crystal structure of an ACh-binding protein reveals the ligand-binding domain of nicotinic receptors. *Nature* **411**, 269-276 (2001); published online EpubMay 17 (10.1038/35077011).
42. N. Unwin, Structure and action of the nicotinic acetylcholine receptor explored by electron microscopy. *FEBS Lett* **555**, 91-95 (2003); published online EpubNov 27 (
43. A. Miyazawa, Y. Fujiyoshi, N. Unwin, Structure and gating mechanism of the acetylcholine receptor pore. *Nature* **423**, 949-955 (2003); published online EpubJun 26 (10.1038/nature01748).
44. N. Unwin, Refined structure of the nicotinic acetylcholine receptor at 4A resolution. *J Mol Biol* **346**, 967-989 (2005); published online EpubMar 4 (10.1016/j.jmb.2004.12.031).
45. W. Y. Lee, S. M. Sine, Principal pathway coupling agonist binding to channel gating in nicotinic receptors. *Nature* **438**, 243-247 (2005); published online EpubNov 10 (10.1038/nature04156).
46. W. Y. Lee, C. R. Free, S. M. Sine, Binding to gating transduction in nicotinic receptors: Cys-loop energetically couples to pre-M1 and M2-M3 regions. *J Neurosci* **29**, 3189-3199 (2009); published online EpubMar 11 (10.1523/JNEUROSCI.6185-08.2009).
47. A. Auerbach, The gating isomerization of neuromuscular acetylcholine receptors. *J Physiol* **588**, 573-586 (2010); published online EpubFeb 15 (10.1113/jphysiol.2009.182774).
48. E. Granseth, S. Seppala, M. Rapp, D. O. Daley, G. Von Heijne, Membrane protein structural biology--how far can the bugs take us? *Mol Membr Biol* **24**, 329-332 (2007); published online EpubSep-Dec (10.1080/09687680701413882).
49. R. J. Hilf, R. Dutzler, X-ray structure of a prokaryotic pentameric ligand-gated ion channel. *Nature* **452**, 375-379 (2008); published online EpubMar 20 (10.1038/nature06717).
50. N. Bocquet, H. Nury, M. Baaden, C. Le Poupon, J. P. Changeux, M. Delarue, P. J. Corringer, X-ray structure of a pentameric ligand-gated ion channel in an apparently open conformation. *Nature* **457**, 111-114 (2009); published online EpubJan 1 (10.1038/nature07462).
51. O. Beckstein, M. S. Sansom, A hydrophobic gate in an ion channel: the closed state of the nicotinic acetylcholine receptor. *Phys Biol* **3**, 147-159 (2006); published online EpubJun (10.1088/1478-3975/3/2/007).
52. R. Dutzler, in *Gordon Conference*. (Il Ciocco, 2010).
53. O. Beckstein, M. S. Sansom, The influence of geometry, surface character, and flexibility on the permeation of ions and water through biological pores. *Phys Biol* **1**, 42-52 (2004); published online EpubJun (10.1088/1478-3967/1/1/005).
54. T. Konno, C. Busch, E. Von Kitzing, K. Imoto, F. Wang, J. Nakai, M. Mishina, S. Numa, B. Sakmann, Rings of anionic amino acids as structural determinants of ion selectivity in the acetylcholine receptor channel. *Proceedings. Biological sciences / The Royal Society* **244**, 69-79 (1991); published online EpubMay 22 (10.1098/rspb.1991.0053).
55. S. Vernino, M. Amador, C. W. Luetje, J. Patrick, J. A. Dani, Calcium modulation and high calcium permeability of neuronal nicotinic acetylcholine receptors. *Neuron* **8**, 127-134 (1992); published online EpubJan (
56. R. Zwart, R. G. Van Kleef, J. M. Milikan, M. Oortgiesen, H. P. Vijverberg, Potentiation and inhibition of subtypes of neuronal nicotinic acetylcholine receptors by Pb2+. *European journal of pharmacology* **291**, 399-406 (1995); published online EpubNov 30 (
57. C. J. Dacosta, J. E. Baenziger, Gating of pentameric ligand-gated ion channels: structural insights and ambiguities. *Structure* **21**, 1271-1283 (2013); published online EpubAug 6 (10.1016/j.str.2013.06.019).
58. I. Zimmermann, R. Dutzler, Ligand activation of the prokaryotic pentameric ligand-gated ion channel ELIC. *PLoS Biol* **9**, e1001101 (2011); published online EpubJun (10.1371/journal.pbio.1001101).

59. S. B. Hansen, G. Sulzenbacher, T. Huxford, P. Marchot, P. Taylor, Y. Bourne, Structures of Aplysia AChBP complexes with nicotinic agonists and antagonists reveal distinctive binding interfaces and conformations. *Embo J* **24**, 3635-3646 (2005); published online EpubOct 19 (10.1038/sj.emboj.7600828).
60. C. Bouzat, F. Gumilar, G. Spitzmaul, H. L. Wang, D. Rayes, S. B. Hansen, P. Taylor, S. M. Sine, Coupling of agonist binding to channel gating in an ACh-binding protein linked to an ion channel. *Nature* **430**, 896-900 (2004); published online EpubAug 19 (10.1038/nature02753).
61. G. Duret, C. Van Renterghem, Y. Weng, M. Prevost, G. Moraga-Cid, C. Huon, J. M. Sonner, P. J. Corringer, Functional prokaryotic-eukaryotic chimera from the pentameric ligand-gated ion channel family. *Proc Natl Acad Sci U S A* **108**, 12143-12148 (2011); published online EpubJul 19 (10.1073/pnas.1104494108).
62. M. S. Prevost, L. Sauguet, H. Nury, C. Van Renterghem, C. Huon, F. Poitevin, M. Baaden, M. Delarue, P. J. Corringer, A locally closed conformation of a bacterial pentameric proton-gated ion channel. *Nat Struct Mol Biol* **19**, 642-649 (2012); published online EpubJun (10.1038/nsmb.2307).
63. G. Gonzalez-Gutierrez, L. G. Cuello, S. K. Nair, C. Grosman, Gating of the proton-gated ion channel from Gloeobacter violaceus at pH 4 as revealed by X-ray crystallography. *Proc Natl Acad Sci U S A* **110**, 18716-18721 (2013); published online EpubNov 12 (10.1073/pnas.1313156110).
64. W. Y. Lee, C. R. Free, S. M. Sine, Nicotinic receptor interloop proline anchors beta1-beta2 and Cys loops in coupling agonist binding to channel gating. *J Gen Physiol* **132**, 265-278 (2008); published online EpubAug (10.1085/jgp.200810014).
65. W. Y. Lee, C. R. Free, S. M. Sine, Binding to gating transduction in nicotinic receptors: Cys-loop energetically couples to pre-M1 and M2-M3 regions. *J Neurosci* **29**, 3189-3199 (2009); published online EpubMar 11 (10.1523/JNEUROSCI.6185-08.2009).
66. B. Schwappach, N. Zerangue, Y. N. Jan, L. Y. Jan, Molecular basis for K(ATP) assembly: transmembrane interactions mediate association of a K+ channel with an ABC transporter. *Neuron* **26**, 155-167 (2000); published online EpubApr (
67. I. Zimmermann, A. Marabelli, C. Bertozzi, L. G. Sivilotti, R. Dutzler, Inhibition of the prokaryotic pentameric ligand-gated ion channel ELIC by divalent cations. *PLoS Biol* **10**, e1001429 (2012)10.1371/journal.pbio.1001429).
68. R. Spurny, B. Billen, R. J. Howard, M. Brams, S. Debaveye, K. L. Price, D. A. Weston, S. V. Strelkov, J. Tytgat, S. Bertrand, D. Bertrand, S. C. Lummis, C. Ulens, Multisite binding of a general anesthetic to the prokaryotic pentameric Erwinia chrysanthemi ligand-gated ion channel (ELIC). *J Biol Chem* **288**, 8355-8364 (2013); published online EpubMar 22 (10.1074/jbc.M112.424507).
69. J. Pan, Q. Chen, D. Willenbring, K. Yoshida, T. Tillman, O. B. Kashlan, A. Cohen, X. P. Kong, Y. Xu, P. Tang, Structure of the pentameric ligand-gated ion channel ELIC cocrystallized with its competitive antagonist acetylcholine. *Nat Commun* **3**, 714 (2012)10.1038/ncomms1703).
70. P. S. Miller, T. G. Smart, Binding, activation and modulation of Cys-loop receptors. *Trends Pharmacol Sci* **31**, 161-174 (2010); published online EpubApr (10.1016/j.tips.2009.12.005).
71. R. L. A. Marabelli, L. G. Sivilotti, in *37th Congress of IUPS*. (Proceedings of The Physiological Society, Birmingham, UK, 2013), vol. 37.
72. Dustin K. Williamsa, Jingyi Wangb, R. L. Papkea, Positive allosteric modulators as an approach to nicotinic acetylcholine receptor-targeted therapeutics: Advantages and limitations. *Biochem Pharmacol* **82**, 915-930 (2011).
73. K. Imoto, C. Busch, B. Sakmann, M. Mishina, T. Konno, J. Nakai, H. Bujo, Y. Mori, K. Fukuda, S. Numa, Rings of negatively charged amino acids determine the acetylcholine receptor channel conductance. *Nature* **335**, 645-648 (1988); published online EpubOct 13 (10.1038/335645a0).
74. D. Bertrand, J. L. Galzi, A. Devillers-Thiery, S. Bertrand, J. P. Changeux, Mutations at two distinct sites within the channel domain M2 alter calcium permeability of neuronal alpha 7 nicotinic receptor. *Proc Natl Acad Sci U S A* **90**, 6971-6975 (1993); published online EpubAug 1 (

75. K. Imoto, C. Methfessel, B. Sakmann, M. Mishina, Y. Mori, T. Konno, K. Fukuda, M. Kurasaki, H. Bujo, Y. Fujita, et al., Location of a delta-subunit region determining ion transport through the acetylcholine receptor channel. *Nature* **324**, 670-674 (1986); published online EpubDec 18-31 (10.1038/324670a0).
76. M. Xu, M. H. Akabas, Amino acids lining the channel of the gamma-aminobutyric acid type A receptor identified by cysteine substitution. *J Biol Chem* **268**, 21505-21508 (1993); published online EpubOct 15 (
77. M. H. Akabas, C. Kaufmann, P. Archdeacon, A. Karlin, Identification of acetylcholine receptor channel-lining residues in the entire M2 segment of the alpha subunit. *Neuron* **13**, 919-927 (1994); published online EpubOct (
78. D. C. Reeves, E. N. Goren, M. H. Akabas, S. C. Lummis, Structural and electrostatic properties of the 5-HT3 receptor pore revealed by substituted cysteine accessibility mutagenesis. *J Biol Chem* **276**, 42035-42042 (2001); published online EpubNov 9 (10.1074/jbc.M106066200).
79. B. Hsiao, D. Dweck, C. W. Luetje, Subunit-dependent modulation of neuronal nicotinic receptors by zinc. *J Neurosci* **21**, 1848-1856 (2001); published online EpubMar 15 (
80. S. B. Hansen, H. L. Wang, P. Taylor, S. M. Sine, An ion selectivity filter in the extracellular domain of Cys-loop receptors reveals determinants for ion conductance. *J Biol Chem* **283**, 36066-36070 (2008); published online EpubDec 26 (10.1074/jbc.C800194200).
81. B. K. Ho, F. Gruswitz, HOLLOW: generating accurate representations of channel and interior surfaces in molecular structures. *BMC structural biology* **8**, 49 (2008)10.1186/1472-6807-8-49).
82. S. C. Lummis, D. L. Beene, L. W. Lee, H. A. Lester, R. W. Broadhurst, D. A. Dougherty, Cis-trans isomerization at a proline opens the pore of a neurotransmitter-gated ion channel. *Nature* **438**, 248-252 (2005); published online EpubNov 10 (10.1038/nature04130).
83. W. Kabsch, Xds. *Acta crystallographica. Section D, Biological crystallography* **66**, 125-132 (2010); published online EpubFeb (10.1107/S0907444909047337).
84. E. Potterton, S. McNicholas, E. Krissinel, K. Cowtan, M. Noble, The CCP4 molecular-graphics project. *Acta crystallographica. Section D, Biological crystallography* **58**, 1955-1957 (2002); published online EpubNov (
85. P. D. Adams, P. V. Afonine, G. Bunkoczi, V. B. Chen, I. W. Davis, N. Echols, J. J. Headd, L. W. Hung, G. J. Kapral, R. W. Grosse-Kunstleve, A. J. McCoy, N. W. Moriarty, R. Oeffner, R. J. Read, D. C. Richardson, J. S. Richardson, T. C. Terwilliger, P. H. Zwart, PHENIX: a comprehensive Python-based system for macromolecular structure solution. *Acta crystallographica. Section D, Biological crystallography* **66**, 213-221 (2010); published online EpubFeb (10.1107/S0907444909052925).
86. P. Emsley, K. Cowtan, Coot: model-building tools for molecular graphics. *Acta crystallographica. Section D, Biological crystallography* **60**, 2126-2132 (2004); published online EpubDec (10.1107/S0907444904019158).
87. M. F. Sanner, A. J. Olson, J. C. Spehner, Reduced surface: an efficient way to compute molecular surfaces. *Biopolymers* **38**, 305-320 (1996); published online EpubMar (10.1002/(SICI)1097-0282(199603)38:3<305::AID-BIP4>3.0.CO;2-Y).
88. A. M. Seddon, P. Curnow, P. J. Booth, Membrane proteins, lipids and detergents: not just a soap opera. *Biochim Biophys Acta* **1666**, 105-117 (2004); published online EpubNov 3 (10.1016/j.bbamem.2004.04.011).
89. M. le Maire, P. Champeil, J. V. Moller, Interaction of membrane proteins and lipids with solubilizing detergents. *Biochim Biophys Acta* **1508**, 86-111 (2000); published online EpubNov 23 (
90. M. Luckey, *Membrane Structural Biology: With Biochemical and Biophysical Foundations*. Membrane Structural Biology (2008).
91. R. Phillips, T. Ursell, P. Wiggins, P. Sens, Emerging roles for lipids in shaping membrane-protein function. *Nature* **459**, 379-385 (2009); published online EpubMay 21 (10.1038/nature08147).

92. L. J. Berliner, J. Grunwald, H. O. Hankovszky, K. Hideg, A novel reversible thiol-specific spin label: papain active site labeling and inhibition. *Anal Biochem* **119**, 450-455 (1982); published online EpubJan 15 (
93. M. Pannier, S. Veit, A. Godt, G. Jeschke, H. W. Spiess, Dead-time free measurement of dipole-dipole interactions between electron spins. *J Magn Reson* **142**, 331-340 (2000); published online EpubFeb (10.1006/jmre.1999.1944).
94. Y. Polyhach, E. Bordignon, G. Jeschke, Rotamer libraries of spin labelled cysteines for protein studies. *Phys Chem Chem Phys* **13**, 2356-2366 (2011); published online EpubFeb 14 (10.1039/c0cp01865a).
95. N. L. Absalom, P. R. Schofield, T. M. Lewis, Pore structure of the Cys-loop ligand-gated ion channels. *Neurochem Res* **34**, 1805-1815 (2009); published online EpubOct (10.1007/s11064-009-9971-2).
96. P. Velisetty, S. V. Chalamalasetti, S. Chakrapani, Structural basis for allosteric coupling at the membrane-protein interface in GLIC. *J Biol Chem*, (2013); published online EpubDec 13 (10.1074/jbc.M113.523050).
97. J. Borch, T. Hamann, The nanodisc: a novel tool for membrane protein studies. *Biol Chem* **390**, 805-814 (2009); published online EpubAug (10.1515/BC.2009.091).
98. R. Lape, D. Colquhoun, L. G. Sivilotti, On the nature of partial agonism in the nicotinic receptor superfamily. *Nature* **454**, 722-727 (2008); published online EpubAug 7 (10.1038/nature07139).
99. J. L. Galzi, S. Bertrand, P. J. Corringer, J. P. Changeux, D. Bertrand, Identification of calcium binding sites that regulate potentiation of a neuronal nicotinic acetylcholine receptor. *Embo J* **15**, 5824-5832 (1996); published online EpubNov 1 (
100. R. M. Krause, B. Buisson, S. Bertrand, P. J. Corringer, J. L. Galzi, J. P. Changeux, D. Bertrand, Ivermectin: a positive allosteric effector of the alpha7 neuronal nicotinic acetylcholine receptor. *Mol Pharmacol* **53**, 283-294 (1998); published online EpubFeb (